University of Twente

EEMCS / Electrical Engineering
Control Engineering

Modelling of direct drive motors for performance improvement by design and control

Jeroen Scholten

M.Sc. Thesis

Supervisors
prof.dr.ir. J. van Amerongen
dr.ir. P.C. Breedveld
ir. P.T. Rutgers, ir. J.M. Zwikker

October 2004

Report nr. 029CE2004
Control Engineering
EE-Math-CS
University of Twente
P.O. Box 217
7500 AE Enschede
The Netherlands

University of Twente

EEMCS / Electrical Engineering
Control Engineering

In cooperation with:
demcon

Modelling of direct drive motors for performance improvement by design and control

Jeroen Scholten

M.Sc. Thesis

Supervisors
prof.dr.ir. J. van Amerongen
dr.ir. P.C. Breedveld
ir. P.T. Rutgers, ir. J.M. Zwikker

October 2004

Report nr. 029CE2004

Control Engineering
EE-Math-CS
University of Twente
P.O. Box 217
7500 AE Enschede
The Netherlands

SUMMARY

In this thesis a direct drive permanent magnet motor has been modelled to improve its performance by means of design and control.

An electromagnetic motor model has been made which uses construction design parameters to calculate specific properties of a direct drive permanent magnet motor like its steepness, motor constant, reluctance torque, saturation losses, inductance and windings resistance. The model is based on a parametric magnetic equivalent circuit that calculates the flux balance for a three phase motor as a function of the rotor angle. It is generalized for any combination of pole shoes and magnet poles, takes magnetic saturation into account and is validated against three motors. Also a thermal model has been made which uses the same design parameters as input to simulate the thermal behaviour of a motor.

By varying the design parameters while calculating the motor performance the electromagnetic model can be used for improving the constructional design of a motor. By using the calculated motor properties like motor constant and reluctance torque in a closed loop model, the performance of a motor design can be improved by means of control. For example the effect of learning control on two motor designs has been simulated.

PREFACE

This thesis has been made in close cooperation with Demcon Twente B.V. For seven months I had the honour to join the staff of Demcon and practise to be a hard working citizen (instead of a student) such as my friends started to call me. Although I worked fulltime I really liked the time at Demcon and therefore I want to thanks all my ‘colleagues’ especially Rini, Andre, Wouter, Pieter and the others of the Mechanical Engineering department for the good discussions, their help, but most important the fun we had. As a student Electrical Engineering joining the Mechanical Engineering department was a valuable experience.

Especially Peter Rutgers (Demcon) deserves many credits. Due to his incredibly large practical experience I learned a lot of him. We discussed a lot about all kinds of problems, not only within the scope of this thesis. I liked the productive brainstorming sessions and teamwork we sometimes had. For me it was a pleasure to be able to do at least something in return by assisting you with making the Simulink model of the ML drive.

Furthermore I would like to thank my supervisors Peter Breedveld and Job van Amerongen of the University of Twente. Thanks Peter for the substantive discussions when reviewing this thesis. Thanks Job for providing me with this assignment at Demcon at the first place.

This thesis is the finish of my study Electrical Engineering at the University of Twente. Looking back on the past six years I can say I have had a beautiful time in Enschede. I would like to thank my colleague truckers of the ERC, fellow members of board ’00-’01 of rowing club Euros, fellow students and all other friends for the good times we had. Above all I am grateful to my girlfriend Petra and my parents who supported me.

Jeroen Scholten
Enschede, October 2004

CONTENTS

1 INTRODUCTION

1.1 Origination

This MSc project originated from the demand of Thales Nederland B.V. for knowledge about large direct drive motors for usage in several applications amongst which the mechanical actuation of radar devices. The research has been done in close cooperation with Demcon Twente B.V.

1.2 Problem definition

The goal of this MSc project is to gain knowledge about direct drive motors for usage in several purposes and to make a model for designing and evaluating brushless permanent magnet motors. The model should be useful when choosing or designing a motor, designing a controller for a drive or reviewing a purchased motor. Due to the quite wide-ranging purpose certain generalisation will be necessary in the calculations, modelling and documentation.

A lot has been written about electric drives. Complex theories exist for modelling every detail in an electrical motor. Important is to discern what is relevant and important to know for the applications this project is used for. This thesis will focus on the construction design parameters of permanent magnet motors influencing the electromagnetic transduction properties, especially torque performance because the motor is directly coupled to the load.

Goal is to be able to reproduce motor dependent properties as motor constant, windings resistance and inductance by using a quasi static approach. This knowledge can then be used for improving motor performance by construction design. An additional goal is to investigate how to improve the performance by means of control.

2 ANALYSIS

2.1 Introduction

To get into the topic of brushless permanent magnet motors this chapter treats the most relevant theory, starting with the energy balance of a permanent magnet motor for identifying the electromechanical transduction principles, followed by an introduction to magnetic equivalent circuits which are used in this thesis to model the magnetic behaviour of motors. Afterwards motor theory, the use of permanent magnets and the thermal behaviour of a motor will be addressed. Finally this chapter shows a way to match a motor to an application.

In the end of this chapter it should be clear
- how a permanent magnet motor works,
- what the characterising parameters and performance measures of a motor are,
- how the influence of the motor dimensions on the performance can be modelled,
- what electric, magnetic, mechanical and thermal effects are important or negligible,
- how to choose or design the right motor for certain application.

Technical aspects of the permanent magnet motor that are treated are saturation, cogging, peak and continuous torque, power, efficiency, dissipation and cooling.

In a brushless permanent magnet motor the rotor contains permanent magnets, which are to be rejected and attracted by powering the coils of the stator. Direct drive stands for a drive without gearings directly connected to the load. Mostly a direct drive motor runs at lower speeds than motors with gears. This results in more low frequent torque disturbances acting on the load and a lower efficiency. The working principle of the motor is the generation of a magnetic field such that poles reject and attract each other periodically at the right moment and therefore the rotor starts to move to reduce this energetic undesired situation. This principle can be derived from the magnetic energy balance, which will be started with.

2.2 Magnetic energy balance

In figure 1 a simple sketch shows the concept of permanent magnets generating a flux along a path through stator and rotor. The naming of the elements used in this thesis is also shown.

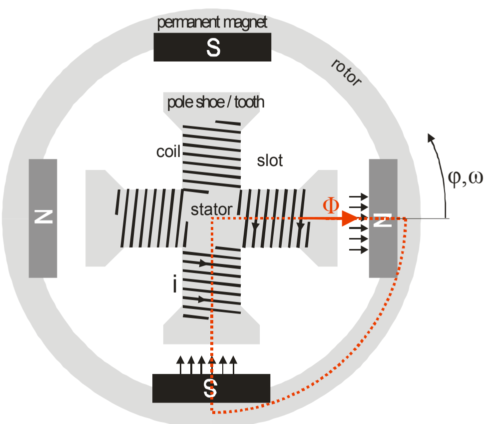

figure 1 naming of the elements and illustration of the magnetic flux induced by coils and permanent magnets

Both coils and magnets contribute to the flux in the motor. The coils add magnetic field due to driving current and the magnets add magnetic field due to their remanence. Assuming that the influence of the current through the coils on the magnets can be neglected, the contribution of the permanent magnets to the coupled flux in the coils can be seen as an applied flux λ_{pm}. Since the magnets are fixed to the moving rotor this applied flux is a nonlinear function of the rotor angle: $\lambda_{pm}(\varphi)$. As long as we have no saturation the coupled flux in the coil can be seen as the sum of both individual contributions.

$$\lambda_{coil}(i,\varphi) = Li + \lambda_{pm}(\varphi) \qquad \text{[Wb] (1)}$$

L is the self induction of the coils and i is the current. In this analysis we assume a flat rotor surface without extrusions except permanent magnets. This implies that the self inductance is independent on the rotor angle. So the coupled flux due to the coils is a function of the current through the coils only.

The energy balance of the magnetic domain gives insight in the relations between electric, magnetic and mechanical coupling of the motor. Assuming that the magnetic flux is the only energy storage in the motor we can write the stored magnetic energy as

$$E_{magn}(\lambda,\varphi) = \frac{\lambda_{coil}^2}{2L} = \frac{\left(Li + \lambda_{pm}(\varphi)\right)^2}{2L} = \frac{1}{2}Li^2 + \lambda_{pm}(\varphi)\cdot i + \frac{1}{2L}\lambda_{pm}^2(\varphi) \qquad \text{[J] (2)}$$

The first term is the magnetic energy stored in the coil due to induction. The second term is a cross term connecting the mechanical and electrical port which are coupled via magnetic energy. The third term expresses the energy stored in the magnetic field interacting with the mechanical domain and is responsible for the current independent reluctance torque or cogging.

The electromechanical transduction principle becomes clear when deriving the motor torque.

$$T = \frac{\partial E_{magn}(\lambda,\varphi)}{\partial\varphi} = 0 + \frac{\partial\lambda_{pm}(\varphi)}{\partial\varphi} i + \frac{1}{L}\lambda_{pm}(\varphi)\frac{\partial\lambda_{pm}(\varphi)}{\partial\varphi} \qquad \text{[Nm] (3)}$$

It can be concluded that the delivered torque is linearly related to the current through the coils due to the second term with a cogging offset due to the third term. It can also easily be seen that the induction term does not contribute to the delivered torque. The factor between current and torque, also defined as the motor constant K_m, can be read from (3).

$$K_m(\varphi) = \frac{d\lambda_{pm}(\varphi)}{d\varphi} \qquad \text{[Vs/rad] (4)}$$

In case of a rotor with two magnet poles passing the coils as the rotor moves, the flux will vary periodically from positive to negative. As one can see from relation (4) the motor constant is therefore a periodical wave. Depending on the motor design the shape of the motor constant can be for example trapezoid or sinusoid.

According to (3) the reluctance torque equals

$$T_r(\varphi) = \frac{1}{L}\lambda_{pm}(\varphi)\frac{\partial\lambda_{pm}(\varphi)}{\partial\varphi} \qquad \text{[Nm] (5)}$$

One can see that the reluctance torque is equal to the total torque when the current is zero.

$$T_r(\varphi) = \left(\frac{dE_{magn}(i,\varphi)}{d\varphi} \right)_{i=0} \qquad \text{[Nm] (6)}$$

This cogging torque tries to prevent the rotor to move since that is a energetic undesired situation: magnets moving along coils create a varying field and flux. So when moving the rotor along the stator reluctance torque is produced regardless if the motor is driven by a power supply.

An electric motor can be modelled in electric domain by a resistance, inductance and gyrator in series for respectively the dissipation in the copper windings, the magnetic energy stored in the coils due to the induction and the energy transformed from electrical into mechanical domain and vice versa. Since the reluctance torque only operates in the mechanical domain it does not appear in the electrical model.

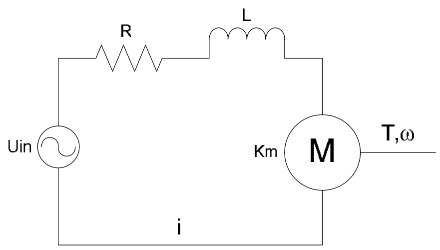

figure 2 elementary model of an electric motor

When deriving the voltage equation for the magnetic circuit it becomes clear that the visualisation of figure 2 of the electric domain holds for permanent magnet motors.

$$u_{in} = u_r + u_{induction}$$

$$u_{induction} = \frac{d\lambda(i,\varphi)}{dt} = \frac{d\left(Li + \lambda_{pm}(\varphi)\right)}{dt} = L\frac{di}{dt} + \frac{d\lambda_{pm}(\varphi)}{dt} = L\frac{di}{dt} + \frac{d\lambda_{pm}(\varphi)}{d\varphi}\frac{d\varphi}{dt} \qquad \text{[V] (7)}$$

$$u_{in} = iR + L\frac{di}{dt} + K_m(\varphi)\cdot\omega$$

This paragraph showed the relations between electric and mechanical domain via the magnetic domain. Once the resistance, inductance and the flux due to the permanent magnets are known all motor properties and behaviour can be deducted. In paragraph 2.3 equivalent circuits will be introduced which are used to calculate the flux and inductance of a motor.

2.3 Equivalent circuits

In this thesis magnetic equivalent circuits have been used to simplify the interpretation of the motor principle. A static representation using electric circuits makes it easy to identify and work with the algebraic structure of magnetic fields and fluxes.

In a magnetic circuit a coil is a magneto motive force source. It creates a magnetic field H that causes a flux through the yoke. The yoke and airgaps are reluctances blocking the flux.

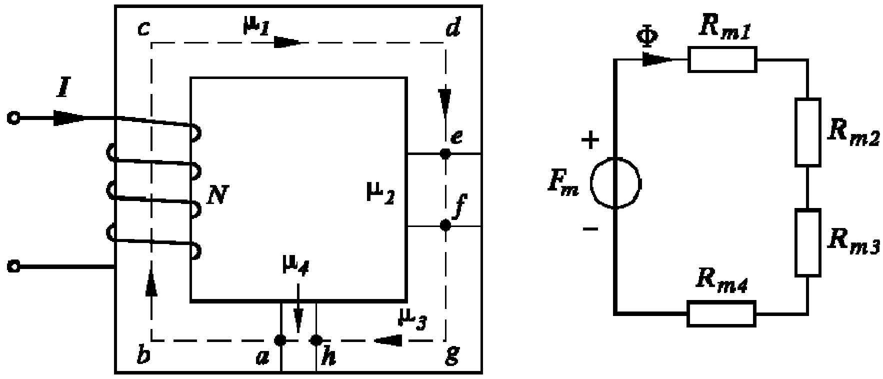

figure 3 magnetic circuit replaced by a equivalent circuit (from Hoeijmakers[2])

This analogy has no meaning in dynamic or energetic context and is only a static representation of the algebraic relations. According to Hopkinson's law the flux through a magnetic circuit can be calculated by dividing the magneto motive force F_m through the reluctance R_m of the whole path.

$$\Phi = \frac{F_m}{R_m} \qquad \text{[Wb] (8)}$$

where the magneto-motive force induced by a coil with N windings and current i is defined as

$$F_m = H \cdot l = N \cdot i \qquad \text{[A] (9)}$$

The reluctance of a circuit of length l, permeability μ and cross-sectional surface A is defined as

$$R_m = \frac{l}{\mu \cdot A} \qquad \text{[A/Wb] (10)}$$

According to (9) and Maxwell's equations (66) and (63) a permanent magnet with remanence B_r can also be seen as a coil with a magneto motive force, also called number of ampere-turns, equal to:

$$F_{m,pm} = \frac{B_r \cdot l}{\mu} \qquad \text{[A] (11)}$$

Self-inductance is the factor that relates the current through a coil with the coupled flux induced through that coil. In other words self-inductance is the reciprocal of reluctance times squared winding.

$$L_m = \frac{N^2}{R_m} \qquad \text{[H] or [Wb/A] (12)}$$

The total inductance per phase equals (12) times the number of coils per phase.

In chapter 3 equivalent circuits will be applied for calculating the flux through a motor. This will be done by constructing a network of sources of magneto motive force and reluctances representing the magnetic circuit of stator, rotor, airgap, coils and permanent magnets. But first in next paragraphs relevant motor theory will be treated, which is necessary to design this motor model.

2.4 Motor theory

This paragraph handles the elements from the motor model of figure 2 in more detail. Besides motor theory attention is paid to the way motor performance is judged in this thesis. Quantities like steepness, motor constant and resistance will be treated for later usage, but we start with the use of multiple phases.

2.4.1 Multiple phases

This thesis will focus on three phase motors. Most used power signals for brushless electric motors are three phase signals. Three phases are used to transfer a constant power. Furthermore the conductor losses are reduced because the phases can have one common ground while their sum equals zero. The more or less linear electricity network does not distort sine waves and therefore all sorts of loads and sources can be designed for a sine shape excitation.

The use of multiple phases has influence on the design and control of permanent magnet motors. As mentioned in paragraph 2.2 the motor constant is a periodic function of the motor angle. To obtain a constant power transfer or a constant torque the sum of the products of current and motor constants should be constant.

$$T = \sum_{phases} K_i(\varphi) i_i \qquad \text{[Nm] (13)}$$

To minimize the dissipation for a certain torque it can be seen that the current should be proportional to the motor constant: if the current is high the motor constant should be high and vice versa. Otherwise the current could be high when the motor constant is low and the motor would only heat up the windings without producing torque.

These two conditions are fulfilled when the motor constant is a sine function of the motor angle and the current is a sine wave exactly in phase with the motor constant as derived by equations (14), (15) and (17).

Having a supply voltage per phase of u_a, u_b and u_c

$$\begin{aligned} u_a &= U\sqrt{2}\cos(\omega t) \\ u_b &= U\sqrt{2}\cos\left(\omega t - \frac{2\pi}{3}\right) \\ u_c &= U\sqrt{2}\cos\left(\omega t - \frac{4\pi}{3}\right) \end{aligned} \qquad \text{[V] (14)}$$

and a resulting current per phase of i_a, i_b and i_c

$$\begin{aligned} i_a &= I\sqrt{2}\cos(\omega t - \varphi) \\ i_b &= I\sqrt{2}\cos\left(\omega t - \varphi - \frac{2\pi}{3}\right) \\ i_c &= I\sqrt{2}\cos\left(\omega t - \varphi - \frac{4\pi}{3}\right) \end{aligned} \qquad \text{[A] (15)}$$

the sum of the currents is zero

$$i_a + i_b + i_c = 0 \qquad \text{[A] (16)}$$

and the resulting transferred power is constant and equals

$$p = u_a i_a + u_b i_b + u_c i_c = 3UI\cos(\varphi) \qquad \text{[W] (17)}$$

where φ is a phase shift due to the load and the inductance of the motor.

Conclusion: the motor constant and current should be a sine function of the motor angle. This is obtained when the flux in the airgap is also a sine function of the motor angle according to (4). The shape of the flux is influenced by the design of the magnetic circuit of a motor and the choices for the dimensions of pole shoes, number of magnet poles, etc. Since one of the goals of this thesis work is to investigate the influence of the motor dimensions on the motor performance, chapter 5 will go into details about these design choices using simulation results.

2.4.2 Copper resistance

The copper resistance is a important characteristic of a motor. As one can see from equation (3) or (7) the produced torque is proportional to the current. A low copper resistance means that a lot of current can be achieved having low supply voltage.

Following relation approximates the resistance of the copper windings per phase

$$R = \frac{pf \cdot N \cdot \rho_{copper} \cdot 2(w+l)}{A_{copper}} \qquad [\Omega] \text{ (18)}$$

where *pf* is the number of coils per phase, *N* the number of windings per pole shoe, ρ_{copper} the specific resistance of copper, *w* and *l* are approximately the width and length of the contour of the centre of the wire bundle around the pole shoe and A_{copper} is the surface of the cross-section of the copper wire.

The inductance and copper resistance determine the electrical time constant for the current through the motor.

$$\tau_i = L/R \qquad \text{[s] (19)}$$

2.4.3 Torque versus speed

As stated in paragraph 2.2 an important characteristic specifying the gyrator ratio of a motor is the motor constant K_m. As we know K_m is not a constant but depends on the motor angle. However when taking all three phases into account and assuming a perfect sinusoidal motor constant and current, the motor constant can be seen as if it were a real constant. Under these assumptions K_m is the constant factor which relates the effort of the electric port with the flow of the mechanical port, and the effort of the mechanical port with the flow of the electric port. In other words it relates the current through the coils with the generated torque due to this current and it relates the rotational speed with the induction voltage.

$$\begin{bmatrix} T_m \\ u_e \end{bmatrix} = K_m \cdot \begin{bmatrix} i \\ \omega \end{bmatrix} \qquad (20)$$

Looking at the static case where L can be neglected the voltage relation of the motor of figure 2 can be written as

$$u_{in} = \frac{R}{K_m} T + K_m \cdot \omega \qquad \text{[V] (21)}$$

where $K_m \cdot \omega$ is called the back-EMF.

To illustrate the interaction between torque, speed, voltage and current a simple three phase motor is simulated for a given maximum supply voltage using three versions of figure 2 with sinusoid motor constant in parallel fixed to one inertia. Parameters are: R=0.433Ω, L=1.2mH, K_{max}=1.36Vs/rad and J=1.8kgm^2.

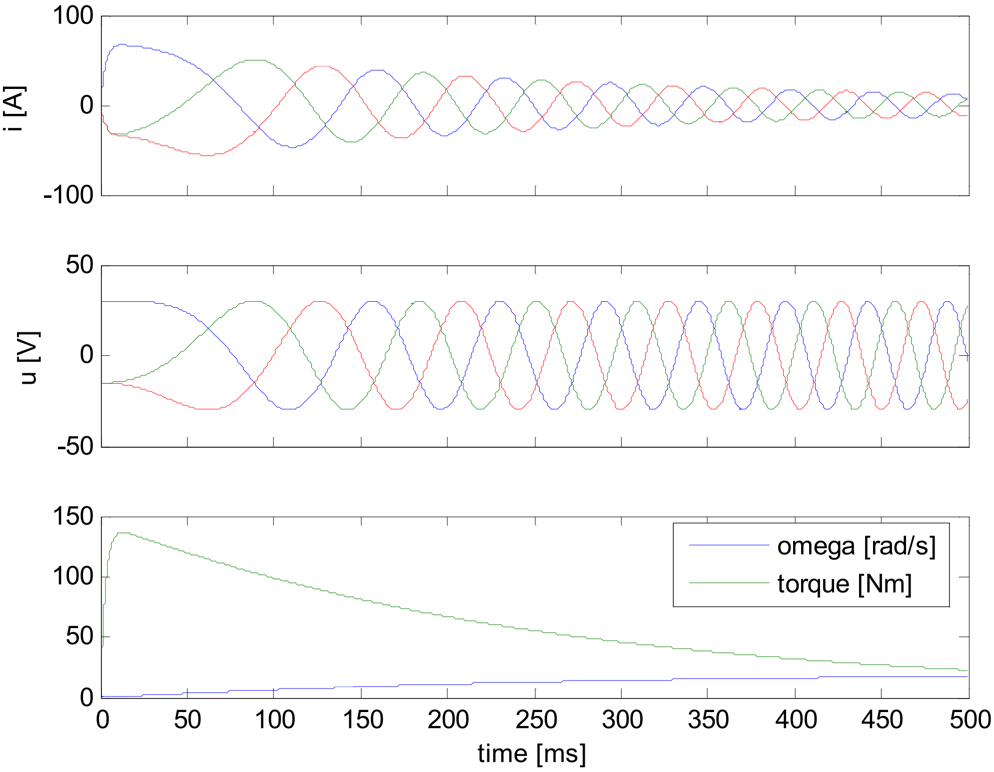

figure 4 supply current & voltage and motor speed & torque of a three phase motor

Equation (21) can be rewritten into an equation expressing the torque as a function of voltage and angular velocity.

$$T = \frac{K_m}{R}\left(u_{in} - K_m \cdot \omega\right) \qquad \text{[Nm] (22)}$$

This relation is depicted in a torque versus angular velocity graph in figure 5.

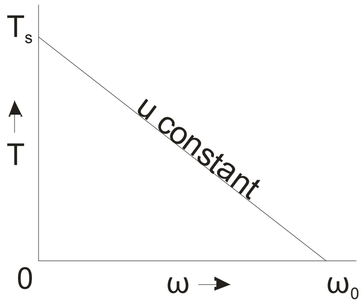

figure 5 torque versus angular velocity

The plot immediately shows a maximum torque (stall torque) and maximum angular velocity (no-load speed) for a certain voltage:

$$T_s = K_m \frac{u_{in}}{R} \qquad \text{[Nm] (23)}$$

$$\omega_0 = \frac{u_{in}}{K_m} \qquad \text{[rad/s] (24)}$$

Both are proportional to the voltage. This implies that the available voltage is an important restriction to the achievable maximum torque and speed.

At full supply voltage an expression for the maximum current through the windings follows from (23) by dividing it through K_m. No supply voltage is used by the back-EMF because the speed is zero.

$$i_{stall} = \frac{u_{in}}{R} \qquad \text{[A] (25)}$$

At this maximum current the motor will likely saturate. Note that the maximum torque then decreases and (23) does not hold anymore. Proper design can reduce saturation and minimize the torque drop at high currents.

The motor constant is approximately quadratic related to the windings resistance. This can easily be reasoned. Doubling the number of windings while keeping the same motor dimensions results in a doubled motor constant but a quadrupled resistance: twice the copper length and half the copper surface per winding.

$$K_m^2 \sim R \qquad (26)$$

This is also the reason why the motor constant is not a good figure to determine the quality of a motor. Only changing the number of windings, while keeping the rest of the design the same, can easily change the motor constant. A better judgement can be done using the steepness.

2.4.4 Steepness

The steepness of an electric motor is the steepness of the graph in figure 5, which is defined as

$$S = \frac{T_s}{\omega_0} \qquad \text{[Nm.s/rad] (27)}$$

It is a good measure to compare motors, because it is independent on the supply voltage, contains explicitly the maximum torque and speed. The steepness is also insensitive to design changes which influence both K_m and R as described above in (26):

$$S = \frac{T_s}{\omega_0} = \frac{K_m \cdot i}{\frac{u_{in}}{K_m}} = \frac{K_m \frac{u_{in}}{R}}{\frac{u_{in}}{K_m}} = \frac{K_m{}^2}{R} \qquad \text{[Nm.s/rad] (28)}$$

Moreover it takes both torque and dissipation into account, which gives motor specific information about the efficiency of producing torque:

$$S = \frac{{K_m}^2}{R} = \frac{i^2}{i^2}\frac{{K_m}^2}{R} = \frac{T^2}{P_{diss}} \qquad \text{[Nm.s/rad] (29)}$$

A higher steepness means a higher torque while keeping the same dissipation or a lower dissipation while keeping the same torque. The only design parameters S depends on are K_m and R, which can be influenced and are independent of the working torque. According to (26) the steepness is also independent of the copper windings diameter, but on the combination of available copper slot space and number of windings instead.

2.4.5 Efficiency

Besides a high steepness also efficiency is important to take into account. Suppose a motor is running at a certain speed and producing certain torque. Referring to (20) the current needed from the power supply is

$$i = \frac{T}{K_m} \qquad \text{[A] (30)}$$

The supply voltage and maximum speed are related by

$$u_{in} = K_m \cdot \omega_0 \qquad \text{[V] (31)}$$

From its definition it follows that the efficiency of an electric motor depends only on the speed at which the motor is running.

$$\eta = \frac{P_{out}}{P_{in}} = \frac{T \cdot \omega}{u_{in} \cdot i} = \frac{T \cdot \omega}{K_m \cdot \omega_0 \cdot \dfrac{T}{K_m}} = \frac{\omega}{\omega_0} \qquad \text{[-] (32)}$$

So it is smart to design the motor such that it runs almost at maximum speed most of the time. Together with a specified required torque at that speed a desired steepness can be calculated. Knowing the available supply voltage the motor constant can be calculated using (31). The winding resistance follows from the desired steepness and the calculated motor constant (27).

2.4.6 Power electronics

Without getting into details about the electronic supply circuits the maximum torque with a three phase system depend on the input voltage according to:

$$\begin{aligned} T_{\max} &= K_{\max} i_{\max}\left(\sin^2(\varphi) + \sin^2\left(\varphi + \frac{2\pi}{3}\right) + \sin^2\left(\varphi - \frac{2\pi}{3}\right)\right) \\ &= \frac{3}{2}K_{\max} i_{\max} = \frac{3}{2}\frac{K_{\max} \cdot u_{in}}{R} \end{aligned} \qquad \text{[Nm] (33)}$$

assuming a perfect sinusoidal motor constant and current.

Since the three phases are used in parallel the maximum speed still depends on the input voltage according to (24).

When a DC supply u_{dc} is used the maximum torque and speed depend on the used supply electronics. In case of one H-bridge per phase u_{in} equals u_{dc}. Here u_{in} is the amplitude of the AC supply voltage. In case of a bridge circuit with three delta connected branches u_{in} equals $\frac{1}{2}\sqrt{3}\cdot u_{dc}$. A bridge circuit with three wye connected branches results in a phase supply voltage u_{in} equal to $\frac{1}{2}u_{dc}$.

2.5 Permanent magnets

Advantages of the use of permanent magnets on the rotor instead of coils are:

- No copper losses as a result of current through coils
- No windings and copper wires are needed on the rotating part of the machine
- Small volume

Besides these advantages permanent magnets have been used more often because strong rare-earth magnets have become cheaper.

The choice of the magnets is very important since they influence the overall performance of the motor very much. They function as sources of magnetic motive force creating a magnetic field over the air gap, repelling the magnetic field created by the coils.

In principle the magnets should

- have high remanence (Br) to gain high magnetic motive forces,
- have high coercivity (Hc) to avoid demagnetisation when reverse field is applied,
- be not susceptible for high temperatures
- have a low mass
- be cheap.

Between these requirements a trade-off has to be found when choosing the right magnetic material.

Permanent magnets demagnetise when they become too hot (δBr/°C) or when a strong reverse field is applied. The latter occurs when stall current is supplied to the permanent magnet motor. When temperature rises the remanence decreases and coercivity changes in positive or negative direction depending on the type of material.

Following table shows relevant magnetic properties of the ferromagnetic materials Barium ferrite (ferroxdure), Aluminium-Nickel-Cobalt (AlNiCo), rare earth material Samarium-Cobalt (SmCo) and bonded rare earth material Neodymium-Iron-Boron (NdFeB).

Material	Br (T)	Hc (kA/m)	δBr/°C	δHc/°C	ρ (Ωm)	Tc (°C)	cost price (euro)
Ferroxdure	<0.4	250	-0.2%	0.34%	1,0E+06	450	5
Alnico	1.3	130	-0.02%	0.01%	5,0E-07	850	?
SmCo	1	700	-0.05%	-0.3%	5,0E-07	750	>200
NdFeB	1.4	1000	-0.2%	-0.3%	1,4E-06	300	<100

2.6 Saturation and hysteresis

The relation between H and B in iron is a combination of storage and friction effects. The resistive part of the magnetization curve is the hysteresis effect, related to the existence of magnetic domains in the material. Once the magnetic domains are reoriented, it takes some energy to turn the poles. This effect is also called magnetic memory. The inner surface of the contour in the B-H graph of figure 6 is the energy dissipated into the material due to this friction.

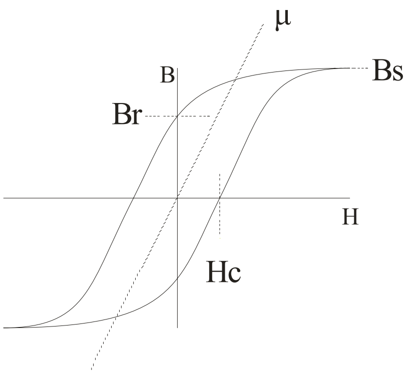

figure 6 hysteresis curve

The storage effect is the fact that flux is stored in the material having a limited storage capacity. Therefore B starts saturating when it approaches its saturation value (B_s). When B is saturated increasing H will not lead to a considerable increase of B. When the flux through iron gets high effectively the permeability of the iron starts to decrease. In [3] a relation between B and H in the magnetic material of a linear motor has been measured. This B-H curve is shown in figure 7 and can be approximated by a function also depicted.

$$\left\{\begin{matrix} H = 150B + 15B^{11} \\ H = \frac{1}{\mu}B \end{matrix}\right\} \leftrightarrow \mu = \frac{1}{150 + 15B^{10}} \qquad (34)$$

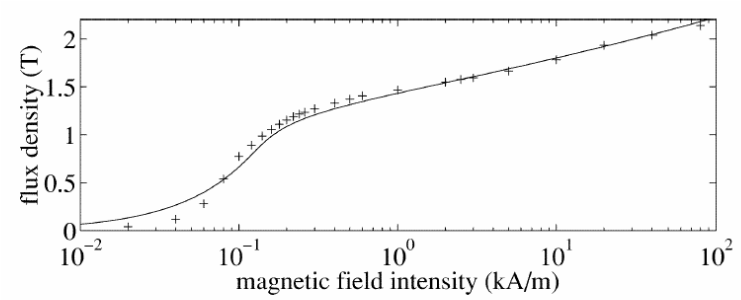

figure 7 measured (+) BH-curve and approximation function of the magnetic material in a linear motor

In chapter 3 this nonlinear relation will be used for taking the saturation into account.

2.7 Thermal domain

Besides a good electromagnetic transduction dissipation is a very important issue in an electric motor. Especially the insulation material and the permanent magnets should not become too hot, because melting insulation can cause fatal short circuit and too hot magnets become demagnetised. In 3.3 a model is made to monitor the thermal behaviour within the motor.

2.7.1 Losses

At several places in the transduction process energy is lost and transformed into heat. Most losses are copper losses in the windings according to Ohms law. Using (27) this is

$$P_{diss,copper} = \frac{T^2}{S} \qquad [W]\ (35)$$

Note that the copper dissipation is proportional to the square of the delivered torque and is independent of the diameter of the copper windings: the only design dependent quantity in (35) is the steepness, which is independent on the windings diameter according to paragraph 2.4.4.

Secondly hysteresis of the magnetic flux in the iron of the magnetic circuit warms up the iron. Its size depends on the amplitude and frequency of the flux and on material properties. (reference 14, page G3/3)

$$P_{hyst} = m_i \cdot \sigma_h \cdot f \cdot B^m \qquad \text{[W] (36)}$$

with iron mass m_i, material constant σ_h (≈0.01 for iron), frequency f, magnetic flux density B and Steinmetz exponent m, which is 1.6 for iron and 2.5 for ferrite 3C8.

Another loss is due to Eddy currents in the iron, which are currents in the iron trying to counter act the current creating the flux in the first place. Eddy current loss depends quadratically on the frequency f, lamella thickness h and flux density B. (reference 14, page G3/4)

$$P_{eddy} = m_i \cdot \sigma_w \cdot \left(h \cdot f \cdot B\right)^2 \qquad \text{[W] (37)}$$

where σ_w is a material constant of about 0.002 for iron.
Another dissipation effect is the Skin effect due to increased copper resistance for thick windings and high frequencies. Compared to the copper losses the hysteresis and eddy currents play an important role, especially at higher frequencies.

2.7.2 Cooling

The copper windings in the motor are the most important source of heat. This heat has to be carried away to the outer environment by means of conduction, air cooling and, in case of a heavy motor, by means of water cooling. Conduction occurs via the construction the motor is mounted to.

The way thermal heat flows through the motor depends on the thermal resistance properties of the construction (reference 12, page D25). Thermal resistance gives the relation between temperature differences and resulting heat flow $\dot{Q}$. Three types of thermal resistance are responsible for the heat flow in the motor:

1. conduction by the material, given by

$$\dot{Q} = \lambda A \frac{T_1 - T_2}{d} = \frac{\Delta T}{R} \qquad \text{[W] (38)}$$

$$R = \frac{d}{\lambda \cdot A} \qquad \text{[W/K] (39)}$$

where d is the distance and A the surface of the path through the material and λ the specific heat conductance coefficient.

2. contact resistance / convection, given by

$$R = \frac{1}{k \cdot A} \qquad \text{[W/K] (40)}$$

where k is the heat transition coefficient.

3. radiation, according Stefan Boltzmann's law of black radiators

$$\dot{Q}_{12} = \sigma \cdot A \cdot \left(T_1^4 - T_2^4\right) \qquad \text{[W] (41)}$$

where σ is the radiation coefficient of $5.67 \cdot 10^{-8}$ [W/m^{2}K^4].
Radiation is not written as a thermal resistance, because there is no linear relation between the temperature difference and the resulting flow.

Heat is temporarily stored by heat capacities. Capacity depends on the specific heat ρ and the mass m of the material.

$$C = \rho \cdot m \qquad \text{[J/K] (42)}$$

The thermal time constant of the motor equals

$$\tau_{th} = R_{therm,tot} C_{therm,tot} \qquad \text{[s] (43)}$$

In 3.3 an electric equivalent model is made to monitor the thermal behaviour using the elements above.

2.8 Matching application and motor

How to decide whether a motor design is good? What are desired properties of a motor? How to transform specifications in terms of application parameters into design parameters of a motor? This paragraph tries to answer these questions.

2.8.1 Design strategy

The application determines the requirements of the motor. Before getting into design details one should clearly define the requirements, restrictions and optimization criteria.

Requirements

1. maximum speed
2. maximum torque
3. minimum angular accuracy
4. minimum duty cycle
5. maximum cogging force
6. minimum shock stability
7. minimum lifetime

Restrictions or limitations

1. maximum supply voltage
2. maximum supply current
3. maximum dimensions and mass

Optimization criteria

1. minimize losses
2. minimize costs

Firstly the required speed and restricted supply voltage determine the maximum required mean value of the motor constant. The required maximum torque and restricted maximum supply current determine the minimum mean value of the motor constant. The combination of required maximum speed and torque determine the required steepness. The actual desired value of the motor constant should be chosen in combination with the windings resistance such that this required steepness is achieved according relation (27).

Once the size of the required motor constant and windings resistance are known an appropriate size of the motor can be chosen, which is restricted by the specified maximum dimensions and mass. Whereas requirement 1 determined the size of the motor constant, the other requirements influence the shape of it. These requirements influence the completion of the construction design. Minimizing the losses is therefore also a matter of choosing the right construction design at detailed level.

In following paragraph the design strategy will be illustrated using an example motor design.

2.8.2 Calculating required motor constant and winding resistance

Suppose we have an application where a maximum torque of 1 kNm and a maximum speed of 10 rps are required. According to (27) the motor design should have a steepness of

$$S = \frac{T_s}{\omega_0} = \frac{10^3}{10 \cdot 2\pi} \approx 15.92 \qquad \text{[Nms/rad] (44)}$$

Having a supply voltage of 360V according to (24) we get a required motor constant of

$$K_{\max} = \frac{u_{in}}{\omega_0} = \frac{360}{10 \cdot 2\pi} \approx 5.73 \qquad \text{[Vs/rad] (45)}$$

and the maximum winding resistance can be calculated from (44) and (27)

$$R = \frac{{K_{\max}}^2}{S} \approx 2.06 \qquad [\Omega] \text{ (46)}$$

A simple simulation of a motor with load shows that with this motor constant and windings resistance the required speed and torque are met.

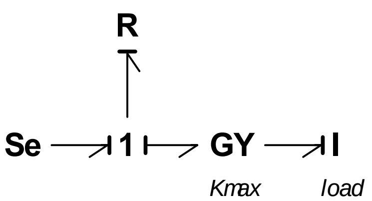

figure 8 bond graph model of figure 2

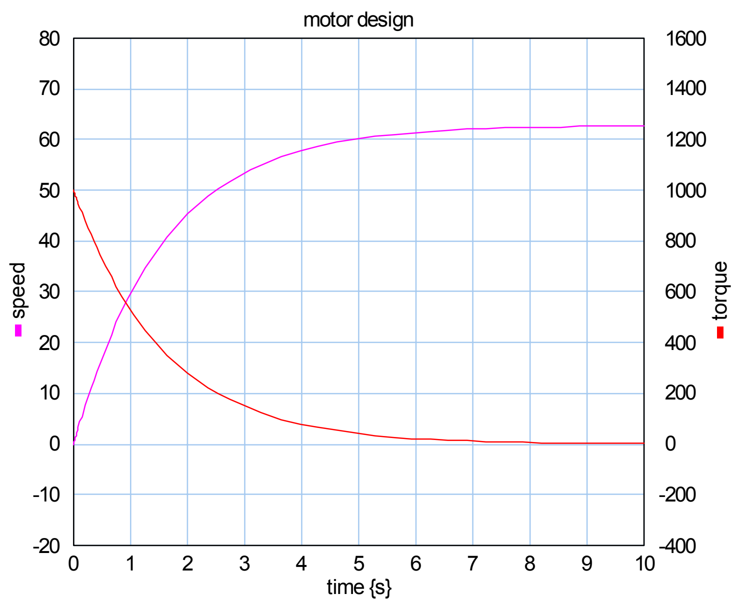

figure 9 results using the calculated values

In the bond graph of figure 8 for convenience the phases are added and discounted in the parameter values.

In practice one could specify a certain required torque at certain speed. This constraints the maximum required torque-velocity combination in the torque-velocity graph of figure 5, but not the steepness. When the desired efficiency at that working point is also given, the required steepness can be calculated.

2.8.3 Construction design

Once the sizes of the motor constant and winding resistance are defined the construction design can start. Goal is to minimize the losses while achieving the required motor constant, minimize the windings resistance and fulfilling the other requirements as good as possible.

Following design aspects help making the first choices.

2.8.3.1 Motor dimensions

To gain the high required torque the magnets and airgap should be placed at maximum allowed diameter. The steepness is approximately proportional to the length of the motor. To gain the maximum steepness the length should be chosen equal to the maximum (restricted) value.

The smaller the airgap the higher the steepness, because the motor constant increases when the reluctance of the magnetic flux path decreases. But when the airgap is chosen too small the chance increases that rotor and stator hit each other and the motor gets damaged. For a shockproof application this is limited by the shock stability requirement. In the end magnetic saturation in the iron yoke limits the advantage of decreasing the air gap height.

2.8.3.2 Magnetic circuit

The magnetic circuit of the motor should be designed such that a maximum flux flows through the air gap. This implies a trade-off between very large windings empowered by large currents versus a low reluctance due to large iron volumes in the flux path. In the design of the magnetic flux path one should take care of locations where saturation takes place and the lamella thickness to reduce eddy currents. Places where the flux variation is smaller can have less or no lamellas to reduce costs. In case of a permanent magnet motor this holds for the rotor, because the phase fluxes approximately add up to zero. This implies that a permanent magnet motor is very easy to implement in a design: just place magnets on the inner surface of a construction to let it function as rotor.

A motor for higher speeds should have a low number of poles, because the higher number of poles, the higher the frequency of the current through the coils, the higher the hysteresis losses and eddy currents. On the other hand a motor for lower speeds should have many poles, because when the poles are positioned close to each other less iron is needed to maintain the same reluctance.

The maximum winding resistance limits the amount of copper windings and the thickness of the wires. At the same time the total amount of copper is limited by the space available in the slots. The lower the copper resistance the less losses and the higher the achievable maximum torque.

2.8.3.3 Thermal house holding

The more copper and iron the higher the thermal time constants and the higher the peak torque. The continuous torque depends on the thermal resistance, which is higher when the outer surfaces of rotor and stator are higher and enough fresh air can flow along these surfaces. Water cooling drastically decreases the thermal resistance at the expense of winding space.

3 SYNTHESIS

In this thesis work two models are designed for usage when designing or reviewing a brushless direct drive permanent magnet motor. In this chapter these models will be described and in following chapters they will be validated and their application will be shown.

3.1 Introduction

An electromagnetic parametric model is made to calculate the electromechanical transduction performance of the motor. The model calculates following specifications:

- motor constant,
- steepness,
- losses,
- amount and location of saturation and
- induction and resistance of the motor.

As described in paragraph 2.4 these parameters characterise the motor and give a performance measure of the designed or reviewed motor.

Besides calculating these typical values the model can also optimize a design by varying certain design parameters. Following design parameters can be varied and/or optimized for:

- diameter and length of the motor
- permanent magnets
    - number of pole pairs
    - material
    - height and width
- teeth configuration (pole shoes)
    - number of pole shoes
    - height and width
    - slot size
    - copper wire diameter and number of turns
    - torsion angle
- airgap height

Second model is a thermal model to keep track on the dissipation and heat removal within the motor. This model uses the same design parameters as input and generates following thermal specifications:

- thermal resistance and capacity → time constant
- total thermal resistance (cooling capacity)
- location and amount of heat flow within the motor
- temperature at the copper hotspot, stator and rotor

Later on these models will be described and validated. Afterwards the application is shown such that simulations can be used in order to make design choices for a certain application. First the electromagnetic model will be described in next paragraph.

3.2 Parametric electromagnetic model

This model is the main part of this thesis. As described in paragraph 2.2 the flux in the motor as a function of the rotor angle is the key for calculating the motor constant and reluctance torque. Also the resistance and inductance are important characteristics of a motor. The parametric electromagnetic model is an algebraic model representing the magnetic circuit of a motor. It calculates the flux in the motor at several hotspots as a function of the rotor angle and the inductance follows from the equivalent circuit as well.

3.2.1 Principle

One way to calculate the magnetic flux and inductance is writing out all sets of integral equations along possible flux paths and calculating the unique solution satisfying all sets of equations following from Maxwell's equations (63). Disadvantage of writing out the equations is its restricted generalization. E.g. when changing the number of pole shoes or rotor p.m. poles the number of equations could change. To retain generalization and provide insight in the model the magnetic circuit of the motor is captured in an equivalent circuit (paragraph 2.3).

All magnetic relevant parts of the motor correspond to a branch in the circuit. Most relevant parts of a permanent magnet motor for the electromagnetic domain are:

- the airgap where most of the electromechanical transduction takes place,
- the pole shoe where the magnetic energy is interchanged and where saturation occurs first,
- permanent magnets at the rotor, also interchanging magnetic energy,
- the airgap between pole shoes which enables flux leakage,
- the yoke for estimating the measure of saturation and losses.

These are important to take into account when modelling the motor using an equivalent circuit.

As an example we take figure 10, which represents a part of a permanent magnet motor with two magnet poles and two pole shoes. Both stator and rotor are fixed for the time being.

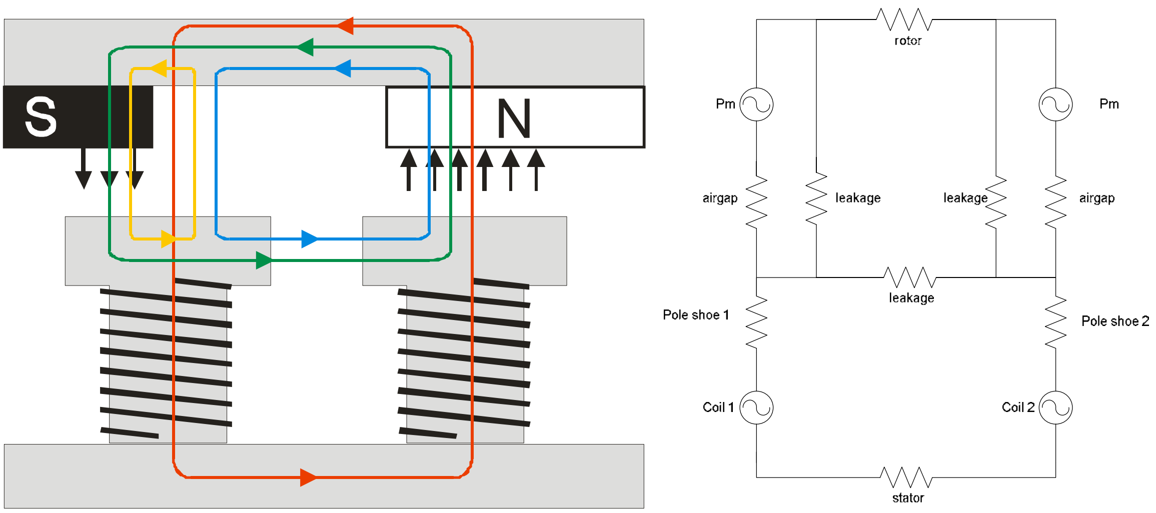

figure 10 illustrating possible flux paths across the airgap (left) and a possible equivalent circuit (right)

To keep a usable model we discern a limited amount of different flux paths in this circuit as will be explained in next paragraph. The paths show all possible branches of the equivalent circuit. Each branch has its specific reluctance and magneto motive source in case of a coil or magnet.
Two lower branches can be discerned: one per phase representing the pole shoe with coil.
Four upper branches can be discerned: two per phase, one through magnets and the other through air.
In this example the rotor, stator and pole shoes are represented as iron reluctances. The airgap between stator and rotor and the air leakage between both pole shoes are modelled as air reluctances. The permanent magnets and coils are magneto motive force sources.

Now we let the rotor move along the stator. The permanent magnets are not phase dependent anymore but move along the pole shoes as the rotor rotates. To capture this rotor movement and to obtain certain generalization for later usage the magnets are modelled as two sources per pole shoe, one representing the north poled magnets and one the south poled magnets. Per separate pole shoe these sources represent the overlap of both magnet poles with that particular pole shoe as a function of the rotor angle. Also the reluctances are modelled per pole shoe separately. As a result we get the same four upper branches as in figure 10 per separate pole shoe, of which all elements vary with the rotor angle. Besides in case of a rotational motor the left and right pole shoe are connected to each other again closing the loop. Assuming that the rotor yoke is thick compared to the pole shoes and knowing that the sum of all phases is zero we can assume that the rotor yoke has zero reluctance and can therefore be neglected. This assumption simplifies the algebraic equations. The resulting equivalent circuit of a rotational permanent magnet motor with two pole shoes and two magnet poles is drawn in figure 11.

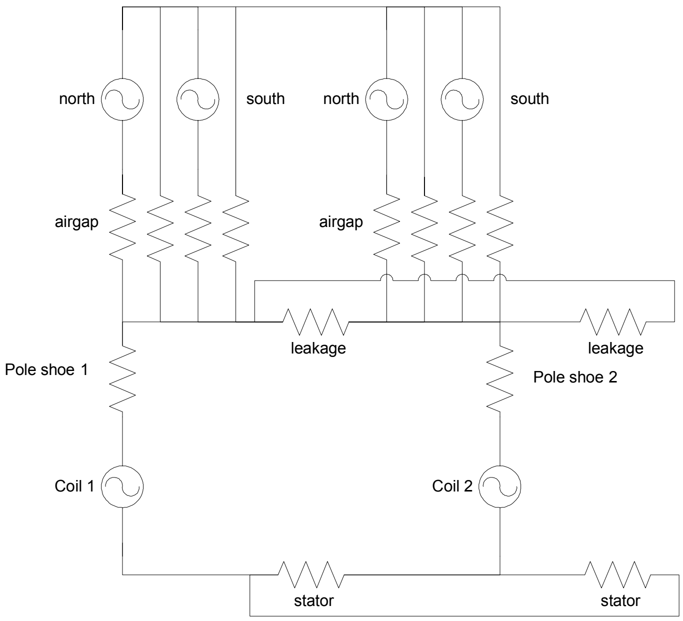

figure 11 equivalent circuit of rotational two phase motor with two magnet poles

If the motor has more than one pole shoe per phase the total motor can be seen as a parallel combination of circuits like figure 11. The circuit can therefore also be seen as a representation of the phases. Since the rotor angle dependent elements in the upper branches vary nonlinearly with the rotor angle, it is not (necessarily) possible to add the parallel upper branches.

The idea behind this model is that the flux in the motor can now be calculated as a function of the rotor angle just by solving the algebraic equations of figure 11 for each rotor angle. Before showing the implementation of the model in Matlab the assumptions and choices are described.

3.2.2 Assumptions and choices

When modelling the magnetic fields and fluxes some assumptions and simplifications had to be made to keep a compact model giving insight and to avoid unnecessary complexity.

Following assumptions are made:

1. Flux crosses the airgap between **rotor and stator** only in a straight line between pole shoe and rotor perpendicular to the airgap.
   In practice flux will somewhat spread out at the boundary of the conducting material. Because the air gap is very small relative to the width of the pole shoe this assumption results only in a very small error and makes the model a lot easier.

2. Flux crosses the airgap between **two teeth (pole shoes)** only in a straight line between the head of the pole shoe where the distance is closest and the coil has ended.
   This assumption is equal to the previous, but for the horizontal flux between two pole shoes.

The flux is assumed to flow in a straight line, but in practice the flux will spread out. For the calculation of the flux leakage between two pole shoes it does not matter where the flux exactly flows. Therefore this assumption can be made without loosing relevant information.

3. Induction takes place linearly along the length of the coil.
   This assumption can be made because the length of the coil is large compared to the diameter.

4. Magnets are fully homogeneously magnetised.
   Although the magnetisation of magnets can vary as a function of the position at the magnet, this is assumed to be constant to simplify the modelling. This assumption should not have influence on the mean value of the calculation results.

5. The permanent magnet motor can be modelled as a linear motor.
   Because the diameters of rotor and stator are large enough this assumption can be made without noticeable loss of accuracy.

We have chosen a three-phase system, because of its standardization and because it is the cheapest multiple phase solution, which gives the well-known advantages like a zero ground (less wires and conductor losses) and a constant transferred power and thus torque.

In literature several types of modelling are used to represent the electromagnetic behaviour of a permanent magnet motor. In [4] and [7] an analytical approach using the vector potential is used to calculate the field due to the current distribution in the airgap. In [5], [6] and [9] magnetic circuit models with magneto-motive force sources are used. [8] uses a power capability analysis and finite element method.

In this thesis work a magnetic circuit model is used, because of its expandability and generality for different configurations. Furthermore the shape of the circuit visually facilitates understanding of the system and its opportunities and bottlenecks. Besides the fact that finite element software was not available it might not have given as much conceptual insight as the circuit has. The drawback of the analytic method is its lower level of insight and lower expandability.

3.2.3 Implementation

We derived a generalized magnetic equivalent circuit representing a three phase permanent magnet motor with two magnet poles like we did in paragraph 3.2.1. In figure 12 the equivalent circuit is schematically drawn. Note that this is just a drawing and not the model used for the calculations. Each phase consists of the elements as described in paragraph 3.2.1. The diagonal line in the reluctances of the pole shoes indicate that these are nonlinear because saturation (paragraph 3.2.9) is taken into account.

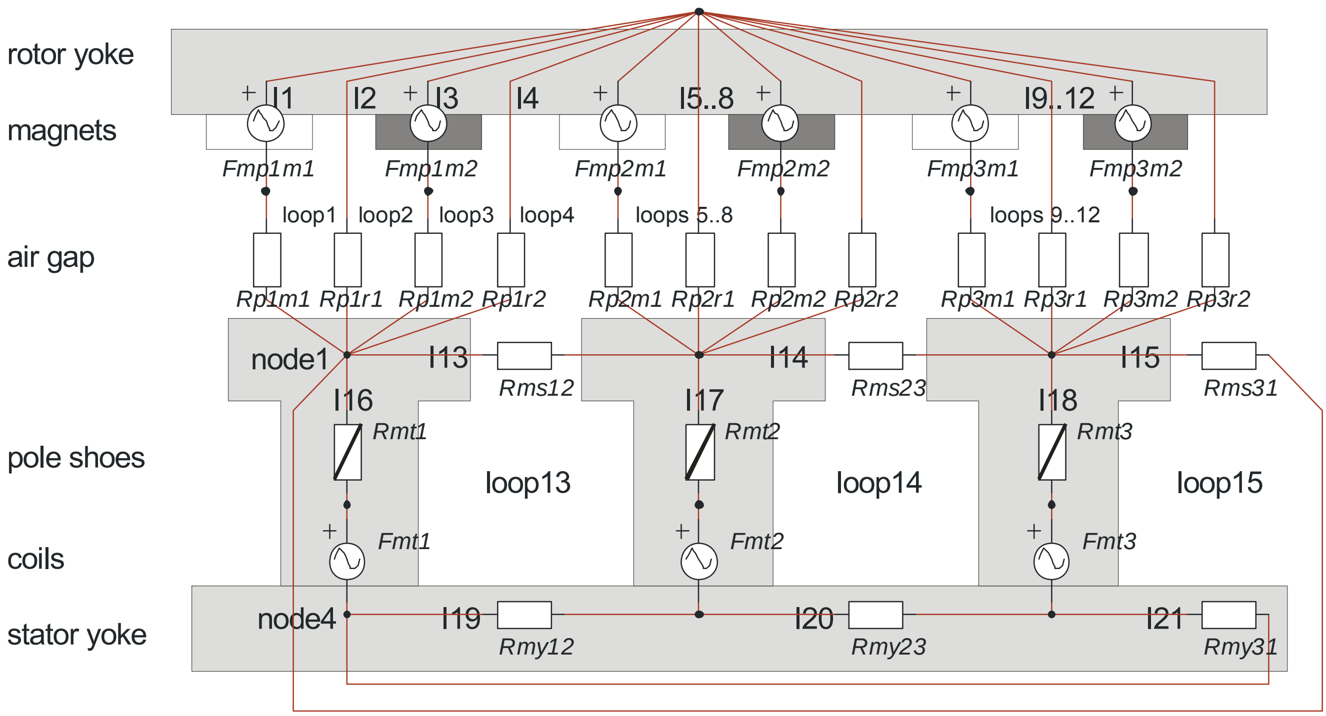

figure 12 magnetic equivalent circuit (3 phases, 3 slots, 2 magnet poles, 1 slot per coil)

The most right part of the circuit is connected to the left part because of the rotary shape of the motor. Since the radius of the motor is assumed to be large compared to the dimensions of the pole shoes, permanent magnets and the airgap we simplify rotations by translations as $x \cong r \cdot \varphi$, where r is the radius of the motor (from the centre to airgap).

Per phase k=1..3 we discern two types of components:

<u>magnetic reluctances</u>

R_{pkm1}	airgap between pole shoes of phase k and magnet 1
R_{pkr1}	airgap between pole shoes of phase k and border 1 (gap between magnets 1 and 2)
R_{pkm2}	airgap between pole shoes of phase k and magnet 2
R_{pkr2}	airgap between pole shoes of phase k and border 2
$R_{msk,k+1}$	air (leakage) between two phases
R_{mtk}	phase k
$R_{myk,k+1}$	yoke between two phases

<u>magneto motive forces</u>

F_{mpkm1} due to all permanent magnets N located above phase k
F_{mpkm2} due to all permanent magnets S located above phase k
F_{mtk} due to all coils of phase k

When all these component values are known as a function of the rotor angle the algebraic equations can be solved. Then we know the flux in the motor as a function of the rotor angle and the inductance of the magnetic circuit. The component values are determined by the constructional design parameters and will be calculated in next paragraph.

3.2.4 Calculation of the component values

This paragraph describes the calculation of the circuit's component values from the construction design parameters.

For later usage we will number the components of the circuit from figure 12 as follows:

$$
\begin{aligned}
&R_{p1m1} \,..\, R_{p3r2}\text{:} \quad \text{No.} \quad 1-12\\
&R_{ms12} \,..\, R_{ms31}\text{:} \quad \text{No.} \quad 13-15\\
&R_{mt1} \,..\, R_{mt3}\text{:} \quad \text{No.} \quad 16-18\\
&R_{my12} \,..\, R_{my31}\text{:} \quad \text{No.} \quad 19-21
\end{aligned}
\tag{47}
$$

According to equation (10) the reluctance can be calculated from the cross-sectional surface, length and permeability of the path. These will now be calculated as a function of the rotor angle.

First the overlapping surfaces of the rotor and stator near the airgap will be calculated. Let $A_{stator}(x_s)$ define the length of the top of the pole shoes that touch the airgap as a function of the position in stator frame for each phase

$$A_{stator}(x_s) = \begin{bmatrix} A_{p1} & A_{p2} & A_{p3} \end{bmatrix} \qquad \text{dimension: 3 phases by n location steps}$$

and let $A_{rotor}(x_r)$ define the length of the four rotor elements given in rotor frame

$$A_{rotor}(x_r) = \begin{bmatrix} A_{m1} & A_{r1} & A_{m2} & A_{r2} \end{bmatrix} \quad \text{dimension: 4 rotor elements by n location steps}$$

These rotor elements are respectively all permanent magnets of pole 1 (e.g. north), borders 1 (space between magnets north and south), permanent magnets 2 (e.g. south) and borders 2 (space between magnets south and north) summed up along the rotor.

We now let the rotor move along the stator and calculate the overlapping surface of stator pole shoes and rotor elements. The rotor position x_r is described relatively to the stator frame. Since we define the rotor to move over the stator this overlapping surface will be a function of x_r. The total overlapping surface $A_{overlap}(x_s, x_r)$ between $A_{stator}(x_s)$ and $A_{rotor}(x_r)$ is calculated by taking the cross-section between $A_{stator}(x_s)$ and $A_{rotor}(x_r)$. For a fixed rotor angle we get for example the cross-sectional surface like in figure 13. We will use motor A (see chapter 4) without torsion angle as an example during this chapter.

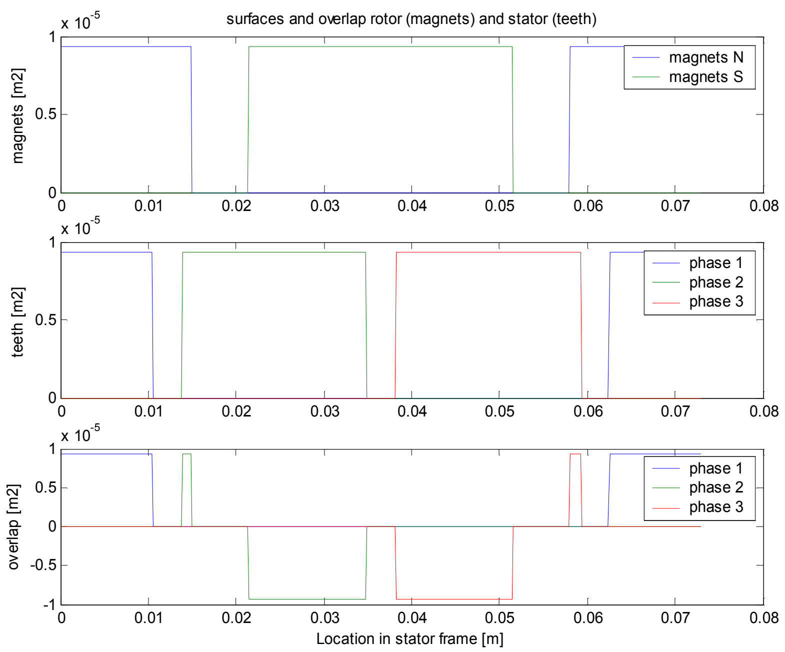

figure 13 overlapping surface between rotor and stator elements near the airgap for fixed rotor

The cross-section is taken at each rotor position x_r. The element wise sum of $A_{overlap}(x_s, x_r)$ over x_s gives $A_{overlap\_sum}(x_r) = \sum_{x_s} A_{overlap}(x_s, x_r)$ which is the total surface between all pole shoes per phase (over the whole stator contour) and a certain rotor element. See figure 14 for the overlapping surface of phase 1 with magnets N and S.

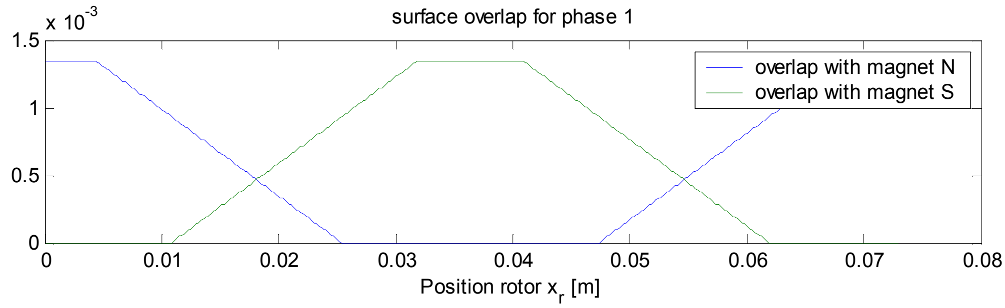

figure 14 surface overlap between rotor magnets and stator teeth (shown for only one phase)

The (rotor position independent) surfaces A_s, A_t and A_y of respectively the stator reluctances R_{ms}, R_{mt}, R_{my} are easily calculated from the physical dimensions of the stator. These surface values are concatenated three times (corresponding to the numbering of the components by (47), once for each phase) to finish with a single surface matrix $A(x_r)$:

$$A(x_r) = \left[A_{p1m1} \quad A_{p1r1} \quad A_{p1m2} \quad A_{p1r2} \quad A_{p2m1} \quad .. \quad A_{p3r2} \quad | \quad A_s^{(3x)} \quad A_t^{(3x)} \quad A_y^{(3x)} \right]$$

Dimension: (12+9) by n.

The physical dimensions of the motor determine the values in this matrix.

In a similar way we define L as the lengths and U as the permeabilities of all path elements that are needed to calculate $R_m(x_r)$. These are independent of x_r and therefore constant; however they depend on the construction design. Now $R_m(x_r)$ follows from equation (10) and gives the reluctances of all elements according to the numbering by (47). For example the reluctances between phase 1 and the four rotor elements are shown in figure 15.

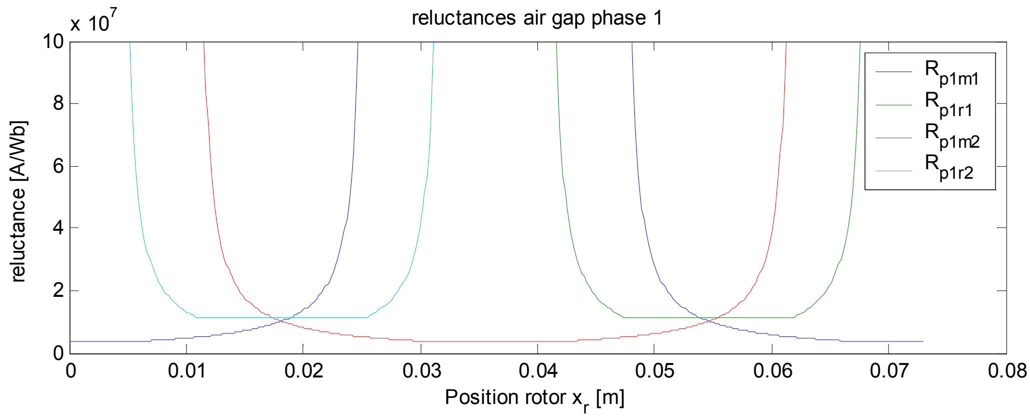

figure 15 air gap reluctances between the first pole shoe and respectively magnet 1, border 1, etc.

Note that these reluctances are defined separately in parallel to describe the rotor movement and the way the magnets insert flux into the several phases. Replacing the four parallel reluctances by one reluctance shows that the effective reluctance is constant. This corresponds to the condition that the reluctance between stator and rotor is independent of the rotor angle and does not vary (see paragraph

2.2). This is an important necessary condition for the derivations of motor constant and reluctance torque in paragraph 2.2.

After having calculated all reluctances within the circuit we now calculate the magneto motive forces. The magneto-motive forces due to the permanent magnets seen by the stator depend also on the rotor position x_r so $F_{m,pm} = F_{m,pm}(x_r)$. Its values follow easily from $A(x_r)$ and (11):

$$F_{m,p1..3m1..2}(x_r) = \frac{B_r \cdot l}{\mu} \cdot sign\left(A_{p1..3m1..2}\right) \text{ [A]} \tag{48}$$

For example the magneto motive forces on phase 1 produced by magnets N and S as a function of the rotor position are shown in figure 16.

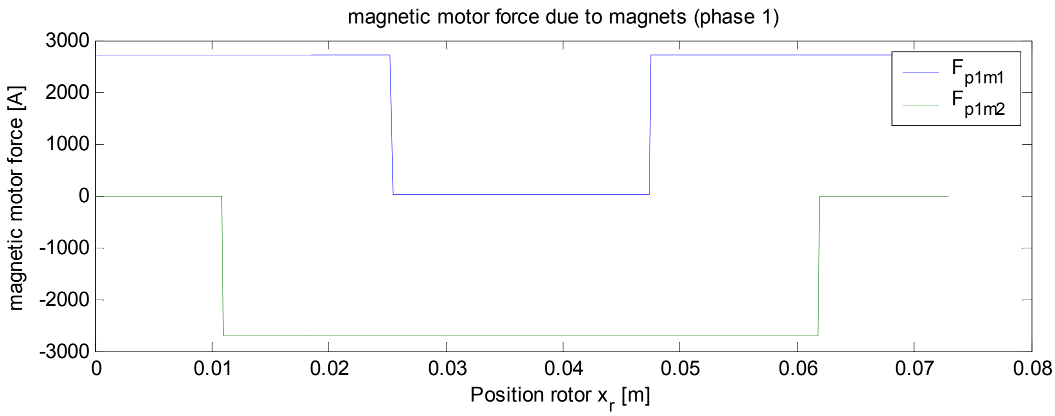

figure 16 magneto-motive force acting on phase 1 due to magnets 1 and 2

The coils are modelled as magneto-motive force sources $F_{mt1..3}$ induced by an user defined AC current (9). As described in paragraph 2.4.1 the current will be chosen as a function of the rotor angle as well, to let it run in phase with the motor constant. Now all ingredients to calculate the flux through the motor are available. In next paragraph this flux will be calculated as a function of the rotor angle.

3.2.5 Flux balance

The circuit of figure 12 has 21 flux paths and therefore 21 unknown fluxes corresponding to the numbering of (47).

$$\Phi = \begin{bmatrix} \Phi_1 & \cdots & \Phi_{21} \end{bmatrix}$$
$$\begin{bmatrix} \Phi_1 \cdots \Phi_{12} \end{bmatrix} = \begin{bmatrix} \Phi_{p1m1} & \Phi_{p1r1} & \Phi_{p1m2} & \cdots & \Phi_{p3r2} \end{bmatrix} \quad \text{[Wb]} \tag{49}$$
$$\begin{bmatrix} \Phi_{13} \cdots \Phi_{21} \end{bmatrix} = \begin{bmatrix} \Phi_{s12} & \Phi_{s23} & \Phi_{s31} & \Phi_{t1} & \Phi_{t2} & \Phi_{t3} & \Phi_{y12} & \Phi_{y23} & \Phi_{y31} \end{bmatrix}$$

For each position of the rotor x_r the flux balance changes and needs to be recalculated. This is done by solving the algebraic equations for each x_r.

Hopkinson's laws are used to set up the flux balance. 4 'force' loops in the airgap, 1 'force' loop in the stator, 1 'flux' node in the top of the pole shoes and 1 'flux' node in the stator yoke can be discerned per phase. In total there are $(4+3)\cdot 3$ algebraic equations for a three phase motor. These are written in matrices. 21 by 21 matrix M contains the reluctances (or multipliers for the fluxes in case of the node equations) and column vector Q contains the magneto-motive forces.

Reluctances of the 12 airgap magnetic force loops:

$$M\left[1:12,1:12\right]=\begin{pmatrix} eq.1 \\ \vdots \\ eq.12 \end{pmatrix}=\begin{bmatrix} -R_{p1m1} & R_{p1r1} & & & & \\ & -R_{p1r1} & R_{p1m2} & & & \\ & & \ddots & \ddots & & \\ & & & & -R_{p3m2} & R_{p3r2} \\ R_{p1m1} & & & & & -R_{p3r2} \end{bmatrix}$$

Reluctances of the 3 stator magnetic force loops:

$$M\left[13:15,13:18\right]=\begin{pmatrix} eq.13 \\ eq.14 \\ eq.15 \end{pmatrix}=\begin{bmatrix} R_{ms} & & & -R_{mt} & R_{mt} & & -R_{my} & & \\ & R_{ms} & & & -R_{mt} & R_{mt} & & -R_{my} & \\ & & R_{ms} & R_{mt} & & -R_{mt} & & & -R_{my} \end{bmatrix}$$

‘Reluctances’ (multipliers) of the 3 top pole shoe flux nodes:

$$M\left[16:18,1:18\right]=\begin{pmatrix} eq.16 \\ eq.17 \\ eq.18 \end{pmatrix}=\begin{bmatrix} 1 & 1 & 1 & 1 & & & & & & & & & -1 & & 1 & -1 & & \\ & & & & 1 & 1 & 1 & 1 & & & & & 1 & -1 & & & -1 & \\ & & & & & & & & 1 & 1 & 1 & 1 & & 1 & -1 & & & -1 \end{bmatrix}$$

‘Reluctances’ (multipliers) of the 3 bottom pole shoe flux nodes:

$$M\left[19:21,16:21\right]=\begin{pmatrix} eq.19 \\ eq.20 \\ eq.21 \end{pmatrix}=\begin{bmatrix} 1 & & & -1 & & 1 \\ & 1 & & 1 & -1 & \\ & & 1 & & 1 & -1 \end{bmatrix} \qquad \text{[A/Wb] (50)}$$

Column vector Q contains the magneto-motive forces of all 21 equations:

$$Q=\begin{pmatrix} eq.1 \\ \vdots \\ eq.21 \end{pmatrix}=\begin{bmatrix} F_{p1m1} \\ -F_{p1m2} \\ \vdots \\ F_{p3m2} \\ -F_{p1m1} \\ F_{mt1}-F_{mt2} \\ F_{mt2}-F_{mt3} \\ F_{mt3}-F_{mt1} \\ 0 \\ \vdots \\ 0 \end{bmatrix} \qquad \text{[A] (51)}$$

After having defined these matrices flux Φ is easily calculated:

$$M\cdot\Phi=Q\leftrightarrow\Phi=M^{-1}\cdot Q \qquad \text{[Wb or Vs] (52)}$$

Since $R_m\left(x_r\right)$ and $F_{m,pm}\left(x_r\right)$ are functions of the rotor position x_r we get the solution of Φ for all rotor positions along the whole stator: $\Phi\left(x_r\right)$. For example figure 17 shows the fluxes of phase 1 of an example motor with zero current.

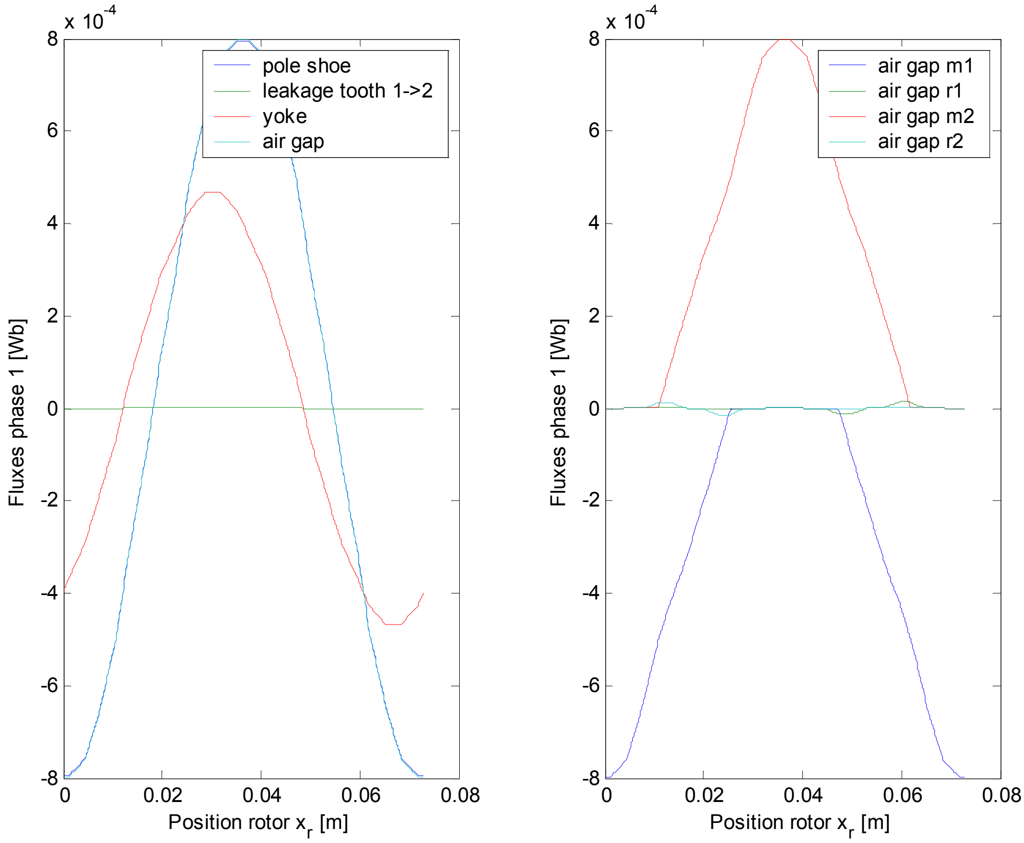

figure 17 fluxes of phase 1 (left) and fluxes of phase 1 passing through the air gap in detail (right)

The left plot shows the size of the flux along all possible paths for one phase. The right plot shows the flux through the airgap in more detail. As can be seen there is only little leakage flux vertically and horizontally crossing the airgap: the flux trough the pole shoe almost equals the flux through the airgap in this specific motor configuration.

$B(x_r)$ is $\Phi(x_r)$ divided by the cross-sectional surface. $H(x_r)$ is equal to $B(x_r)$ except for the scaling factor μ for the linear case. Later on saturation effects will be taken into account. For example the magnetic fields within phase 1 are shown in figure 18.

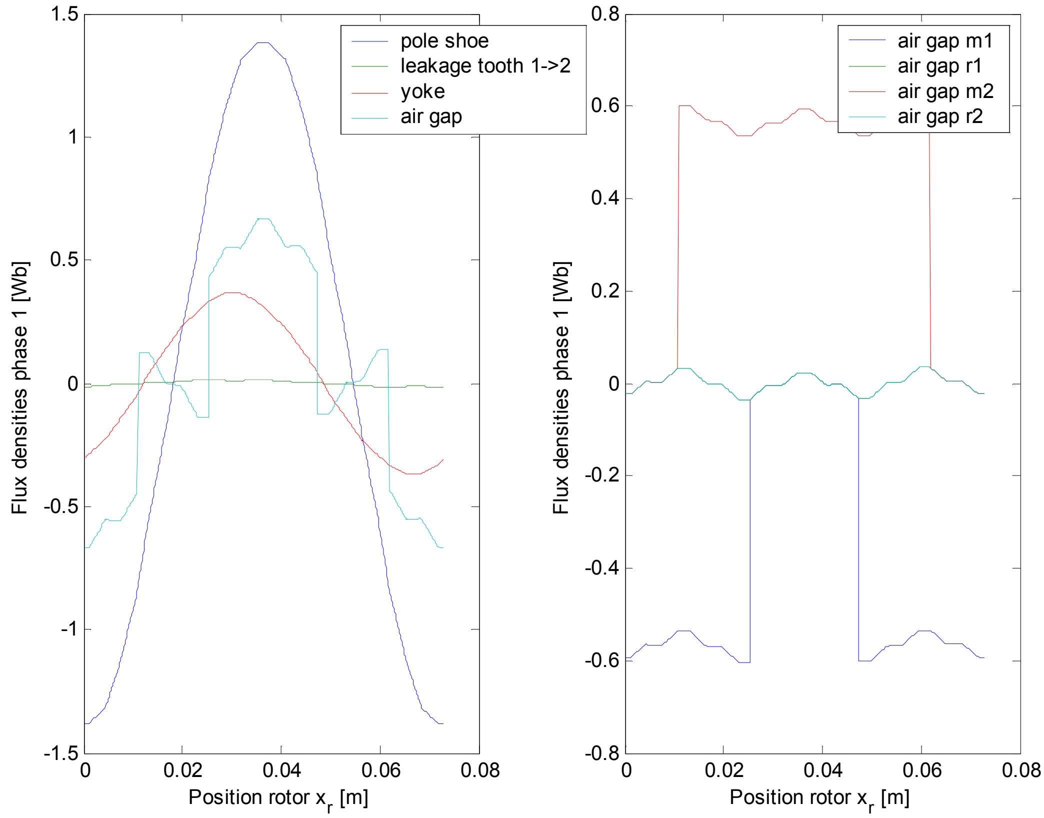

figure 18 magnetic field of phase 1 (left) and magnetic field of phase 1 across the air gap (right)

The rotor angle dependent hysteresis between $H(x_r)$ and $B(x_r)$ is not calculated here, because it would be necessary to remember the states of the flux during calculations, which makes the model too complex. However the amount of hysteresis "friction" is taken into account in paragraph 0.

3.2.6 Model generalization

The reason for the seemingly laborious method using the large matrices of (49), (50) and (51) is, besides the fact that Matlab is very fast in calculating with matrices, the ease to generalize it for other motor configuration with any proportion of phase : teeth : pole.

In practice any motor with a multiple of two magnet poles and three pole shoes can be calculated using the model of figure 12. Let a three phase motor have p pole shoes, n magnet pole pairs and m slots per coil. Before starting calculations these values of p, n and m are divided by their greatest common divisor (gcd) to avoid redundant repetitive calculations and to improve precision with the same number of steps:

$$repeat = \gcd\left(n, \frac{p}{3 \cdot m}\right) \tag{53}$$

After calculations the results are multiplied by this factor to get back the real scale.

The constructed Matlab model is generalized for permanent magnet direct drive motors with three phases having p pole shoes, n magnet pole pairs, and m pole shoes per coil. The number of unknown fluxes and therefore the size of the algebraic matrices is 7p, where 7 is determined by the basic structure of the model: the elements/effects that are taken into account (paragraph 3.2.1). Choosing p=3, n=2 and m=1 we have the circuit from figure 12. For example in figure 19 m=2.

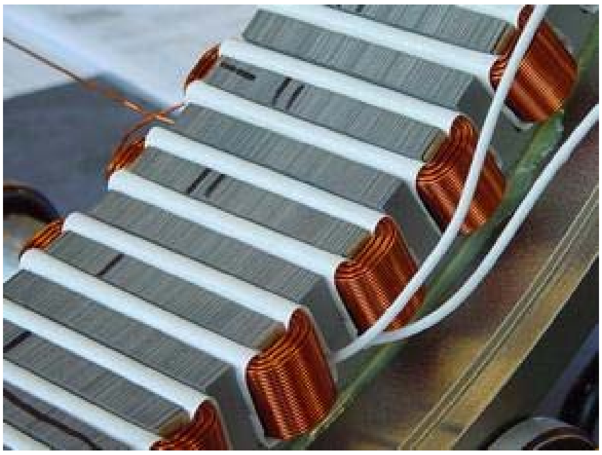

figure 19 permanent magnet motor from ETEL with two pole shoes per coil

Since we now have calculated $\Phi(x_r)$ the motor constant, reluctance torque and inductance can be calculated according to the derivations in paragraph 2.2.

3.2.7 Motor constant

Since K_m is defined as a function of the rotor angle according to (4), we take the derivative of the flux to the angle instead of x_r. This is allowed since the range and number of steps of x_r and φ are the same.

Afterwards Km is multiplied with the repeat factor from (53) to take all pole shoes per phase into account. For each phase k the derivative of the flux through the pole shoe (tooth) to the rotor angle is calculated.

$$K_k(\varphi) = repeat \cdot N_w \cdot \frac{\Phi_{tk}(\varphi + \Delta\varphi) - \Phi_{tk}(\varphi)}{\Delta\varphi} \qquad \text{[Vs/rad or Nm/A] (54)}$$

The result of this calculation is shown in figure 20.

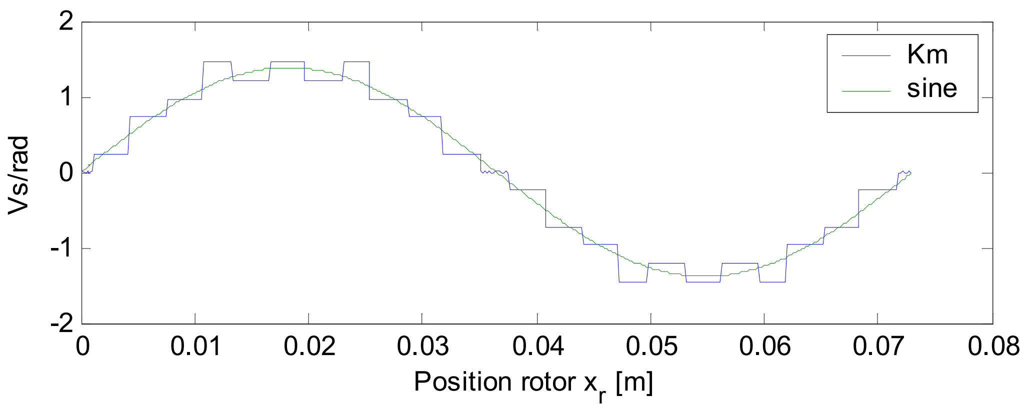

figure 20 motor constant of phase 1 calculated using the flux balance

As expected and required the motor constant has a sine wave shape. It can be written as

$$K(\varphi) \cong K_{\sin} \cdot \sin(\varphi) \qquad (55)$$

The value of amplitude K_{sin} can be calculated from $K(\varphi)$ using the mean of $K(\varphi)$:

$$K_{mean} = \overline{|K(\varphi)|}$$

$$\frac{1}{\pi}\int_0^{\pi} K_{\sin} \cdot \sin(\varphi) \cdot d\varphi \doteq K_{mean} \qquad (56)$$

$$K_{\sin} \cong K_{mean} \cdot \frac{\pi}{2}$$

Besides the electric torque (due to the current through the coils) we have the reluctance torque due to the permanent magnets when moving the rotor.

3.2.8 Reluctance torque, total torque and inductance

According to relation (6) the reluctance torque is calculable from the total magnetic energy at zero current. The total magnetic energy can be calculated from B, H and V.

$$E_{magn} = \int i d\lambda = \int \frac{Hdl}{N} dNBA = \int \mu H dHV = \frac{1}{2}\int \mu H^2 dV = \frac{1}{2}\int BHdV \qquad \text{[J] (57)}$$

Within each component of the equivalent circuit we assume a uniform magnetic field and flux density. Therefore the total magnetic energy as a function of the rotor angle can be calculated by summing the element wise multiplication of $B(x_r)$, $H(x_r)$, $A(x_r)$ times motor length l. Now the reluctance torque can be easily calculated. The result is shown in figure 21.

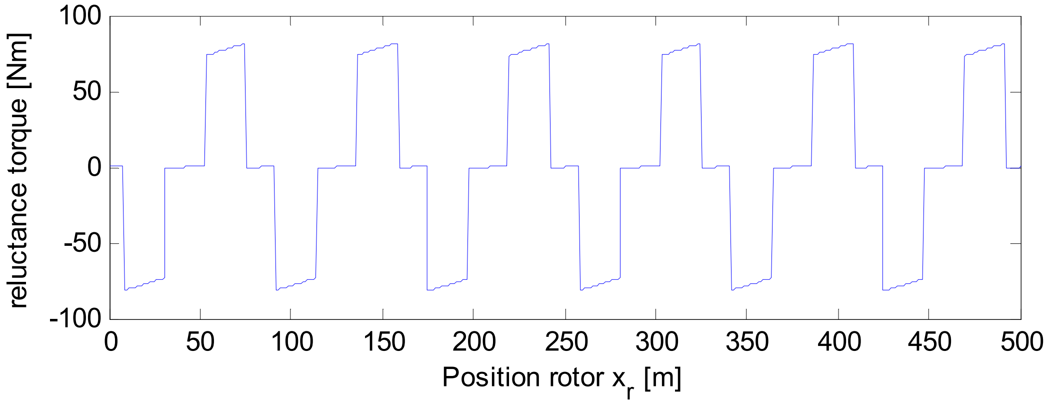

figure 21 reluctance torque motor A calculated from B, H and V at zero current

The electrical torque is the result of multiplying the motor constant with the current through the windings. The total torque generated by the motor can now easily be calculated by summing the reluctance and electrical torque.

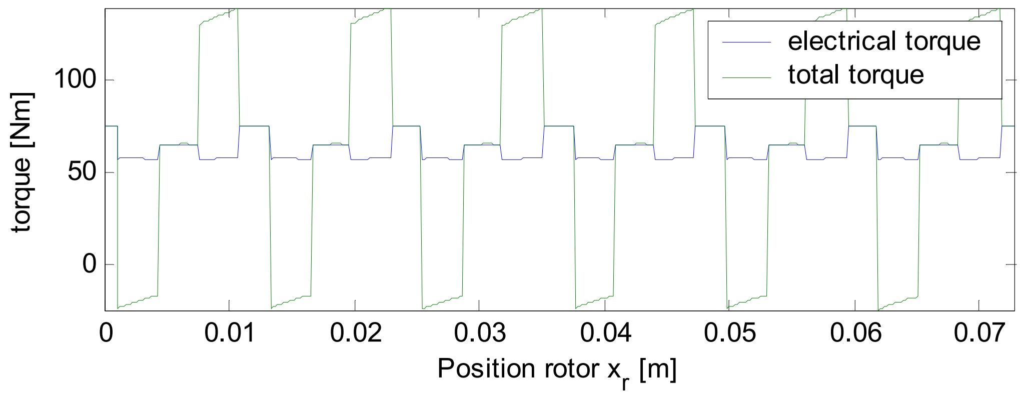

figure 22 electrical torque and total torque motor A at nonzero current

As can be seen the reluctance torque can be very large. For low electrical torques the reluctance torque has a huge influence on the total torque delivered by the motor. Several methods exist to reduce the reluctance torque ripple. One is to rotate the pole shoes with a small angle (torsion angle) to smoothen the flux density at the transitions between the pole shoes when the rotor is moving. The reluctance torque of the same motor as in previous calculations but with a torsion angle of six degrees is shown in figure 23.

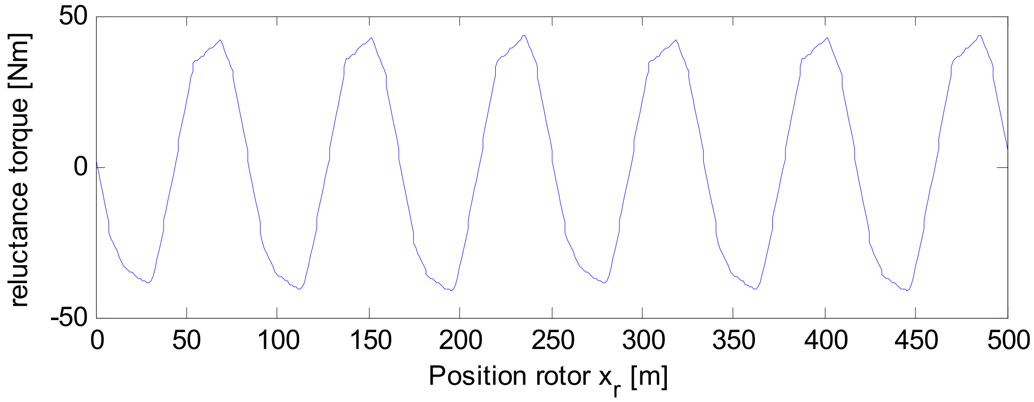

figure 23 reluctance torque motor A with torsion angle of six degrees

As can be seen the transitions are much smoother and the amplitude is smaller, resulting in a smoother total torque.

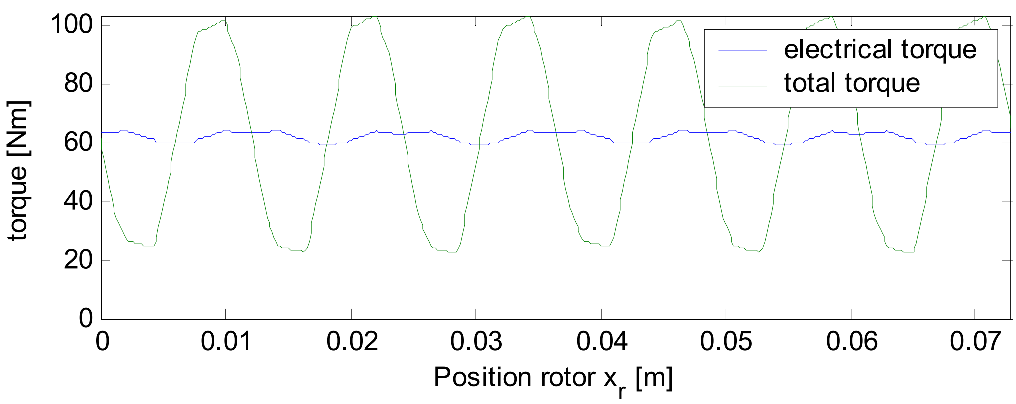

figure 24 electrical and total torque motor A with torsion angle of six degrees

The motor inductance per phase is the inductance per pole shoe times the number of pole shoes per phase. The inductance per pole shoe is calculated using relation (12), where R_m is the replacing reluctance of the whole circuit from and to the coil: the reluctance of pole shoe plus airgap plus all other airgaps and pole shoes in parallel. It turns out that the leakage between the pole shoes can be neglected in this calculation. The copper resistance is calculated using relation (18). Its inputs are directly related to the construction design parameters specified by the user.

Until now it has been shown how motor dimensions determine the reluctance of the magnetic circuit of the motor, which influences the motor constant, reluctance torque and inductance. Until now saturation was neglected. However the model is able to take saturation into account.

3.2.9 Saturation, hysteresis and eddy currents

To take the saturating storage part of the B-H relation into account relation (34) is implemented into the model using the iteration scheme below.

1. The initial solution of $\Phi(x_r)$ is solved using (52). B follows from (66).
2. μ is recalculated using (34).

3. $R_m\left(x_r\right)$ is recalculated using (10).
4. This repeats from step 1 for a fixed number of times to avoid large calculation times. The number of iterations has been empirically chosen large enough to obtain a good estimation of the saturation.

In next figure the resulting BH-relation is calculated for the example motor at 30A.

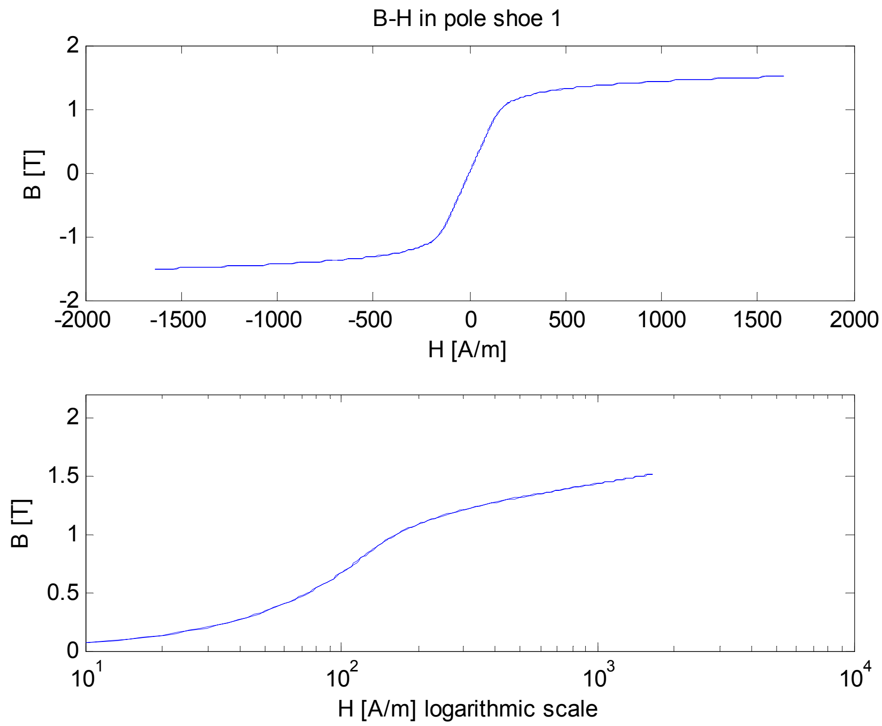

figure 25 B versus H curve illustrating the working area at 30A

The hysteresis in the BH-relation is hard to simulate due to the magnetic memory. The values of B due to H depends on the previous values of B. In general this can be seen as B having a sort of non-linear phase lag with respect to H dependent on the value of the coercivity and remanence of the magnetic material. Taking this nonlinear relation into account would make the model too complex, because it would be necessary to save the state of the BH-relation for all positions within the motor model. Because the nature of this effect is merely dissipation, it is sufficient to take its cumulative size into account.

An estimation of the losses due to Eddy currents and hysteresis are calculated afterwards using relations (36) and (37). The hysteresis losses of motor A without current but with rotor movement is shown in figure 26.

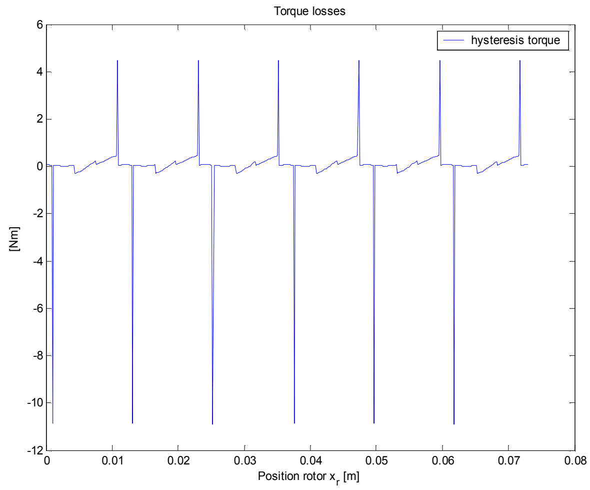

figure 26 torque losses due to hysteresis motor A without torsion angle

Appendix D shows a summary of the Matlab implementation of the algorithm described in previous paragraphs.

In this chapter the parametric electromagnetic model has been presented. All relevant electromagnetic specifications of a motor can be calculated using this model. In chapter 4 the model will be validated against three existing motors. Before validation another model is introduced for giving an indication of the temperature within a motor.

3.3 Thermal model

The motor design will be validated for thermal behaviour using a model. The system is described in port variables of the pseudo thermal domain, temperature and heat flow, because these are related by linear equations defining the heat transfer, conduction and radiation mostly according to Fourier's law. This is allowed since the environmental temperature is assumed to be constant.

$$U = I \cdot R \rightarrow T = \dot{Q} \cdot R \tag{58}$$

The thermal energy flow into the motor is delivered by the dissipation in the copper windings. This thermal power source is assumed to be located in the centre of the copper of the windings and is modelled as a heat flow source.

$$P_{diss} = \dot{Q}_{source} = I^2 R \tag{59}$$

From the windings three heat flow paths are dominant:

1. hotspot → copper/epoxy → water cooling (optional)
2. hotspot → copper/epoxy → stator iron → air cooling
3. hotspot → copper/epoxy → airgap → magnets and rotor iron → air cooling

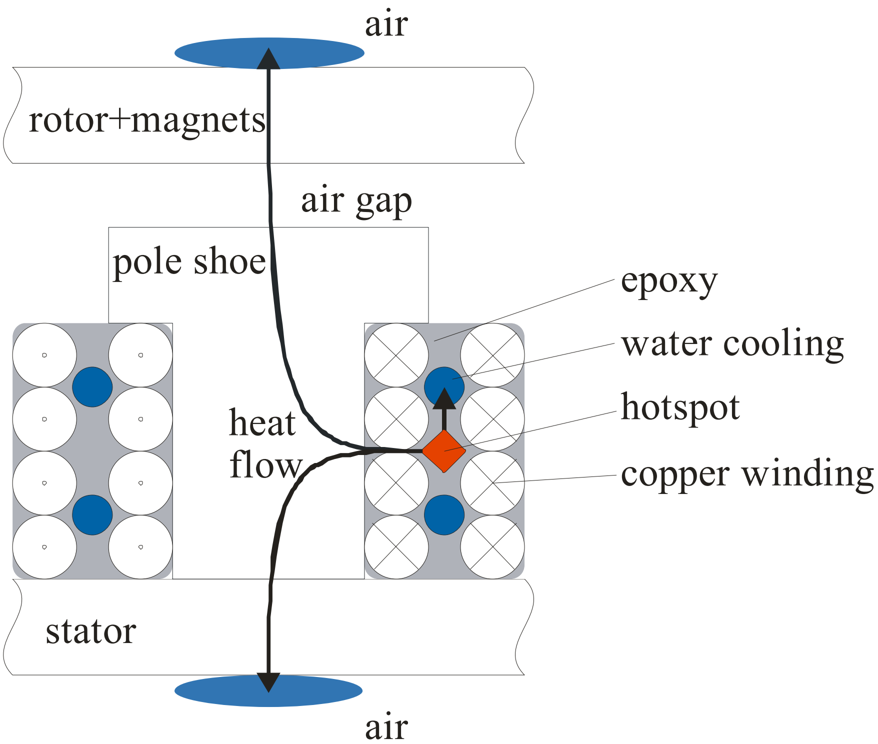

figure 27 cross section of a pole shoe schematically indicating the thermal sources and flow paths due to dissipation and cooling in the motor

The thermal resistance of the copper and epoxy layer in the windings is mainly determined by conduction (38). We assume the epoxy to be perfectly cast in the mold and therefore to have negligible contact resistance with the copper and the iron.

The windings are optionally cooled with water. Most of this heat transfer occurs by means of convection (40). The heat transition coefficient of streaming water with forced convection is between 500 and 10^4.

Another part of the heat flow goes from the windings into the stator or via the airgap into the rotor and is dissipated into the air. The thermal resistance through the iron is mainly determined by conduction. Between the iron and air contact resistance plays a dominant role. The magnitude of convection k through flowing air is between 10 and 100.

Heat transfer through the airgap is determined partly by convection on the contacts, partly by conduction through air and partly by heat radiation (41). In reality the iron radiates somewhat less than ideal black radiators. This is taken into account by multiplying (41) with a constant factor ε (Kirchhoff's law), which is about 0.8 for iron surfaces.

Three elements in the motor act as heat capacitors: the copper windings, stator iron and rotor iron. All relevant thermal elements of the motor can be summarized in the equivalent electric circuit from figure 28. The only nonlinear element is the airgap heat resistance, because the heat through the airgap is mainly caused by radiation.

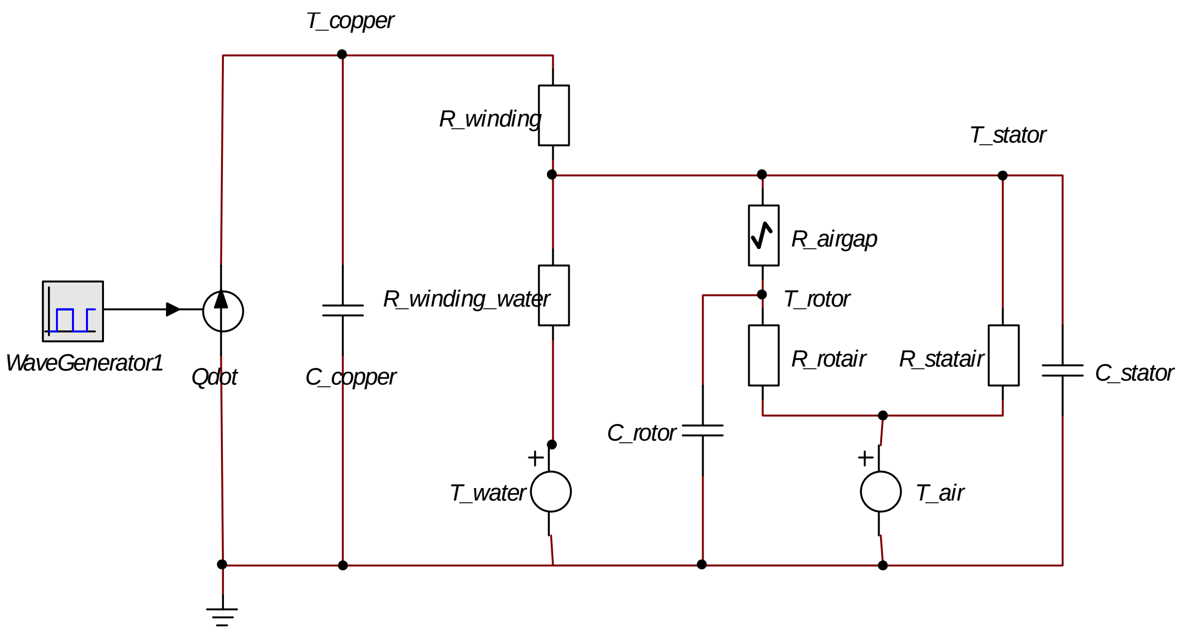

figure 28 thermal circuit of an electric motor based on temperatures and heat flows

For safety reasons the outer surface of the rotor and inner surface of the stator are chosen as the only cooling surfaces. No heat is assumed to be removed from the air gap in another way than via rotor or stator, since the air gap itself is not cooled and could even be a closed system. This way the modelled temperature of air gap and permanent magnets should be a worst case prediction. As an example figure 29 shows the heating, cooling and temperature of a motor.

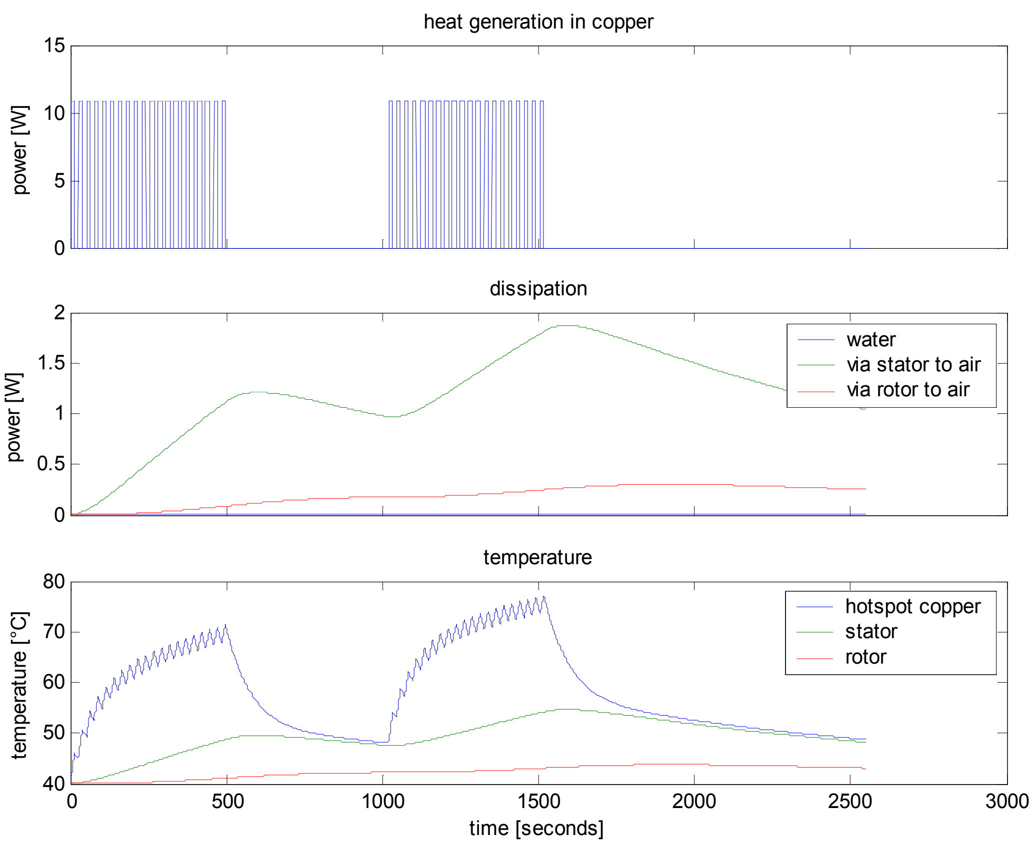

figure 29 heat generation and dissipation in the motor

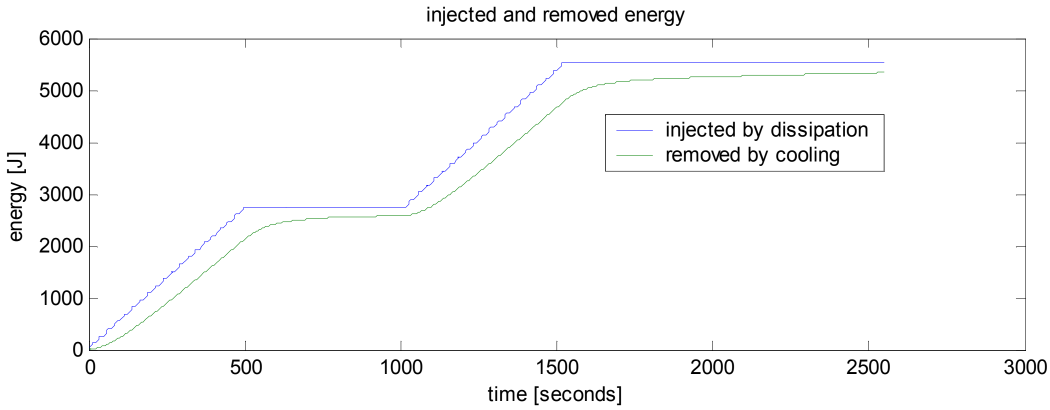

figure 30 total injected and removed thermal energy of the motor in time

4 MODEL VALIDATION

In this chapter the models described in chapter 3 will be validated against following motors:

A) medium sized prototype direct drive motor produced by Demcon
(measured by Peter Rutgers and Andre Hilderink (Demcon) in 1996)
B) medium sized direct drive motor produced by Demcon used for driving wheel chairs
(measured by Martin Ruppert (Demcon) in February 2004)
C) very large direct drive motor produced by Etel Motion Technology: TMA1220-070.
An adapted version of this motor is used by Thales for driving large radar systems.

Following table shows the dimensions and configuration of the motors. Simulations are based on these values. For motor C the original specifications of the TMA1220-070 are used.

table 1 specifications of dimensions and configuration per motor

		motor A	motor B	motor C
<u>armature</u>				
thickness stator ring	[mm]	20	19	51
diameter to air gap	[mm]	186	200	1139
thickness rotor ring	[mm]	8	20	20
lamel thickness	[mm]	4,0	0,66	0,50
airgap height	[mm]	1,0	1,0	1,2
<u>magnets</u>				
pole pairs	[-]	8	8	110
width	[mm]	30,0	26,5	14,0
thickness	[mm]	5,0	4,0	6,0
length (also motor length)	[mm]	64	45	71
remanence	[T]	0,68	1,1	1,2
<u>pole shoes</u>				
phases	[-]	3	3	3
pole shoes per coil	[-]	1	1	2
pole shoes per phase	[-]	8	8	110
width	[mm]	21	18	6
torsion angle pole shoe	[degrees]	6	0	0
torsion angle magnets	[degrees]	0	7	0
head height	[mm]	2	2	0
bottom width	[mm]	9	11	6
bottom height	[mm]	40	30	45
cupper wire surface	[mm2]	1,5	3,4	1,1
number of windings	[-]	27	18	60

For both the electromechanical transduction properties and the thermal behaviour measurements and simulations are compared, starting with the resistance, inductance and back-EMF, which give enough information to validate the electromagnetic model. Afterwards a thermal measurement is used to validate the thermal model.

4.1 Resistance per phase

In table 2 the measured and calculated resistances per phase from terminal to ground are compared.

table 2 measured and calculated resistance per phase from terminal to ground

resistance [Ohm]	motor A	motor B	motor C
measured			
phase U	0,451	0,124	
phase V	0,457		
phase W	0,477		
mean per phase	0,462	0,124	
specified			5,35
calculated	0,439	0,106	6,05
deviation	-5%	-15%	13%

Etel specifies the resistance and inductance from terminal to terminal in Y phase configuration. This means that for one phase (from terminal to ground) the inductance and resistance are half the specified values.

The resistance is calculated according to (18) in paragraph 2.4.2. The measured value of the copper wire diameter has a lot of influence on the calculated resistance.

4.2 Inductance per phase

The inductance can be measured by recording the voltage with a high frequent supply current and discount for the voltage drop over the copper resistance.

table 3 measured and calculated inductance per phase from terminal to ground

inductance [mH]	motor A	motor B	motor C
measured	**1,56**	**0,50**	
specified			**48,75**
calculated	**1,57**	**0,52**	**42,27**
deviation	1%	4%	-13%

4.3 Back-EMF per phase

In next table the measured and calculated back-EMF or motor constant for one phase are shown for each motor. For comparison reasons the motor constant is written according to the definition of K_{sin} (paragraph 3.2.7) for one phase from terminal to ground.

Etel specifies the (sine shaped) back-EMF constant per phase from terminal to terminal, so this is $\sqrt{3} \cdot K_{sin}$. Also a torque constant is given in Nm/A_{rms} for all phases together, which is $\frac{3}{2}\sqrt{2} \cdot K_{sin}$. Verification of the catalogue values showed that the torque constant equals $\frac{3}{2}\frac{\sqrt{2}}{\sqrt{3}}$ times the back-EMF constant indeed.

table 4 measured and calculated back-EMF per phase from terminal to ground

Back-EMF [Vs/rad]	motor A	motor B	motor C
measured			
measurement 1	1,314	0,899	
measurement 2	1,313	0,817	
measurement 3	1,344	0,821	
mean	1,324	0,846	
specified			171,5
calculated	1,369	0,848	174,2
calculated (with saturation)	1,358	0,843	169,9
deviation	3%	0%	2%
deviation (with saturation)	3%	0%	-1%

Two calculations have been made: with and without taking saturation into account. Since the back-EMF or motor constant is calculated with no current through the coils the saturation is not significant.

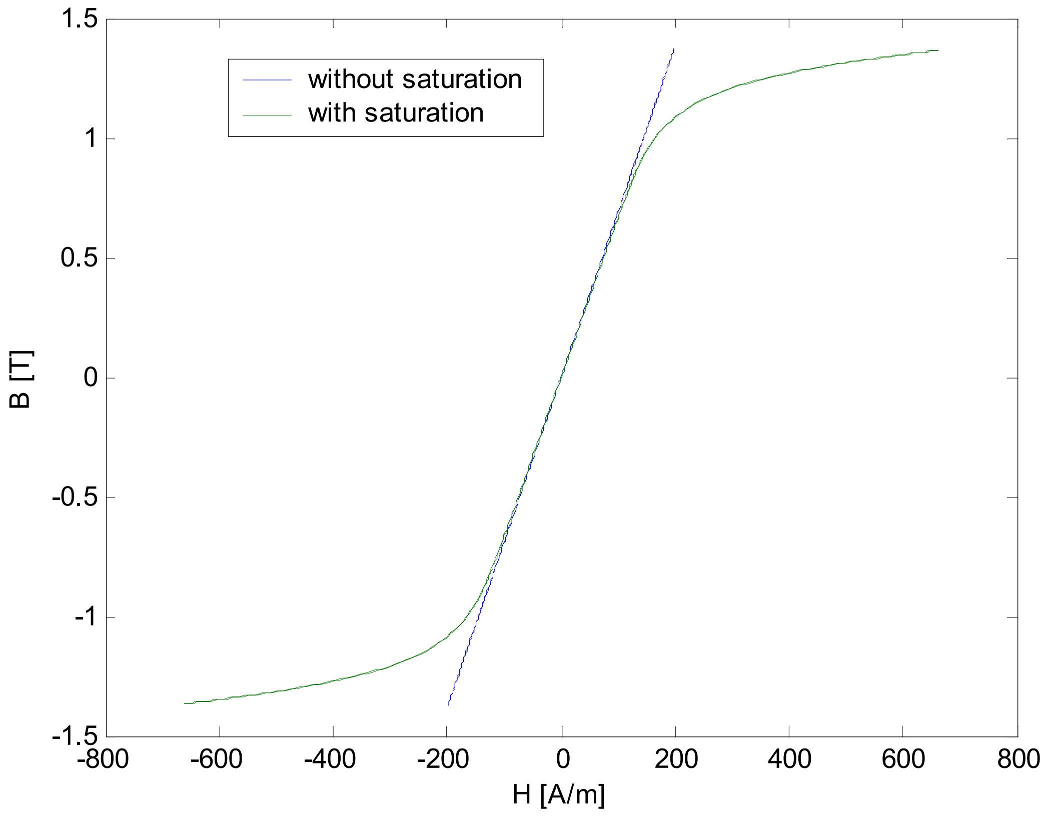

figure 31 B versus H curve while determining the motor constant with and without taking saturation into account

For the prototype motor (motor A) measurements of the shape of the motor constant were available. In figure 32 measured and calculated motor constants per phase are compared.

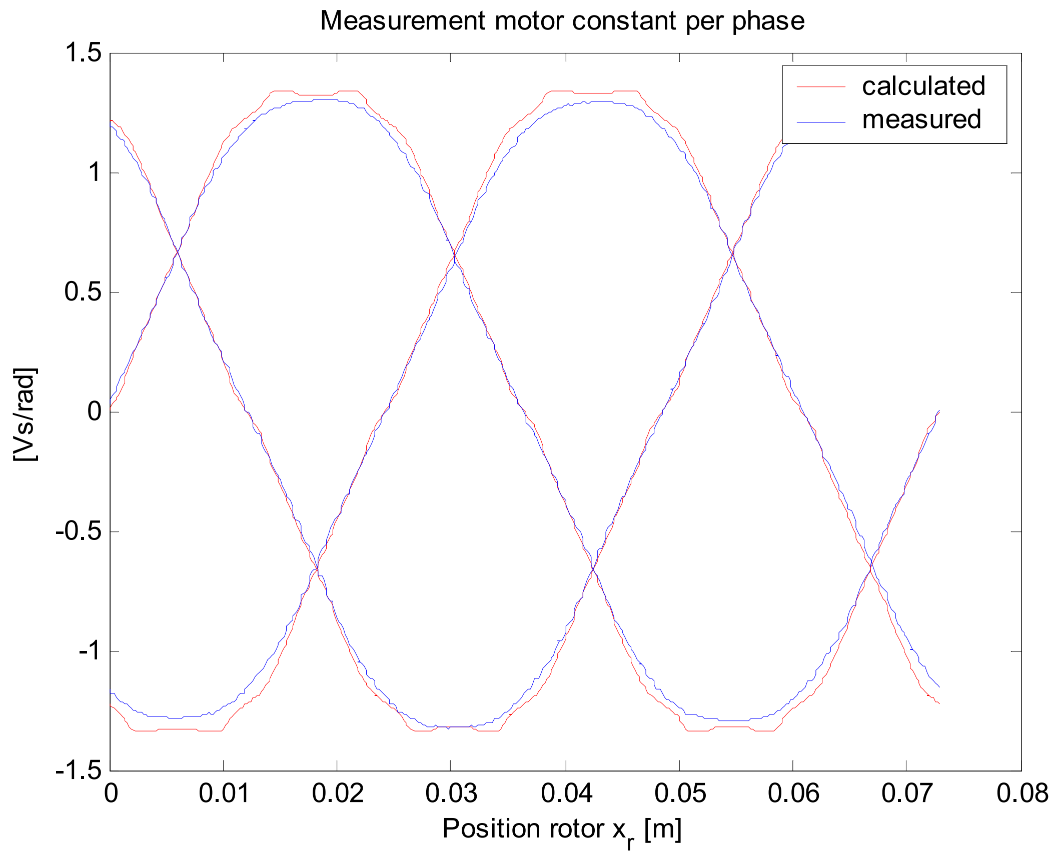

figure 32 measured motor constant of motor A for one phase

The calculated shape of the motor constants per phase of motor B and C are plotted in figure 33 and figure 34 for comparison.

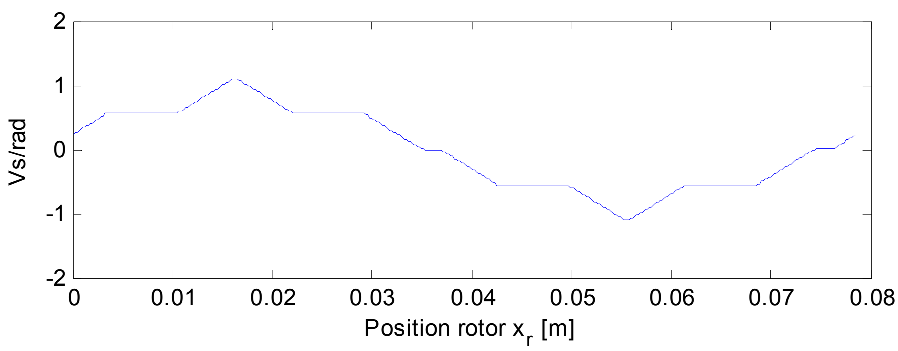

figure 33 calculated motor constant motor B

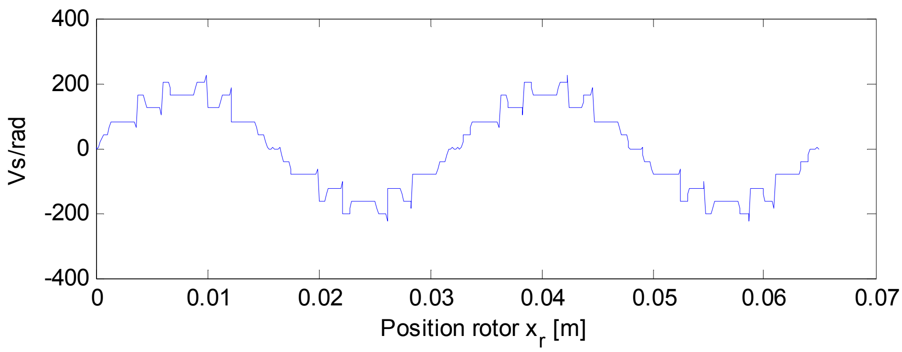

figure 34 calculated motor constant motor C

4.4 Temperature

Three temperature measurements on the Heracles motor done by Thales in 2004 are compared to simulation results of the thermal model. The results are shown in figure 35. Each measurement starts at another initial temperature.

The Heracles motor is a TMA1220-070 with some modifications. The difference of the Heracles motor compared to the original TMA1220-070, which is relevant for the thermal model, is its windings resistance of 0.216Ω per phase instead of 5.33Ω.

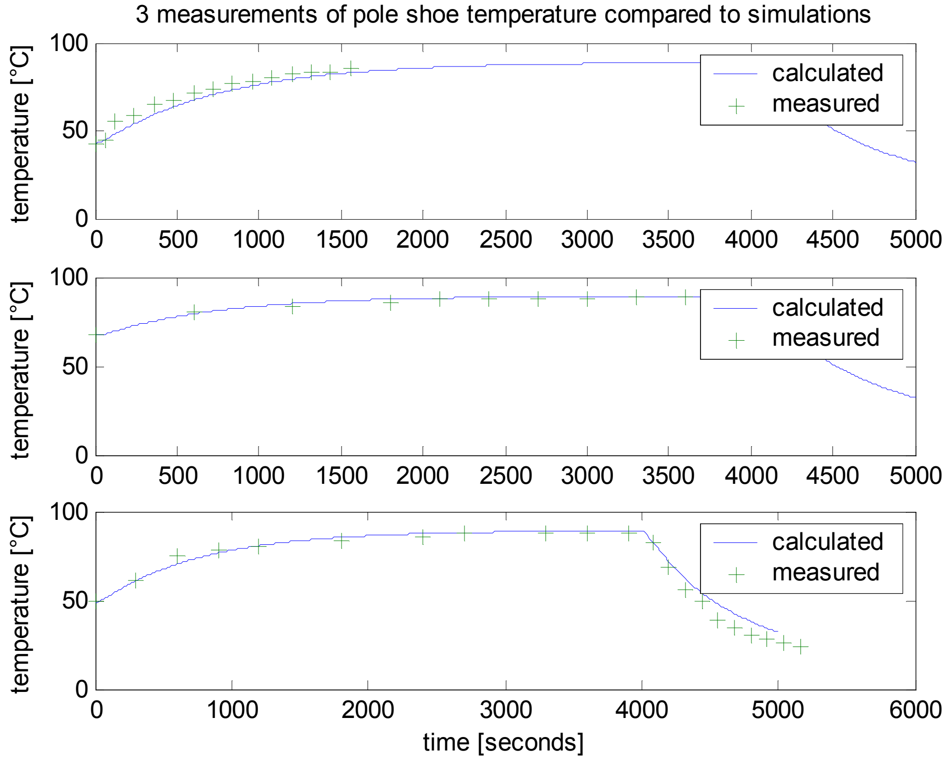

figure 35 temperature measurements Heracles motor (Thales) at 115A compared to simulations

4.5 Conclusions

The models described in chapter 3 are suitable to calculate a good approximation of the specifications of a permanent magnet motor. Both the electromechanical performance in terms of steepness, motor constant, windings resistance and inductance and the thermal performance in terms of thermal time constant and resistance are good predictable. Therefore these models can be used to design or verify a design of a permanent magnet motor. Furthermore they can be used when designing a controller.

In next chapter the models will be used to predict the consequences of changing several design parameters on the electromechanical transduction performance of a motor.

In chapter 6 the influence of the design parameters on the controllability will be simulated. Also learning control will be used to investigate the possibilities to improve torque performance of motors, which have a spiky motor constant and high reluctance torque due to construction design choices.

5 PERFORMANCE IMPROVEMENT BY CONSTRUCTION DESIGN

Having validated the models in previous chapter, now the effects of several design parameters on the motor performance can be calculated by doing simulations using these models. We have chosen to focus on the electromechanical transduction performance of the motor.

In this chapter the parametric electromagnetic model is used to calculate the influence of construction design parameters on the electromechanical transduction performance. Interesting to know is the sensitivity of design parameters on the

- Steepness
  - Motor constant
  - Windings resistance
- Reluctance torque

These indicate the performance of a permanent magnet motor as discussed in paragraph 0.

As starting point we take the Etel TMA1220-070 (motor C) and vary following design parameters while watching the performance:

- Motor dimensions and configuration:
  - diameter
  - length
  - number of magnet pole pairs and pole shoes
  - number of pole shoes per coil
  - airgap height
- Pole shoe dimensions:
  - Torsion angle
  - Foot width
  - Head width
  - Head height
- Magnet dimensions:
  - Torsion angle
  - Width
  - Height

After having simulated the influence of these parameters on the electromechanical performance conclusions can be drawn with respect to the construction design.

5.1 Motor configuration

Consecutively the diameter and length, number of magnet pole pairs, number of pole shoes, number of pole shoes per coil and airgap height will be varied while calculating the winding resistance, motor constant and reluctance torque. For each variation the interesting results are shown. All simulation results are shown in Appendix A. For the parameters not mentioned the original values are used.

5.1.1 Diameter

The motor diameter has been varied from 0.05 to 1 meter. In figure 36 the steepness is shown.

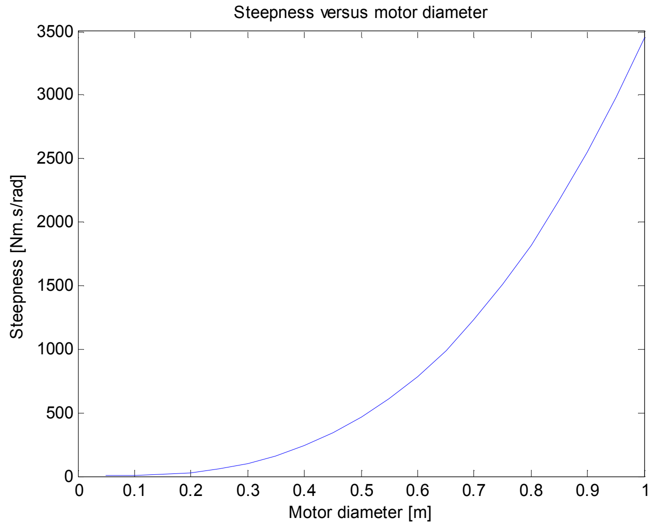

figure 36 steepness for varying motor diameter

The steepness increases more than quadratically when the motor diameter increases, namely to the power of 2.8 at this specific length. As can be seen in Appendix A increasing the diameter decreases the windings resistance about inverse proportionally, because the slot space increases proportionally while the number of windings keeps the same. Because the pole shoe width also increases the winding resistance does not fully decrease proportional. The motor constant increases proportional because as one can imagine the surface of the air gap will increase proportionally with the diameter, so will the total flux. Since the steepness is related to the motor constant and windings resistance according to equation (27) the steepness will be related to the motor diameter with almost the power of 3, which corresponds to the simulations.

The proportionally increased flux causes also a proportional increased reluctance torque, which is shown in Appendix A. Note that for very small diameters the slot space starts to decrease more than proportional, since its shape becomes triangular when the circular shape of the motor cannot be neglected anymore.

5.1.2 Length

The motor length has been varied from 5 to 100 mm.

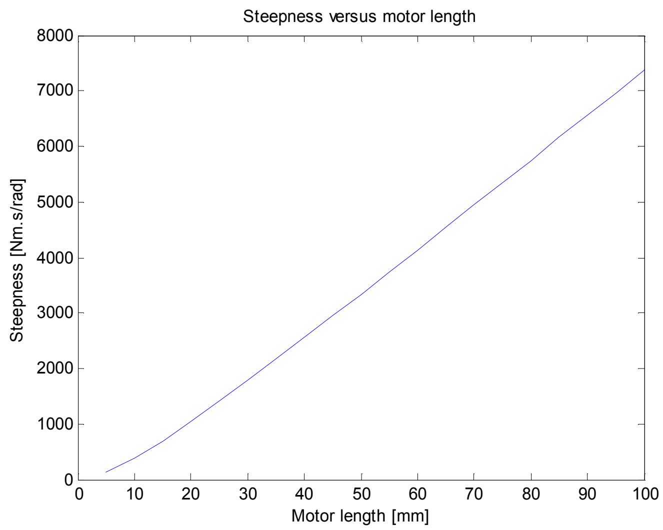

figure 37 steepness for varying motor length

Both resistance and motor constant increase proportionally with the motor length, so is the steepness. The copper wire length is proportional to the motor length for a motor length relatively large compared to the width of a pole shoe. The total airgap surface is also proportional to the length, thus so are the motor constant and reluctance torque.

5.1.3 Number of magnet pole pairs and pole shoes

The number of pole pairs has been varied from 10 to 200. The ratio of magnet pole pairs to pole shoes remains 1:3. This is necessary for a 3 phase system. Doubling the number of pole pairs causes the overlapping surface between rotor and stator to vary faster, resulting in a higher frequency of the flux and motor constant per phase. The resulting steepness is shown in figure 38.

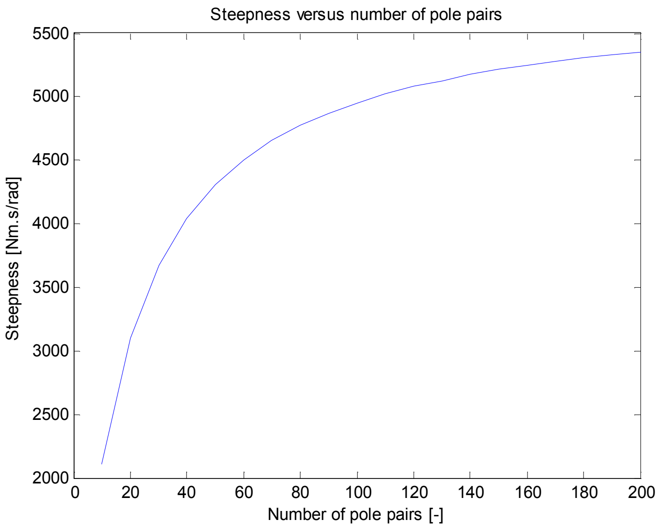

figure 38 steepness for varying number of pole pairs

As mentioned in paragraph 2.8.3.2 a low number of pole pairs results in a low motor constant, which is desirable for high speed applications, see equation (24). This relation between pole number and motor constant is confirmed by the simulations. The motor constant is proportional to the number of pole pairs, because the motor constant is the derivative of the airgap flux to the motor angle, which is proportional to the number of poles. Since the reluctance torque is the derivative of all magnetic energy to the motor angle it is proportional to the number of poles as well.

The resistance is nearly quadratically related to the number of pole pairs. A higher number of poles means smaller slots, thus a smaller copper wire diameter for the same number of windings. Since the pole shoe width also gets smaller the relation is not pure quadratic (but to the power of 1.8 at this specific length). The steepness therefore shows a relation of the number of pole pairs to the power of about 0.2.

5.1.4 Number of pole shoes per coil

In this case the number of pole shoes per coil is varied, while the number of coils is kept constant. This differs from above situation, since there is one pole shoe per coil by default. A second pole shoe per coil introduces an extra flux path through the airgap, however this second yoke goes at the cost of slot space. So on one hand less sources of magnetic force, but on the other hand more iron and less overall reluctance.

For one yoke per coil we have R = 12 Ω, K_{sin} = 347 Vs/rad and S = 10^4 Nm.s/rad.
Keeping the same space available for copper windings, but using two slots per coil we get
K_{sin} = 349 Vs/rad and S = 10^4 Nm.s/rad.

A slight increase is visible for this static case without excitation of the coils. The total flux crossing the airgap is almost the same, while the chance on saturation is less. Since the motor operates in saturation most of the time, adding a second yoke per coil has a positive effect.

5.1.5 Airgap height

The airgap height has been varied from 0.5 to 10 mm. Of course it has no influence on the copper resistance. However the steepness decreases quadratically with the airgap height, because the motor constant is about inverse proportional to the airgap height due to linearly increasing reluctance in the flux circuit.

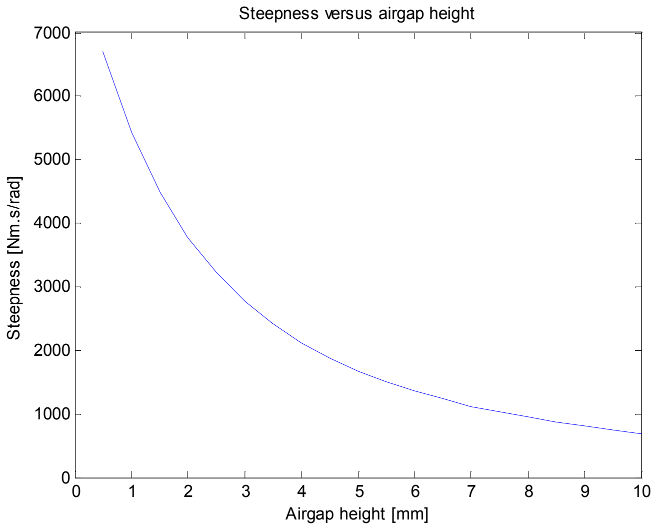

figure 39 steepness for varying airgap height

The reluctance torque shows the same decrease as the motor constant.

5.2 Pole shoe dimensions

In this paragraph the influence of the pole shoe dimensions will be investigated. In figure 40 the varied parameters are illustrated. Angle α is the torsion angle, which will be varied first.

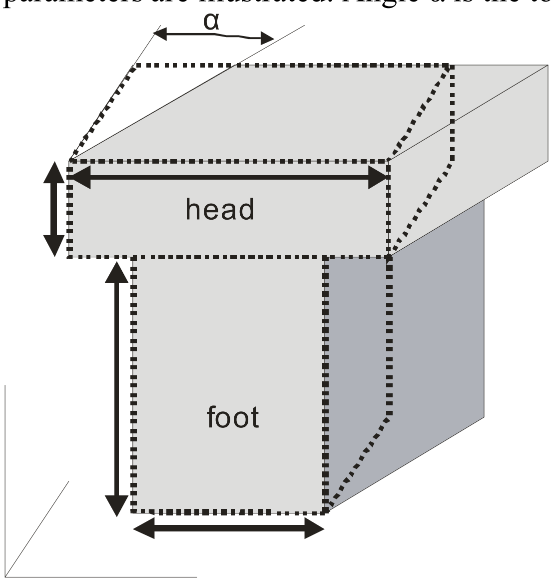

figure 40 schematic pole shoe illustrating the varied design parameters

5.2.1 Torsion angle

The torsion angle has been varied between 0 and 10 degrees. For these small angles the resistance may be assumed to be independent on the torsion angle. However the steepness changes and the reluctance torque even drastically decreases as can be seen in figure 41.

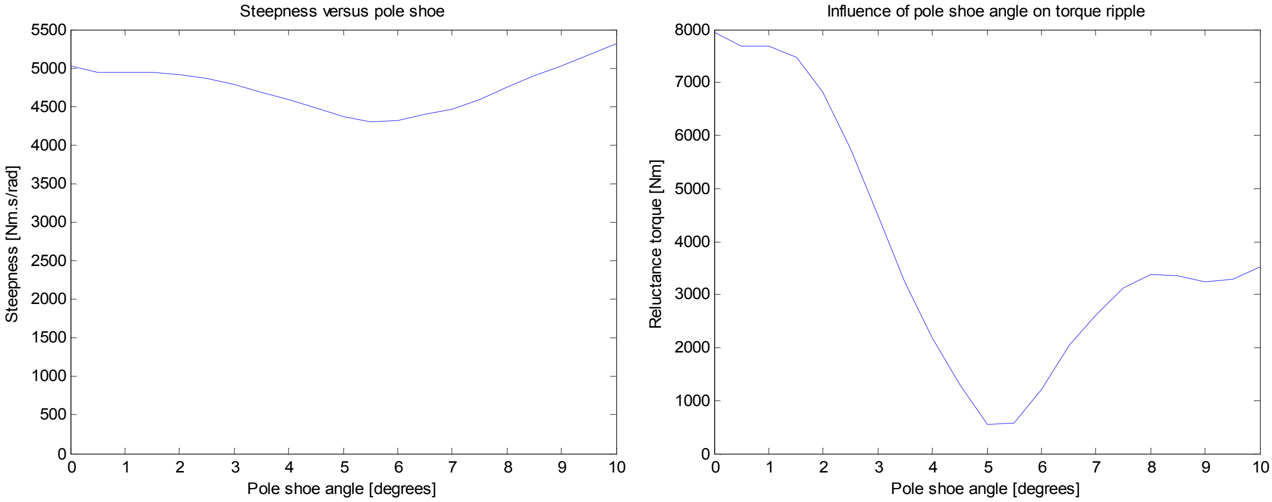

figure 41 steepness (left) en reluctance torque (right) for varying pole shoe angles

For this specific motor configuration a pole shoe torsion angle of 5 degrees drastically reduces the cogging force with 92.5%, while the steepness is only decreased by 15%. Note that both graphs even show an increase again for larger torsion angles. This starts to happen when two pole shoes overlap one magnet pole. It introduces harmonic distortion, which is visible when looking at the overlapping surfaces of magnet poles and pole shoes, shown in Appendix A.

5.2.2 Foot width

The relative foot width of the pole shoes has been varied between 0 and 1 of the fixed head width of 6.196 mm. A trade-off becomes visible in the steepness between slot space for copper to decrease resistance and tooth space for iron to decrease reluctance.

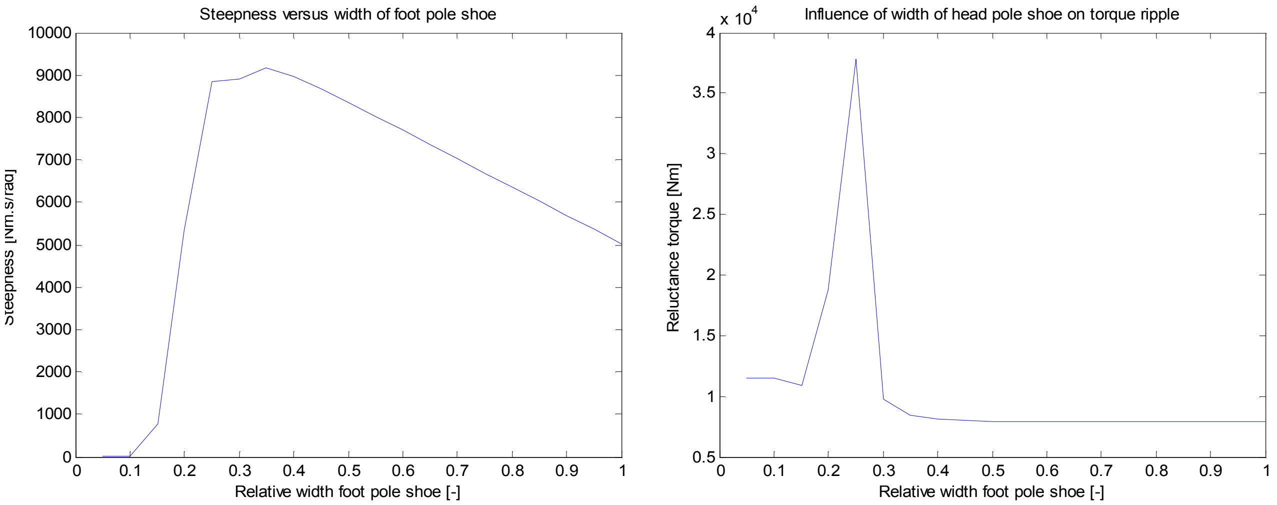

figure 42 steepness for varying foot width

The maximum steepness is achieved at a relative width of about 0.35. From the graph of the motor constant in Appendix A it is clearly visible that at very small foot width reluctance is very high. Whereas at higher widths the motor constant remains the same. It indicates that this effect is caused by saturation. In figure 43 this is illustrated by two B-H curves. Due to the heavy saturation at small foot widths the reluctance torque shows a large peak because of distortion of the flux. The influence on the reluctance at larger widths is constant.

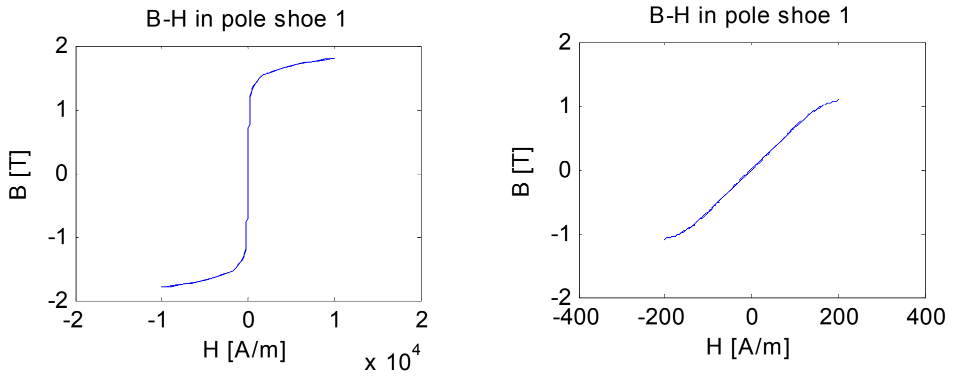

figure 43 foot width of 1.5mm: saturation (left) and foot width of 3.1mm: no saturation (right)

5.2.3 Head width

For this simulation the head height is set to 5mm and the foot width remains constant and equal to the original value. The head width is varied between 0 and 1 relative to the distance between two pole shoes.

Again a trade-off is visible in the steepness graph. This time between a high iron surface at the airgap to decrease the airgap reluctance and a high distance between the pole shoes to increase the leakage reluctance. And clearly the airgap flux plays a dominant role compared to the leakage flux. At a relative width of more than 0.9 the leakage flux starts to become dominant and the steepness collapses. This is because the pole shoes start to touch each other.

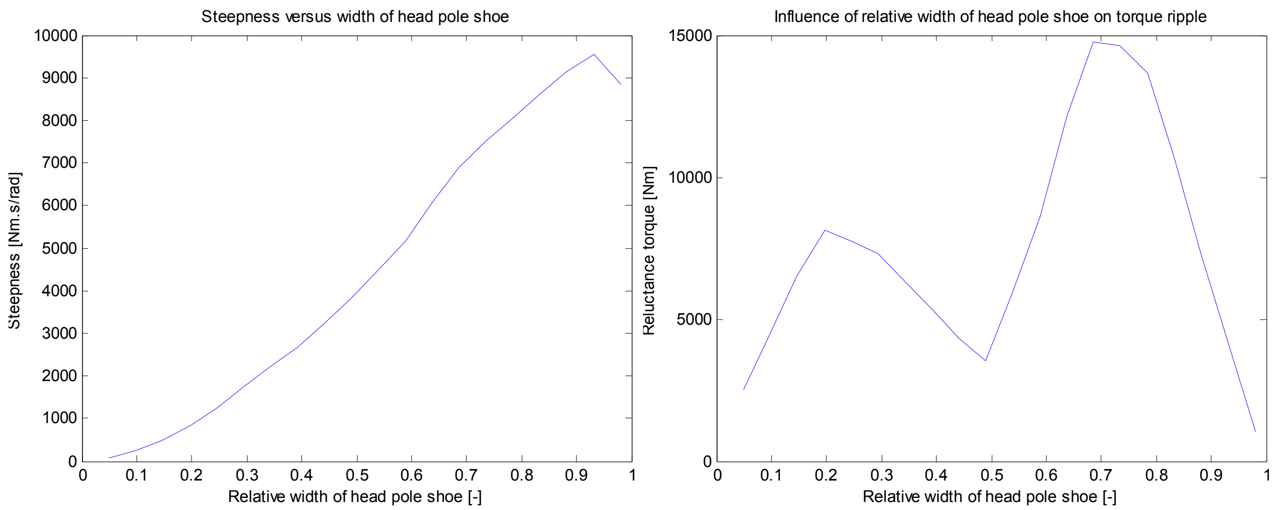

figure 44 steepness (left) en reluctance torque (right) for varying head widths

The reluctance graph shows two local maxima. Looking at the shape of the reluctance torque for three different head widths (Appendix A) shows that head widths of around 0.25 and 0.75 cause wide reluctance spikes whereas a head width of 0.5 causes only small spikes.

5.2.4 Head height

Next the head height has been varied between 0 and 5 mm. The head width is fixed to 6.196 mm (original width) and the foot width is set to half the head width. The airgap height and slot height remain constant, such that only the effect of the head height is visible in the simulation results.

As can be seen in Appendix A the head height seems to have no significant influence on the motor properties. A higher pole shoe head only causes little extra flux leakage and therefore a lower motor constant and steepness. On the other hand too small head height causes saturation at the protruding ends of the head. This effect however is not taken into account in the parametric model and should therefore be calculated using finite element software.

5.3 Magnet dimensions

In this paragraph the influence of the magnet dimensions on the motor performance is investigated. Angle α in figure 45 is the torsion angle, which will be varied first.

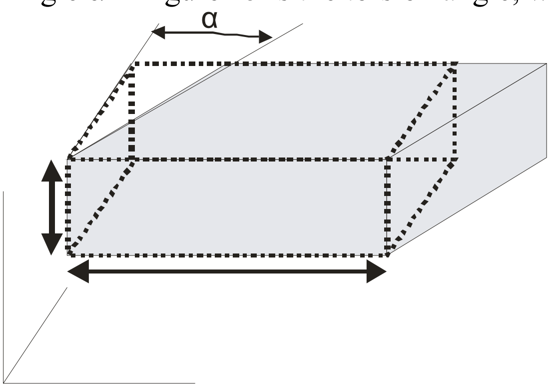

figure 45 schematic magnet illustrating the varied design parameters

5.3.1 Torsion angle

The magnets are rotated between 0 and 7 degrees. As with the torsion angle of the pole shoes this angle causes smoother transitions of the overlapping surface between pole shoes and magnets. As can be seen the reluctance torque decreases due to the angle. The steepness however decreases also a lot, which is more problematic than we had with the pole shoe torsion angle (figure 41).

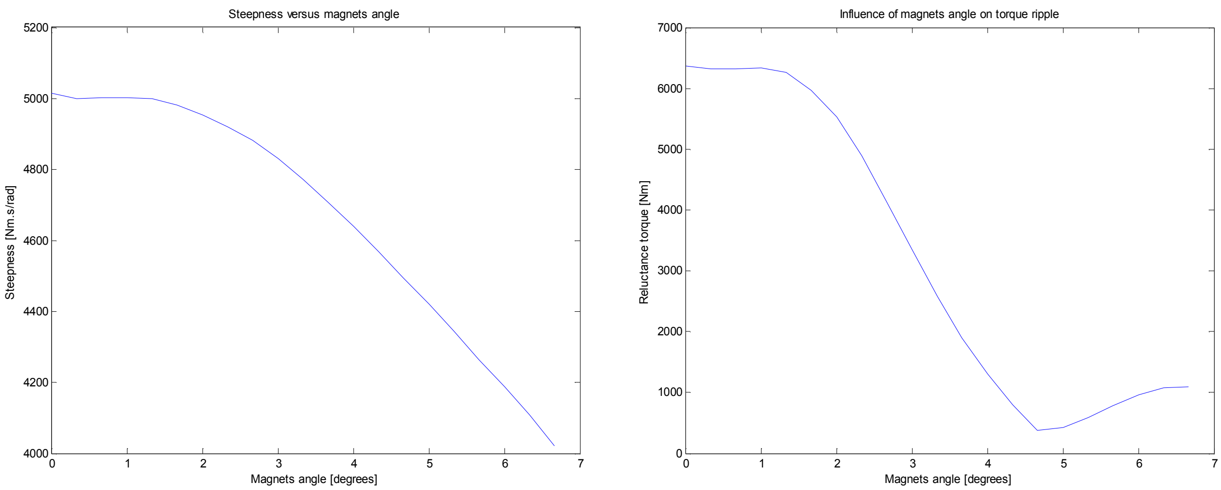

figure 46 steepness (left) en reluctance torque (right) for varying magnet torsion angles

5.3.2 Width

The magnet width has been varied between 0 and 1 relative to the distance between the centres of the magnet poles. Increasing the magnet width has a very positive effect on the steepness. However in the reluctance torque an optimum is present. Therefore the trade-off is between steepness and reluctance torque.

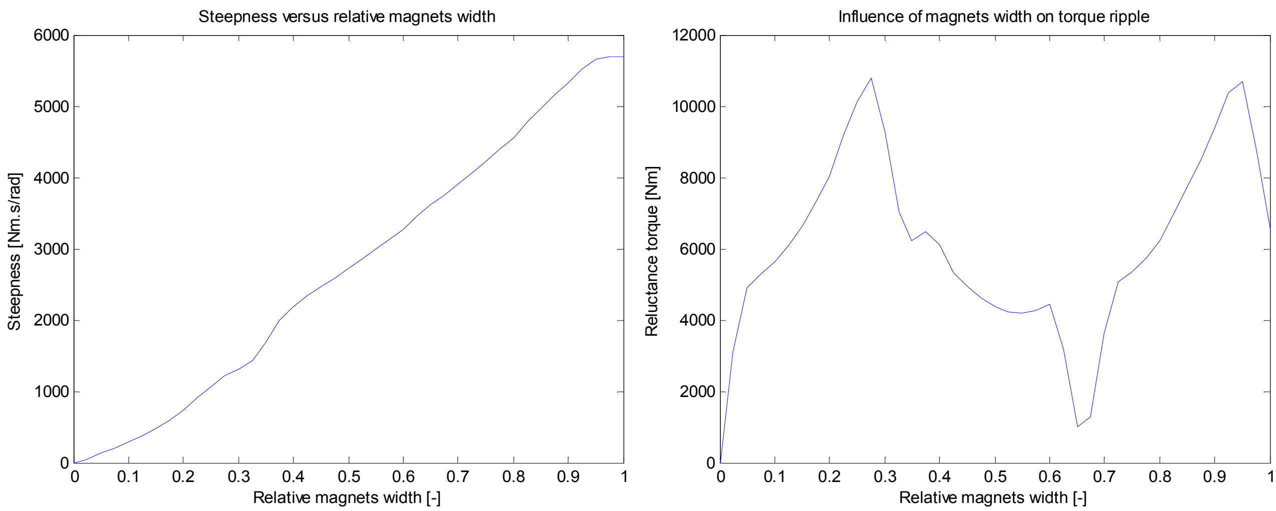

figure 47 steepness (left) en reluctance torque (right) for varying magnet widths

The magnitude of the motor constant increases with the magnet width, but also the shape is relevant. It can be seen in Appendix A that the width of the magnets can be tuned to achieve least harmonic distortion.

5.3.3 Height

The magnets height has been varied between 0 and 10 mm while keeping the airgap height constant. The simulation results are shown in figure 48. As can be seen increasing the magnet height improves the steepness, although there is some kind of saturation in the motor constant which limits this advantage. Since the magnets are modelled as coils in air both the magnetic field and reluctance (airgap) due to the magnets increase, resulting in this saturation effect.

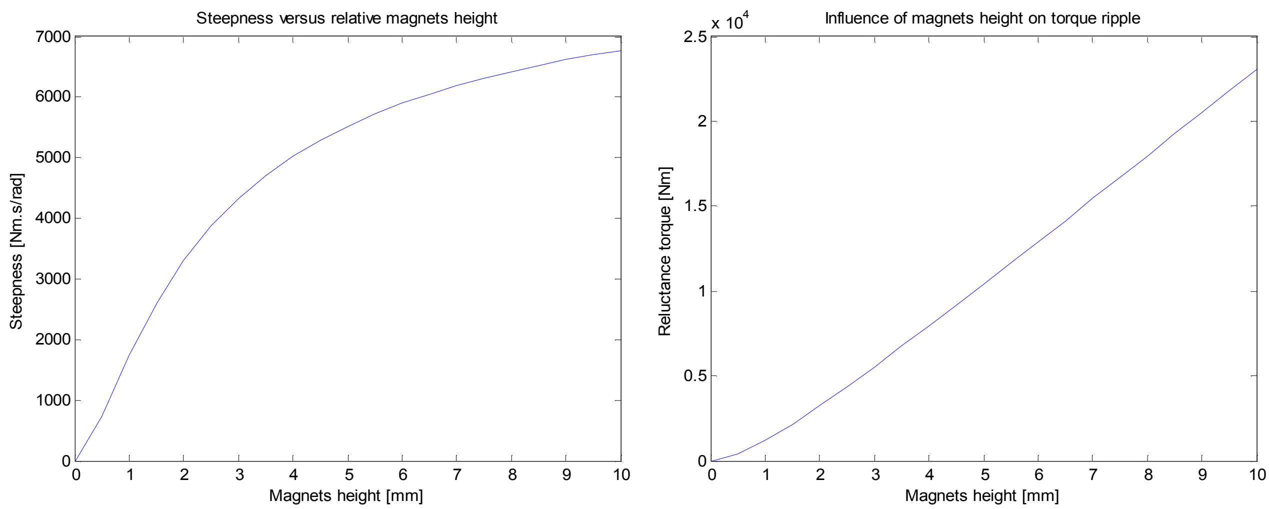

figure 48 steepness (left) en reluctance torque (right) for varying magnet heights

The reluctance torque increases proportionally to the magnet height. Between the steepness and reluctance torque there is a trade-off again, from which clearly an optimum can be chosen.

5.4 Conclusions of construction design

In this chapter the parametric magnetic model has been used to vary several design parameters. Their influence on the motor performance was simulated and evaluated in terms of steepness and reluctance torque. From a torque performance point of view (efficiency and cogging) several construction design parameters can be optimized for.

For the specific motor C following conclusions can be made according to the outcome of the parametric magnetic model.

As expected following design parameters had a pure positive effect on the steepness according to the simulations.

- The diameter and length of a motor should be chosen as large as possible.
- A second pole shoe per coil could be considered to improve the steepness at saturation, or in other words to increase the maximum stall torque.
- The airgap height should be chosen as small as possible, taking eccentricity and shock stability into account.

For following design parameters a trade-off can be made between steepness and reluctance torque.

- Rotating the pole shoes decreases the reluctance torque drastically while the effect on steepness is minimal. Too high angles result in distortion and higher reluctance torques. For motor C an optimal torsion angle of 5 degrees is found.
- The magnets could also be rotated; however this has more negative influence on the steepness.
- The number of poles can be increased to increase the steepness. This however goes at the cost of the size per pole shoe (thus increasing resistance) and a higher reluctance torque. Dependent on the required steepness and resistance the right number can be chosen.
- Increasing the pole shoes head width increases the steepness. However the reluctance torque varies for different widths. For motor C a head width of about 0.9 of the pole shoe distance gives maximum steepness, but 0.5 pole shoe distance gives least reluctance torque for this specific motor configuration.
- The width of the foot of the pole shoes can be calculated using the model such that an optimum is achieved between saturation of the yoke and available slot space for the copper. For motor C this optimum turned out to be about 0.35 of the head width for this specific case with zero current. The optimal width for certain load can be calculated by configuring a desired current. Taking a too small pole shoe foot gives saturation that causes drastically increased reluctance torque and deteriorated torque performance.
- The wider the magnets the higher the steepness. However at certain widths the reluctance torque is clearly higher. So the width of the magnets can be chosen such that a good trade-off between steepness and reluctance torque is achieved. Motor C has an optimal magnet width of about 0.65 of the pole distance for this configuration.
- The magnet height has a positive but saturating influence on the steepness and a proportional relation to the reluctance torque. This means that too short magnets clearly result in too low steepness, but too tall magnets result in too large reluctance torques. Dependent on the importance of both an optimum can be found.

The leakage flux due to a high pole shoe head is negligible compared to the airgap flux for the specific case of motor C. The influence of the head height on the saturation in the top of the head however could be an important restriction on the head width. A finite element package is needed to simulate this.

In following chapter attention is paid to the use of control to improve the motor performance.

6 PERFORMANCE IMPROVEMENT BY LEARNING CONTROL

Besides construction design the performance of a motor can be improved by using smart control. Especially torque ripples can be problematic when high accuracy is required. In this chapter a direct drive permanent magnet motor is modelled and simulated in 20sim. Because direct drive motors are directly coupled to the load, impurities in the motor torque will be fully transferred to the load. Therefore we will focus on the torque performance: the effect of a spiky motor constant and a large reluctance torque.

6.1 Plant model

The following generalized scheme shows a motor in closed loop. The reference produces a desired angle, the controller produces a voltage and the motor transforms this via a torque into an angle.

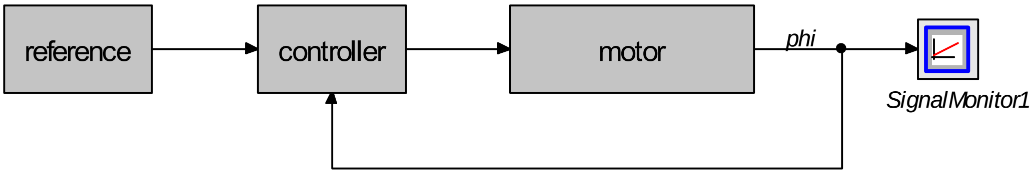

figure 49 simulation setup used to test the influence of design parameters on the controllability

Until now we worked with three phase motors. The motor model of chapter 3 calculates for example the motor constant per phase for a three phase motor. However in this setup the motor will be modelled as a DC motor for simplification, because we are interested in the influence of a spiky motor constant and the reluctance torque and not in the possible effects of phase shifts in the driving currents or encoder errors. A torque actuator adds the reluctance torque to the motor axis.

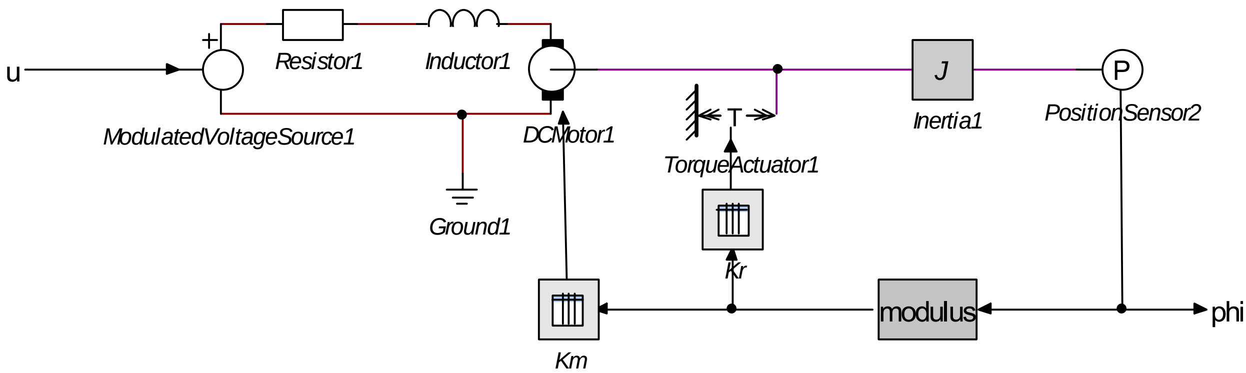

figure 50 motor model using Km and Kr calculated with the Matlab model of chapter 3 (R=1Ω, L=50mH, J=10kgm^2)

Both motor constant and reluctance torque depend on the angle of the motor axis. Their characteristics are calculated by the parametric motor model of chapter 3 and read directly from a *.mat* file using file input blocks. The input to the file input blocks is the motor angle. Since the motor constant and reluctance torque consist of a multiplicity (53) of periods of the same shape we use the modulus of the motor angle to this multiplicity to find the right value of the motor constant and reluctance torque in the lookup table. The motor we used in the simulations has a multiplicity of 8, because it has 8 pole pairs and 24 pole shoes.

As motor constant we use the root of the summed squares of the phase constants, which are calculated by the parametric model of chapter 3.

$$K_m = \sqrt{K_1^2 + K_2^2 + K_3^2} \tag{60}$$

This way the phases do not cancel out each other due to the phase shift of $2\pi/3$ and the spiky and nonlinear shape is retained.

The output of the file input blocks is shown in figure 51 as a function of the motor angle.

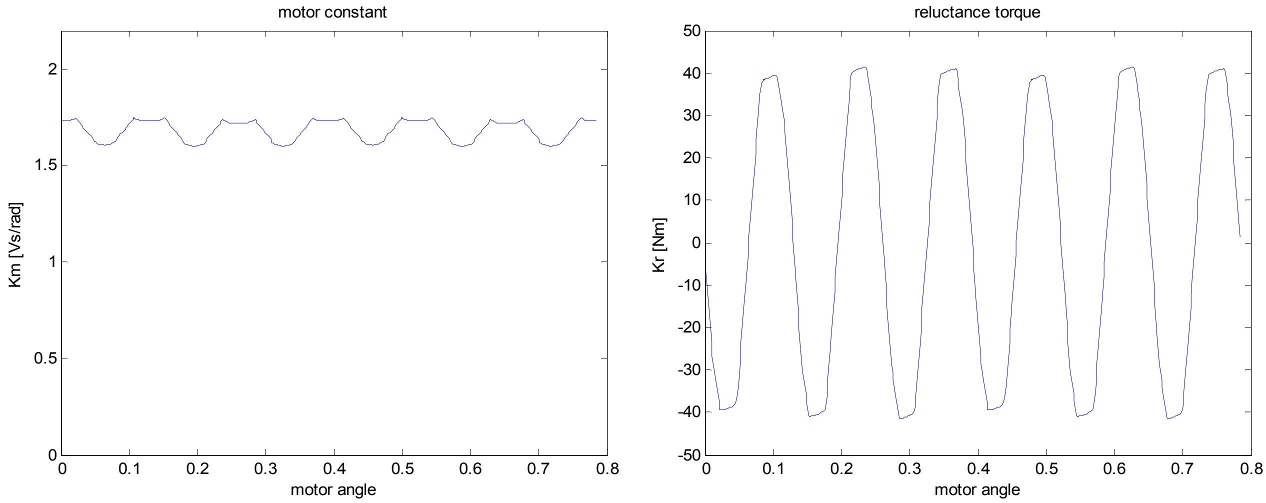

figure 51 file inputs: motor constant (left) and reluctance torque (right) as a function of the motor angle

To control the nonlinear plant a learning controller has been designed.

6.2 Controller with B-Spline network

The motor is controlled by a standard PID feedback controller assisted by a learning feedback controller (B-Spline network) to compensate the negative effects of reluctance torque and spiky motor constant which the PID cannot compensate for (see figure 52). A learning feedback instead of feed forward has been chosen because most likely the measured angle differs much from the set point due to the very nonlinear plant. Besides the error does not depend on the value of the set point, because the motor axis clearly stays in certain energetic preferable positions.

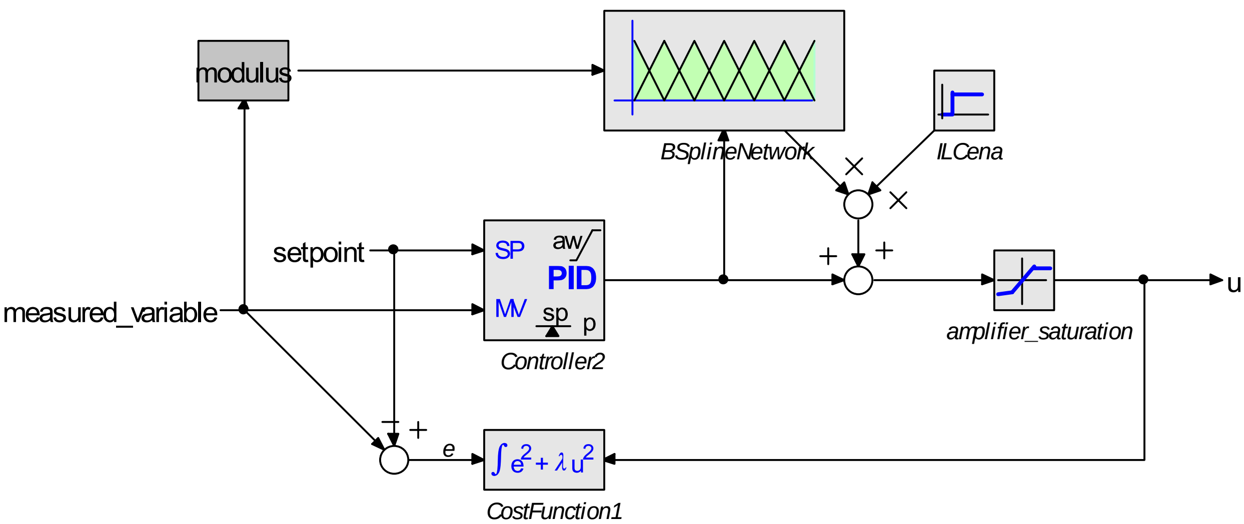

figure 52 controller: PID and a B-Spline network to compensate for the strong torque fluctuations due to reluctance torque and spiky motor constant.

The measured angle and reference set point are inputs of the PID controller. The anti windup function of the PID is set to the limits of the amplifier saturation, which is set to ±100V. Set point weighting is not used. The learning controller consists of a B-Spline Network[13] (BSN) having as inputs the modulus of the measured motor angle and the PID output. The sum of both outputs of the BSN and PID controller is limited by amplifier saturation. We have chosen to use the BSN because of its fast and easy learning mechanism, low computational cost and easy use.

As a measure for the performance a cost function is used:
$\int\left(e^2+\lambda u^2\right)dt$, where $\lambda=10^{-6}$, u is the final controller output, e equals set point minus measured angle.

The concept of learning control with a BSN is based on learning a relation between input values and required output values to minimize an error – in this case respectively the motor angle (input), voltage (output) and PID output (error). The error is used during the training process to adapt the output of the BSN network to. This way the BSN memorizes the PID output behaviour at certain motor angles.

The type of neural network determines the way the relation is stored and learned. In figure 53 the structure of a BSN is schematically drawn.

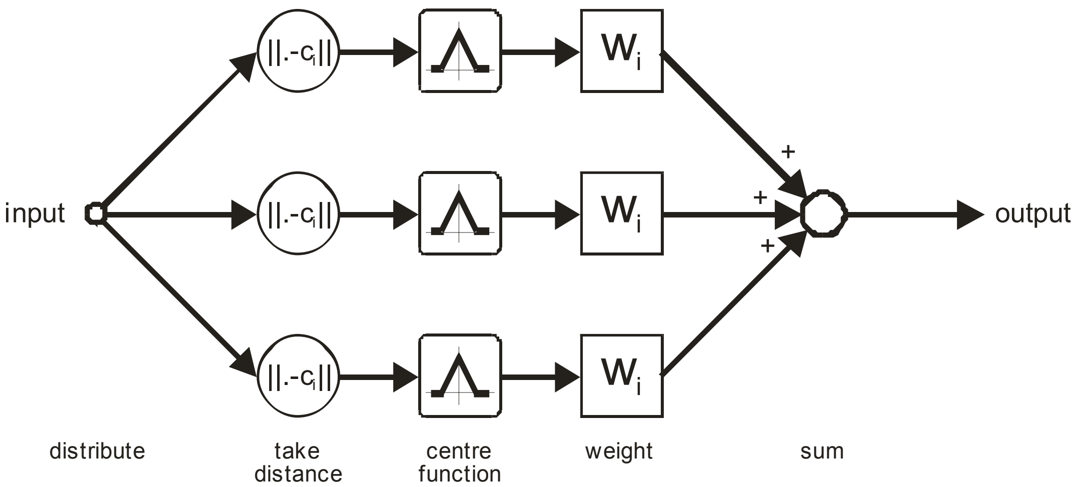

figure 53 working principle of a B-Spline neural network

The BSN consists of three layers: input, hidden and output layer. The input layer distributes the input signal to all neurons of the hidden layer. The hidden layer consists of a number of neurons, of which each is active within a specific part of the input range and of which each has its own contribution to the output of the BSN.

For each neuron a centre is defined on the input space around which the neuron is active with a centre function, a B-Spline in case of a BSN. The distribution of the neurons and their centre functions over the input space is illustrated in figure 54.

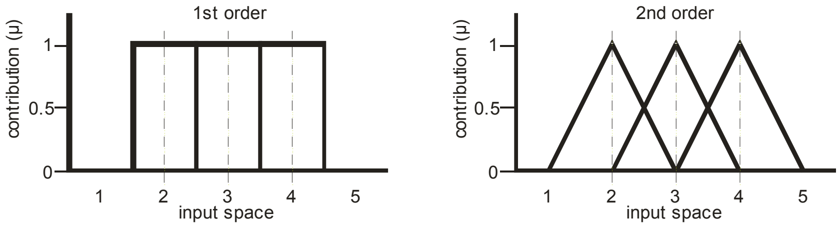

figure 54 Distribution of centre functions over the input space and their contributions

The distance of the input to the centre of a neuron in combination of the shape of the centre function determines the contribution (μ) of a neuron. More neurons can be active at the same input value depending on the order of the centre function. Their sum of contributions is always one. The total output of the BSN is the weighted sum of the contributions of all neurons.

Design parameters of a BSN are the B-Spline order, the number of B-Splines and their distribution over the input space (centres and widths).

The training algorithm of a BSN consists of the determination of the weights. If the centres and widths are chosen the change of weight *j* due to training sample *i* is defined by

$$\Delta w_j = \gamma \sum_i \left(y_{d,i} - y_i \right) \mu_j \left(x_{i,j} \right) \tag{61}$$

where w_j is the weight of the j^{th} neuron, γ is the learning rate, $y_{d,i}$ is the desired output, y_i is the BSN output, $\mu_j(x_{i,j})$ is the outcome of the centre function due to input x_i of the j^{th} neuron.

20sim is used to simulate the model with the BSN. In 20sim a BSN is easily configured using a setup screen (figure 55). The results are discussed in following paragraph.

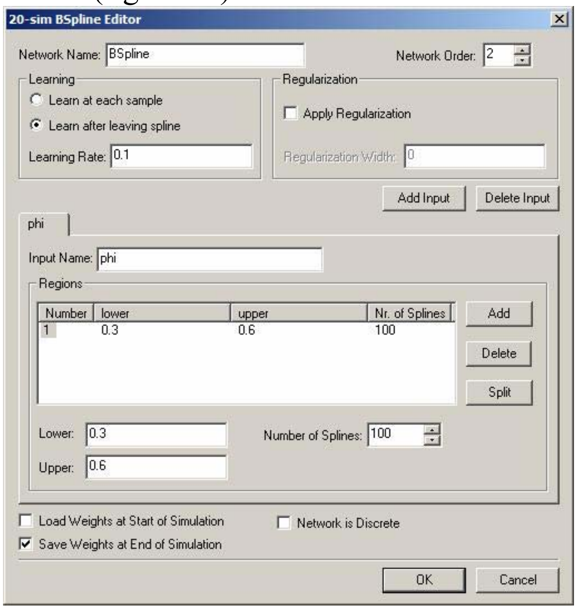

figure 55 setup screen for the BSN

6.3 Simulations

In this paragraph motor A (see chapter 4) will be simulated in closed loop without and with learning control for varying design parameters which influence the torque performance a lot. Two design configurations will be used: one with a pole shoes rotated torsion angle of 6° and one with 0°. Their motor constant and reluctance torque are shown in respectively figure 56 and figure 57. The motor constant is in DC format (60) and the reluctance torque is compared to the electrical torque to illustrate the order of magnitude of this disturbing torque. These figures are calculated using the parametric model made in paragraph 3.2.

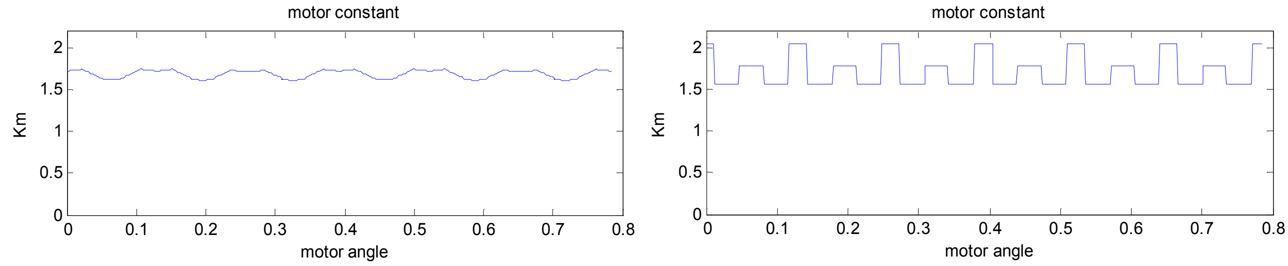

figure 56 motor constant for torsion angles of 6° (left) and 0° (right)

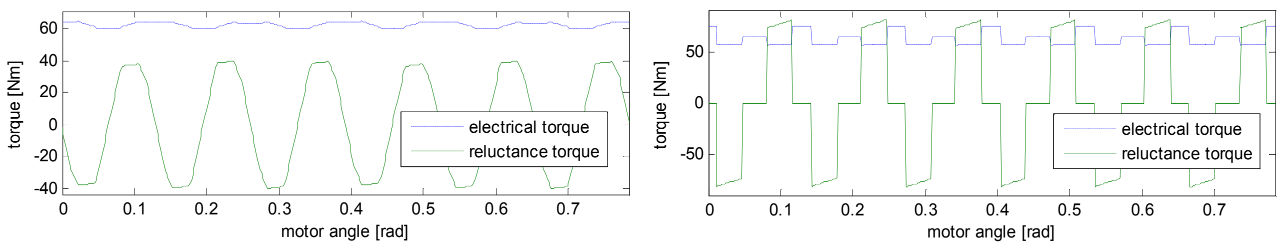

figure 57 reluctance torque compared to electrical torque (30A) for torsion angles of 6° (left) and 0° (right)

The performance of both motor configurations for both controllers is simulated in two applications:

- Servo application where the reference quickly goes to one single (electromagnetic) energetic undesired angle and stays at that angle for a few seconds. This is to compare the achievable accuracy of both motors under influence of high reluctance torques and a spiky motor constant.
- Tracking application where the reference rotates the full 360° – modulus the multiplicity of the motor, see paragraph 6.1 – very slowly, passing all energetic undesired angles. The input range of the learning controller has to be adjusted for this application. Interesting to know is whether the motors stay controllable with a reasonable amount of B-Splines if the whole range has to be covered.

To assure consistency of the weights calculated with the above conditions the simulations are verified with a pulsed ramp.

For each motor configuration and simulated application the PID and B-Spline settings are optimized for the cost function output. This way the effect of the construction design parameters and control method on the maximum achievable performance can be compared.

To illustrate the effect of a torsion angle on the controllability on the one hand and to show the improvement of adding a learning controller on the other hand the results of a pulsed ramp are shown below for both motor configurations. Starting with only a PID controller (figure 57) the motors have to follow a ramp with pulses, passing several energetic unpleasant angles in which the motor hardly stays. Due to large fluctuations in reluctance torque, which disturb the motor axis, the controller has a heavy job to follow the reference. Besides that the motor constant is spiky and fluctuates as well. In figure 58 the performance of the PID controller is shown for the motor with (6°) and without (0°) torsion angle (TA).

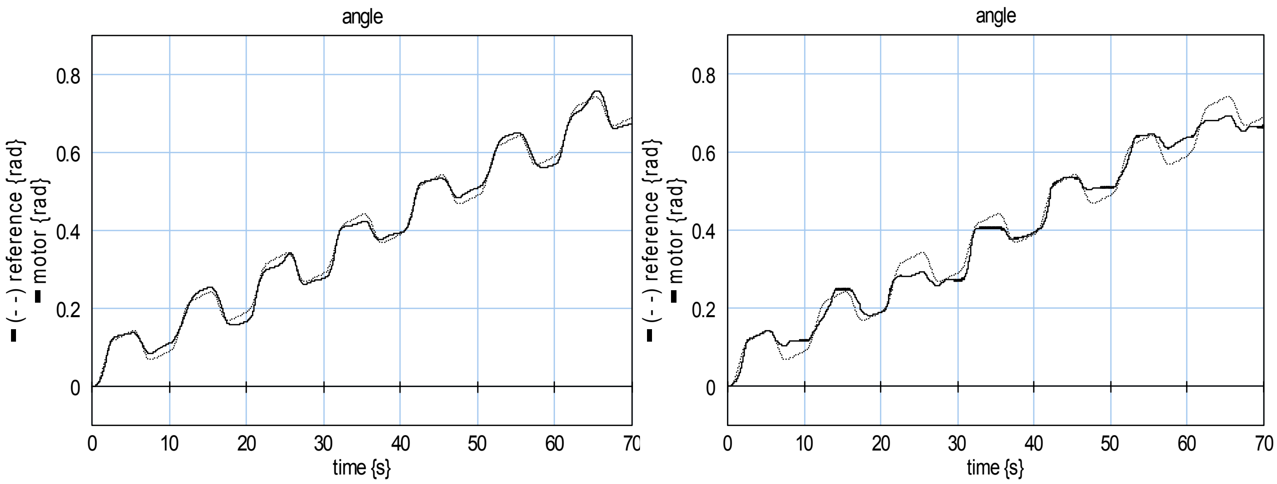

figure 58 PID only: reference and motor angle for 6° (left) and 0° (right) torsion angle

As can be seen the PID controller is able to let the 6° TA follow the reference without too much deviations, but the 0° TA deviates much more. Now the B-Spline network is enabled (figure 59).

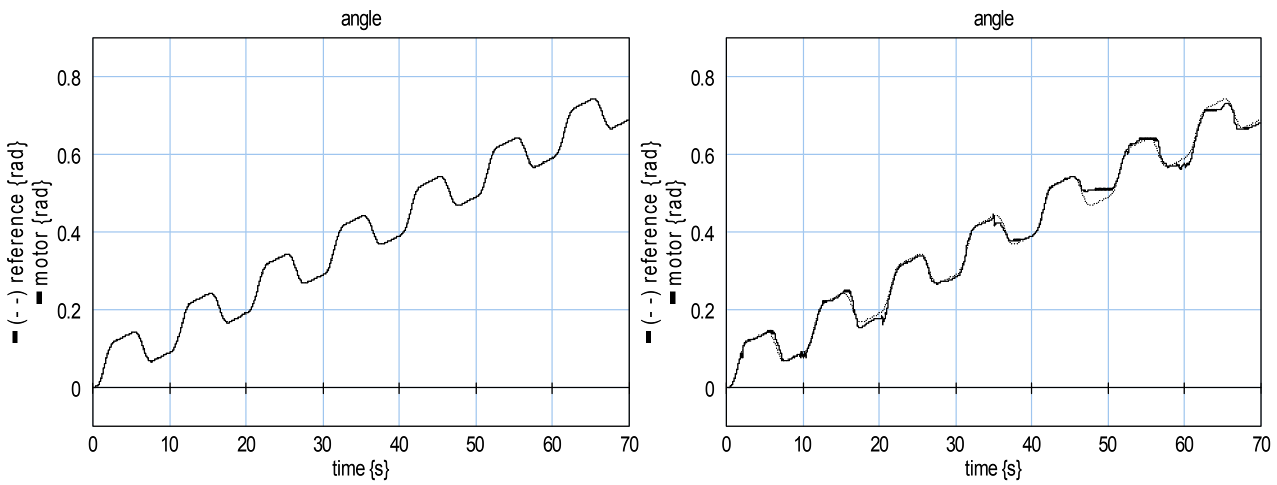

figure 59 PID+B-Spline: reference and motor angle after training for 6° (left) and 0° (right) torsion angle

With enabled B-Spline network the 6° TA follows the reference perfectly. The 0° TA is also improved but still contains deviations. As stated before the errors are weighted by a cost function. The results of the cost functions for all different setups and motor configurations are shown in table 5. More results with other reference signals are shown in Appendix B.

table 5 performance measured by the cost function (mean cost function over time)

application	TA	mean cost function	
		PID only	PID+BSN
Servo	0°	4,2E-03	2,3E-03
	6°	2,7E-03	1,0E-03
Tracking 360°	0°	3,4E-03	2,7E-03
	6°	1,1E-03	5,1E-06
Pulsed ramp	0°	3,0E-03	2,7E-03
	6°	4,6E-04	3,8E-06
Mean	0°	3,5E-03	2,6E-03
	6°	1,4E-03	3,5E-04

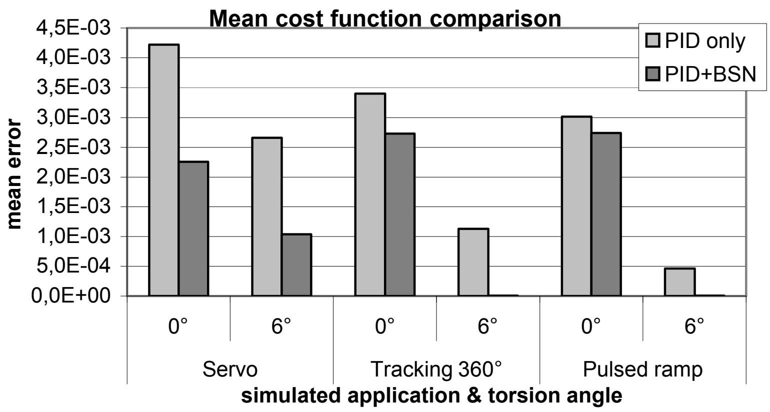

6.4 Conclusions of control

In this chapter a comparison has been made between two motor configurations in closed loop: one with and one without pole shoe torsion angle. Per motor two controllers have been applied and their performance is compared: firstly only a PID controller was used, secondly a B-Spline network was added. For modelling the motor specific characteristics of motor constant and reluctance torque have been used, calculated by the parametric model of chapter 3.

Both motors clearly have energetic preferable angles due to the reluctance torque and motor constant. This causes large errors when the motor has to follow a reference crossing these angles several times. The PID controller is not able to let both motors follow the reference accurately. Adding a learning controller improves the accuracy a lot.

As expected the motor without torsion angle is hard to control due to large spikes in the motor constant and very sudden changes and large amplitudes of the reluctance torque. The performance of the motor with torsion angle is much better. The performance is compared by a cost function that takes both error and steering signal into account.

The results can be summarized as follows. Compared to the motor without torsion angle controlled by a PID controller the performance was improved by

- 25% by adding a B-Spline network to the PID controller
- 60% by using a 6° torsion angle
- 90% by adding a B-Spline network and using a 6° torsion angle

7 CONCLUSIONS

7.1 Conclusions

A parametric electromagnetic model for three phase direct drive permanent magnet motors has been designed and used to simulate the effects of construction design parameters on the torque performance in terms of steepness and reluctance torque. The model calculates the motor properties based on the design parameters and calculates the produced electric and reluctance torque as functions of the rotor angle, while taking saturation into account. Due to the generalized algebraic structure it is possible to simulate any combination of pole shoes, magnet poles and coils. The model has been validated against three different motors. For a specific motor the design parameters has been varied and their influence on the torque performance has been simulated.

Also a closed loop motor model has been made using calculation results of the electromagnetic model to describe the motor constant and reluctance torque. The performance improvement of adding a B-Spline network to a common PID controller has been simulated for a motor with and without torsion angle in the pole shoes. According to the simulations both torsion angle and B-Spline network drastically increase the performance compared to a single PID controller.

7.2 Recommendations

The equivalent circuit of the electromagnetic model consists of a limited amount of elements, of which each represents a part of the motor. Dividing the motor into more parts would increase the accuracy of the model. Moreover the current model assumes the flux always to follow a straight path. This results in discrete transitions in the flux calculations when rotor and stator move along each other. In practice the existence of flux leakage on the edges of the pole shoes would soften the transitions resulting in a smoother motor constant and reluctance torque. To take these effects into account and for obtaining a more accurate model representation a finite element method should be used.

In future work the output of the electromagnetic model could be used for simulating several different permanent magnet motors, for example when testing the performance of learning controllers.

APPENDIX A: SIMULATION RESULTS CONSTRUCTION DESIGN

Appendix A has the same structure as chapter 5 and shows more detailed simulation results of the variation of design parameters and its influence on the motor performance.

Diameter

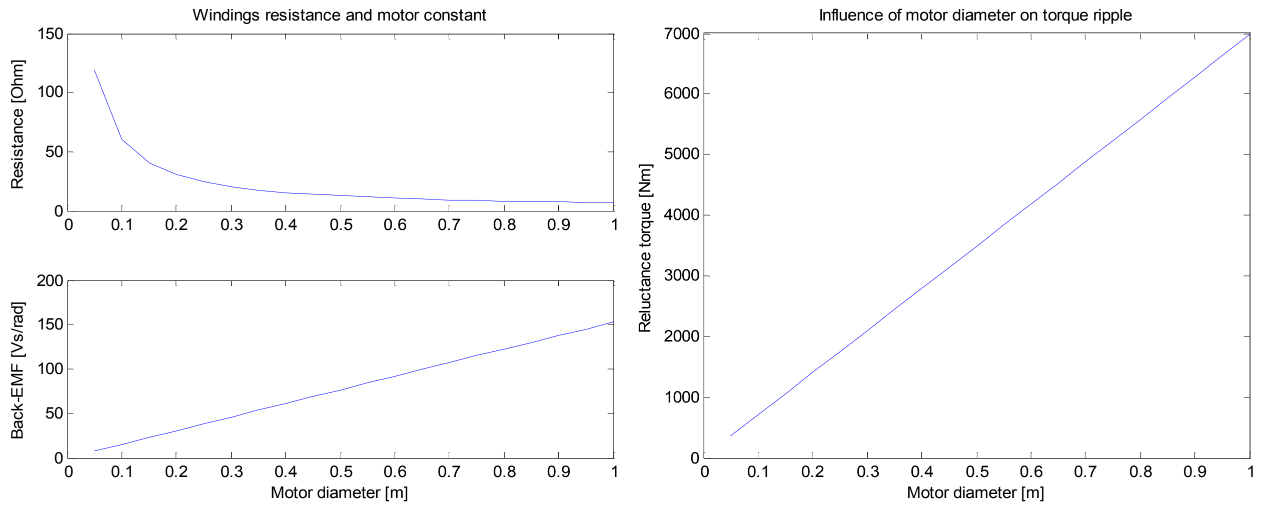

figure 60 resistance and back-emf (left) and reluctance torque (right) for varying motor diameter

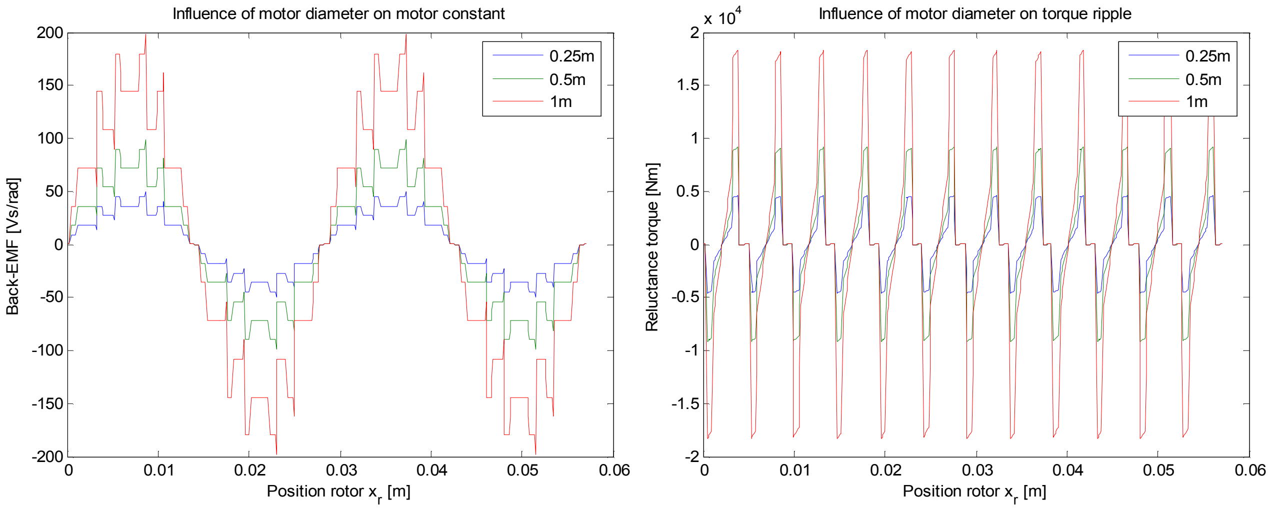

figure 61 back-emf (left) and reluctance torque (right) for three different motor diameters

Length

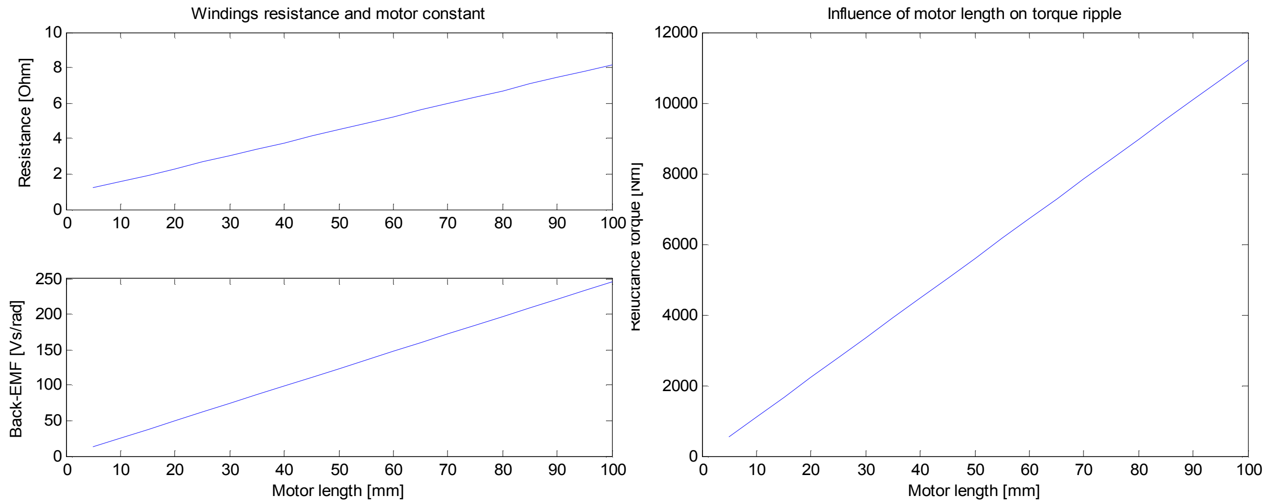

figure 62 resistance and back-emf (left) and reluctance torque (right) for varying motor length

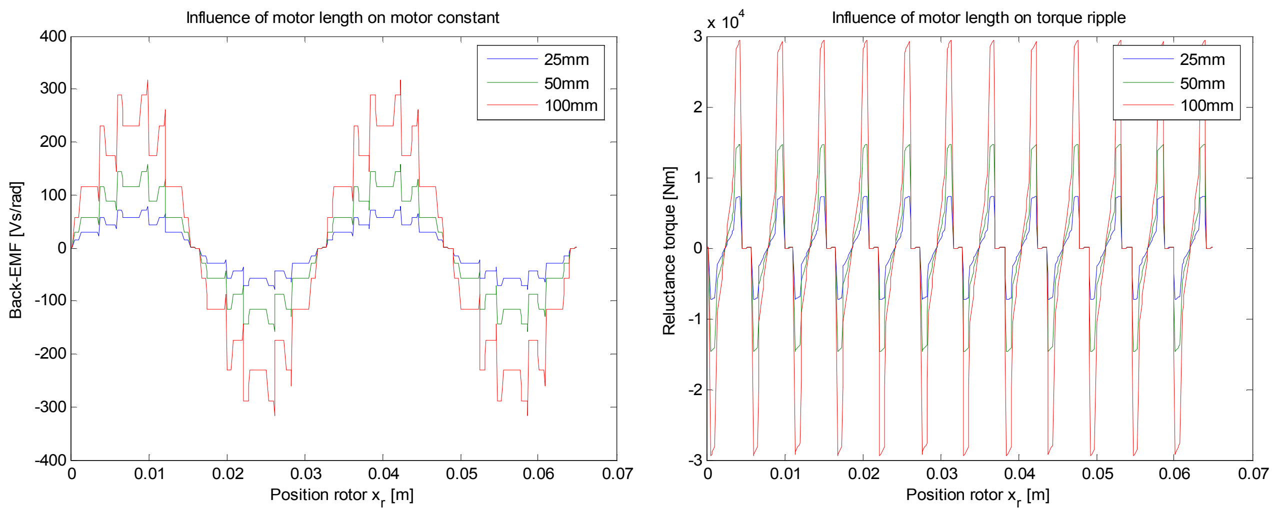

figure 63 back-emf (left) and reluctance torque (right) for three different motor lengths

Number of magnet pole pairs and pole shoes

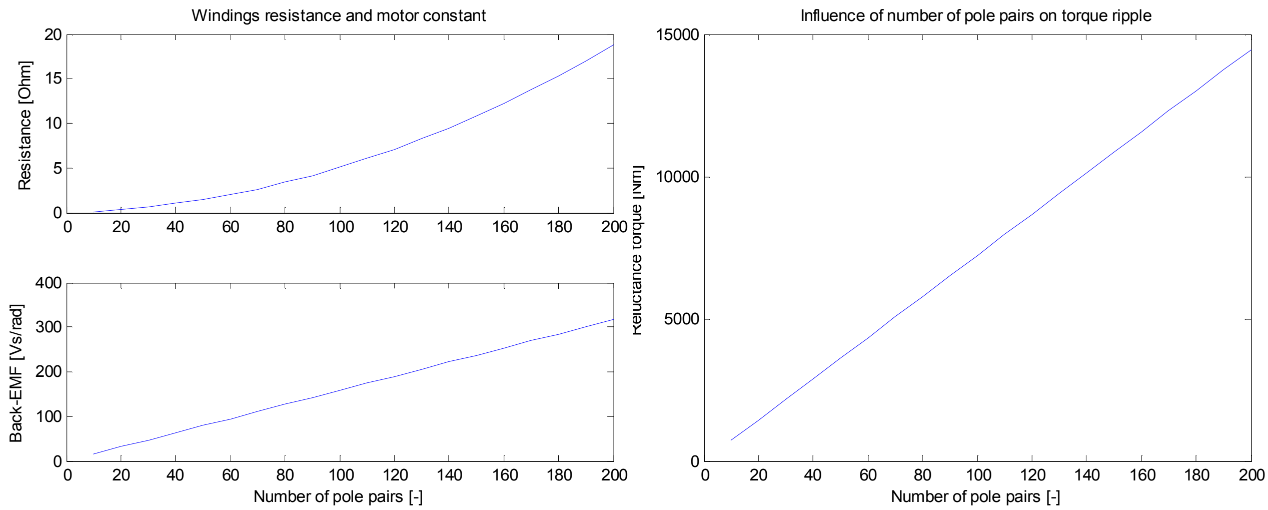

figure 64 resistance and back-emf (left) and reluctance torque (right) for varying number of magnet pole pairs

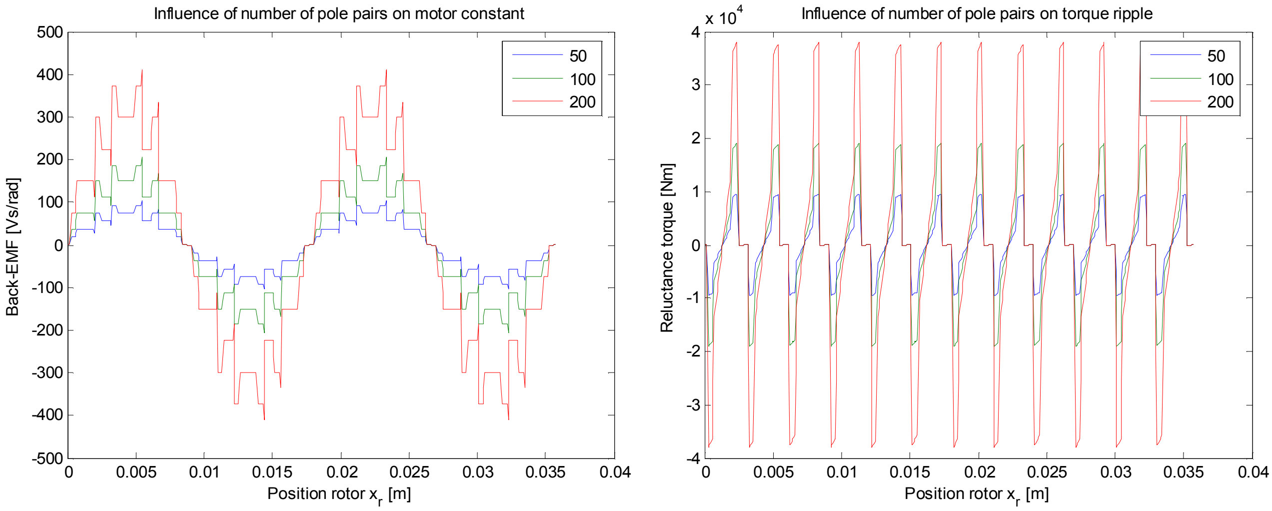

figure 65 back-emf (left) and reluctance torque (right) for three different numbers of magnet pole pairs

Airgap height

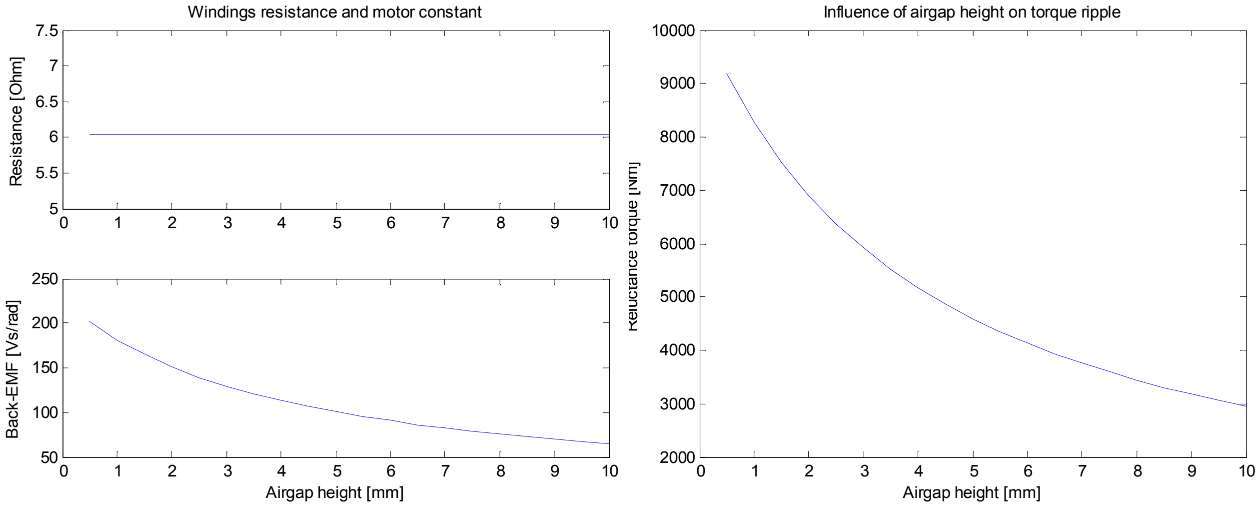

figure 66 resistance and back-emf (left) and reluctance torque (right) for varying airgap height

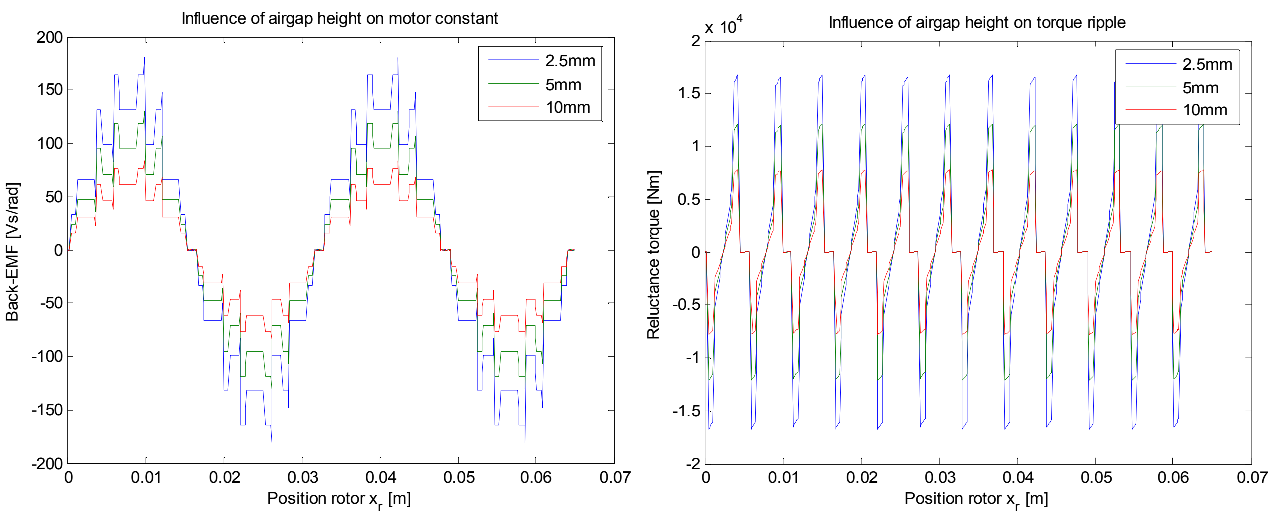

figure 67 back-emf (left) and reluctance torque (right) for three different airgap heights

Torsion angle pole shoe

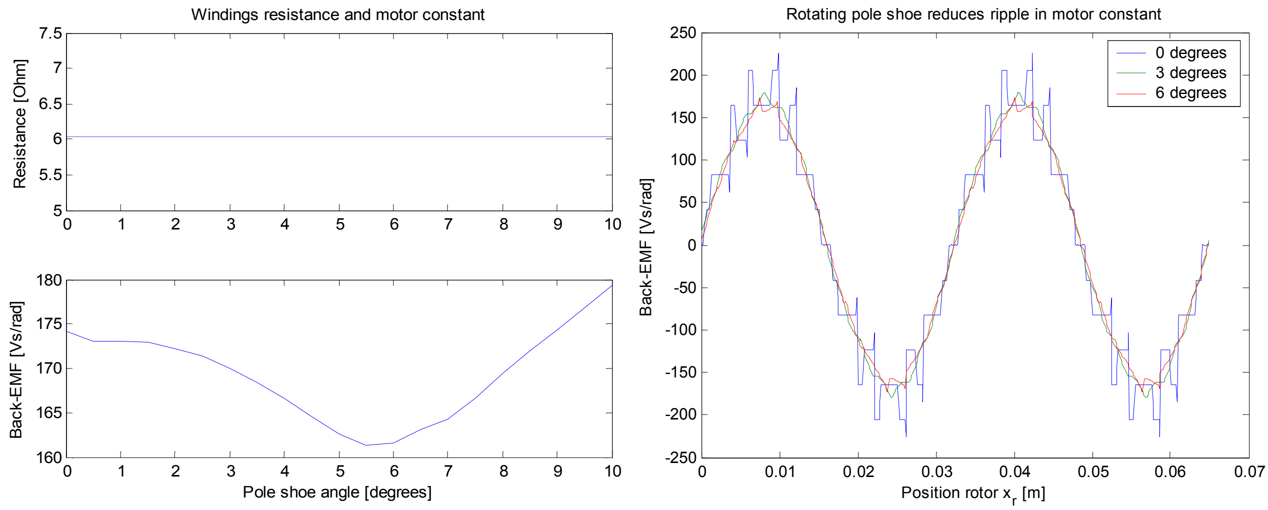

figure 68 resistance and back-emf (left) for varying torsion angle and back-emf for three different angles (right)

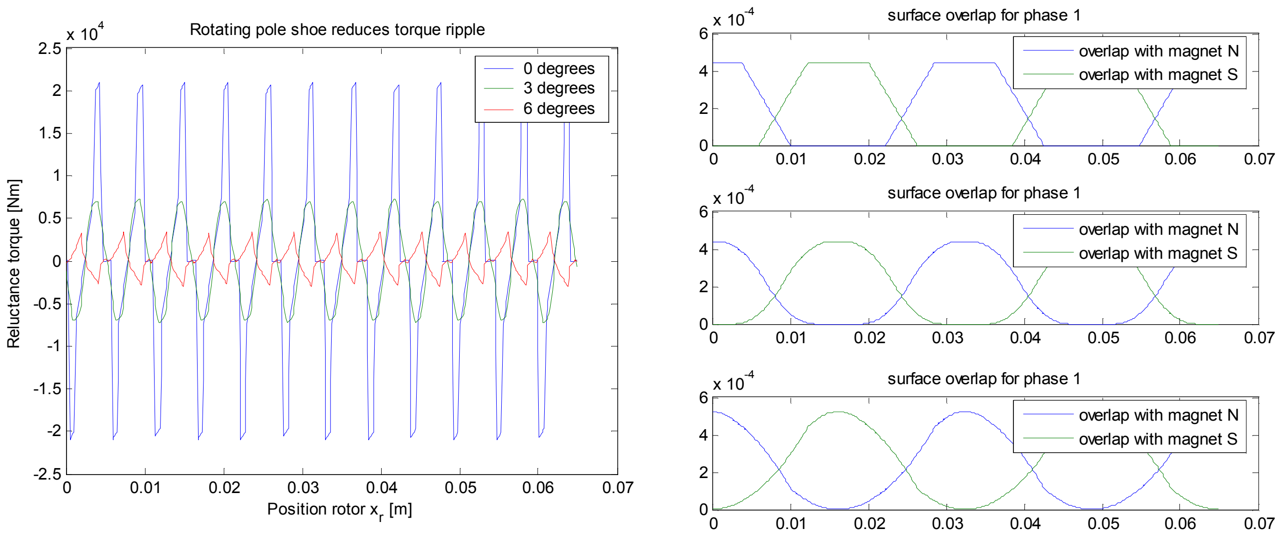

figure 69 reluctance torque for three different torsion angles (left) and overlapping surfaces between magnets and all pole shoes of phase 1 for three different torsion angles: 0°, 5° and 10° (right) illustrating the smoothness but also harmonic distortion at higher angles

Foot width

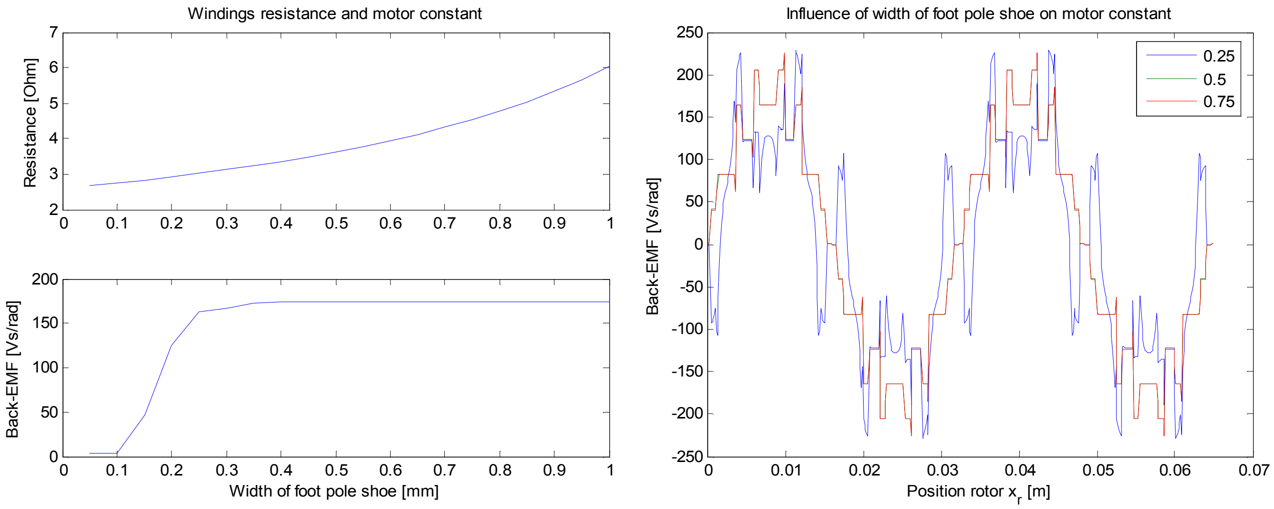

figure 70 resistance and back-emf (left) for varying foot width and back-emf for three different foot widths (right). Foot width is expressed relative to the absolute head width.

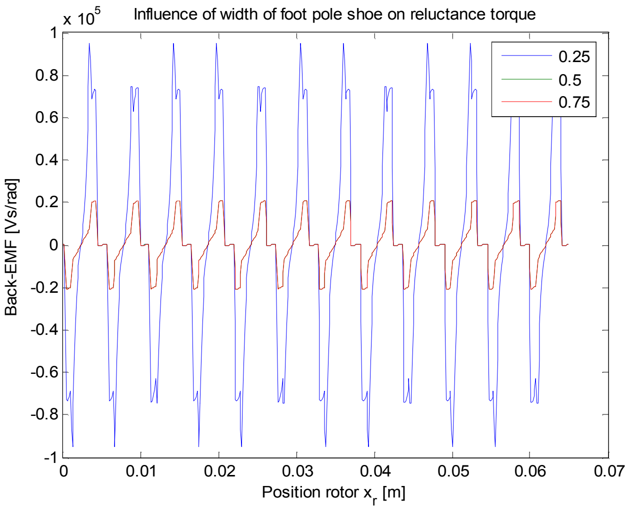

figure 71 reluctance torque for three different head widths. Distortion due to saturation causes a large reluctance torque at small foot widths

Head width

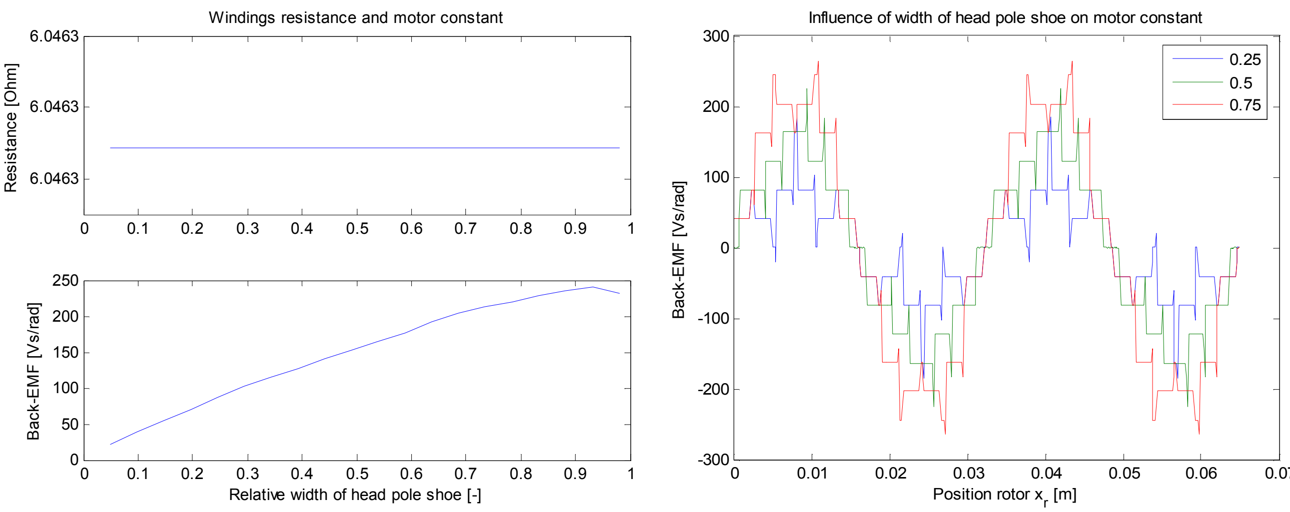

figure 72 resistance and back-emf (left) for varying head width and back-emf for three different head widths (right). Head width is expressed relative to the distance between the centres of two pole shoes.

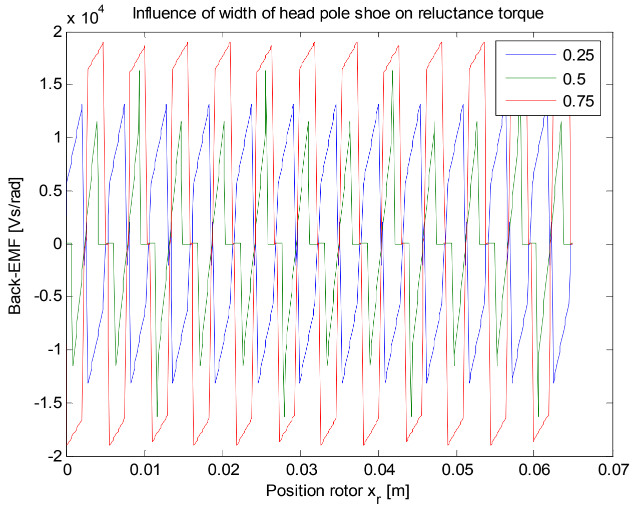

figure 73 reluctance torque for three different head widths

Head height

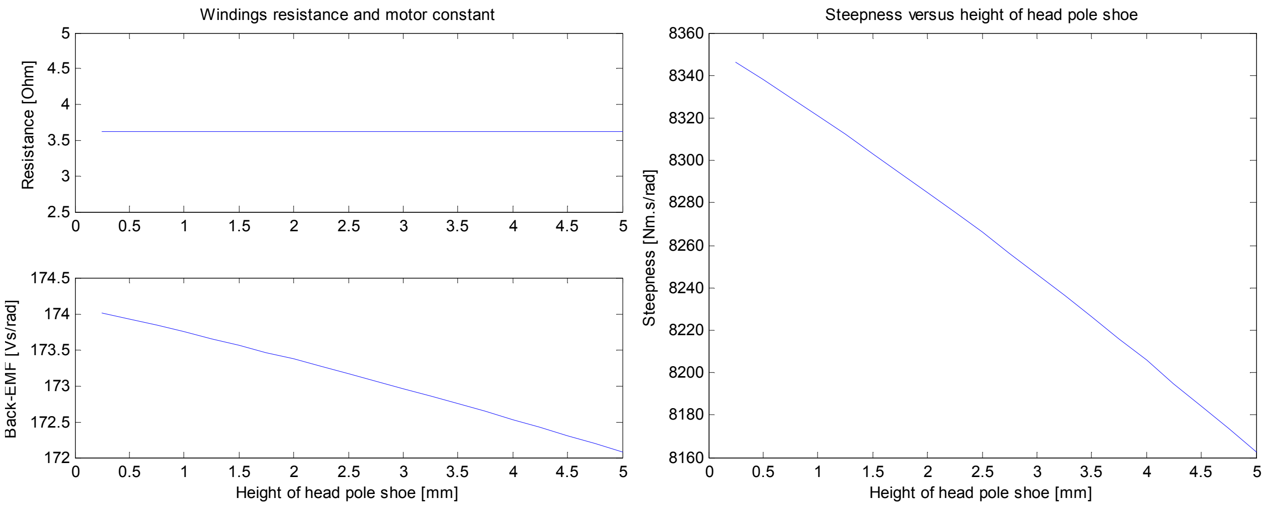

figure 74 resistance and back-emf (left) and steepness (right) for varying pole shoe head height

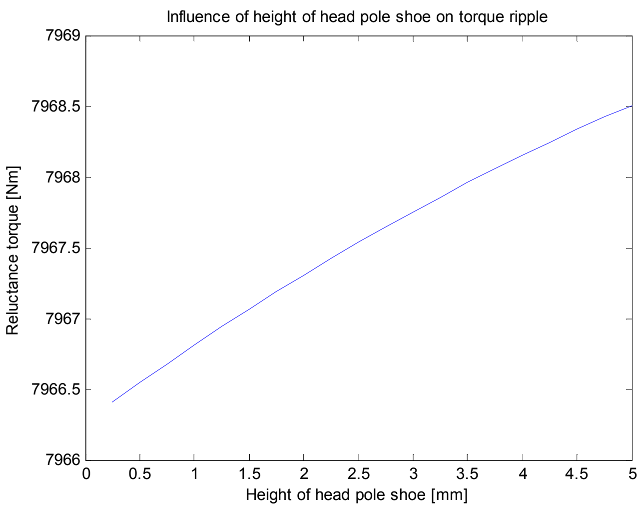

figure 75 reluctance torque for varying pole shoe head height

Torsion angle magnets

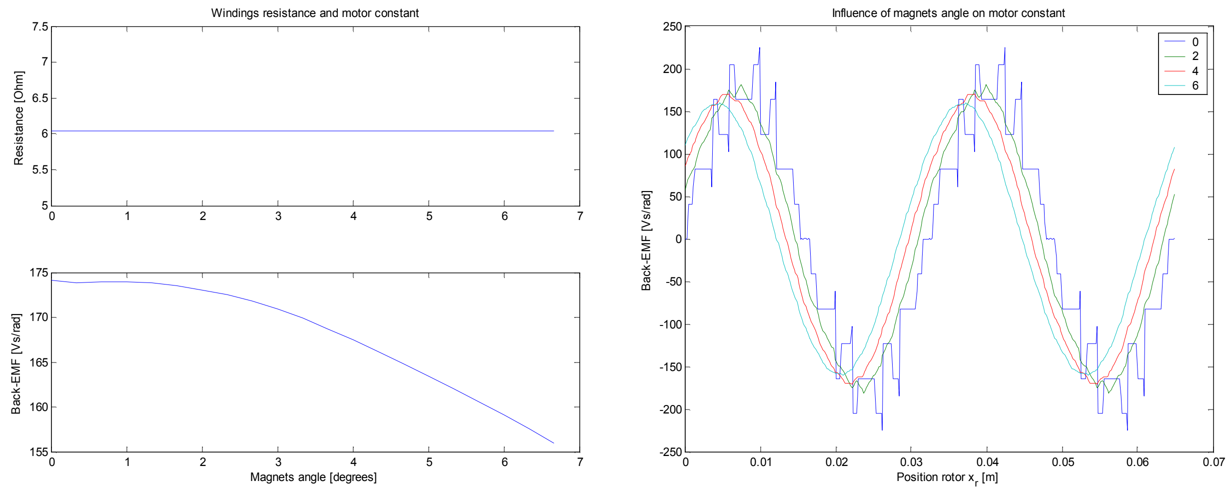

figure 76 resistance and back-emf (left) for varying magnet angle and back-emf for three different angles (right)

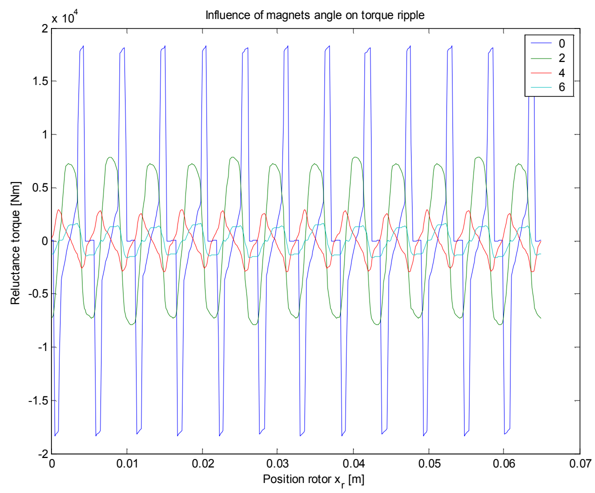

figure 77 reluctance torque for three different magnet angles

Magnet width

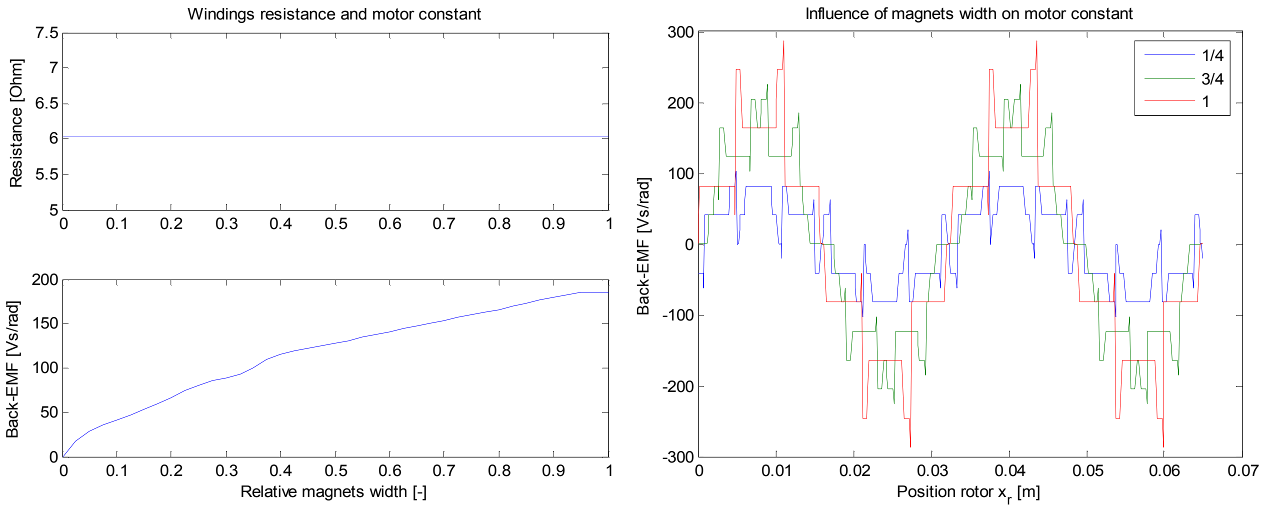

figure 78 resistance and back-emf (left) for varying magnet width and back-emf for three different widths (right). Magnet width is expressed relative to the pole distance (between centres of magnets).

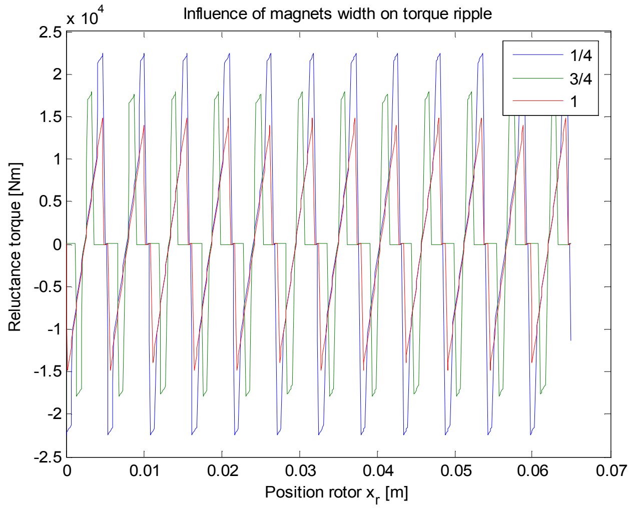

figure 79 reluctance torque for three different magnet widths

Magnet height

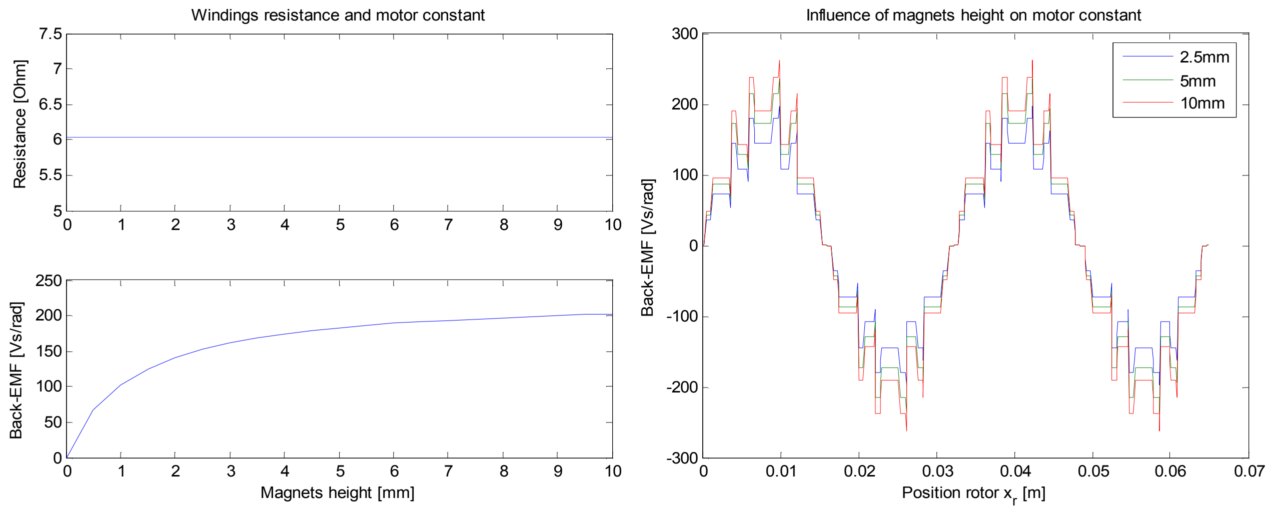

figure 80 resistance and back-emf (left) for varying magnet height and back-emf for three different heights (right)

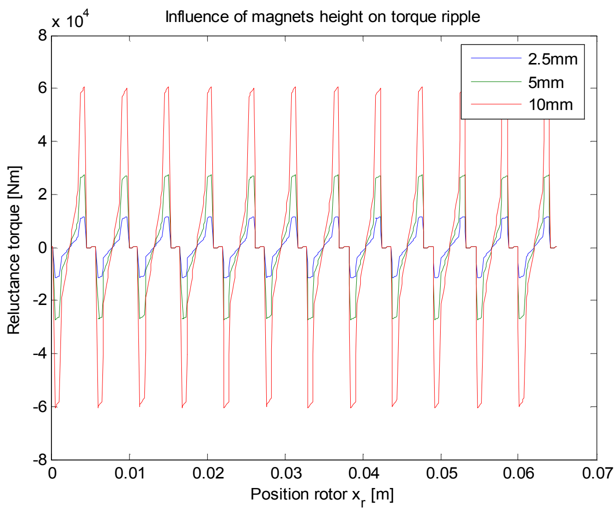

figure 81 reluctance torque for three different magnet heights

APPENDIX B: SIMULATION RESULTS LEARNING CONTROL

This appendix consists of additional simulation results of chapter 6 “Performance improvement by learning control”.

Learning control is compared to PID control applied on motor A in two configurations: with and without torsion angle. Consecutively the results of the repetitive pulse (servo), slow ramp (tracking) and pulsed ramp (for consistency check) are shown.

Servo application: repetitive pulse

<u>6° torsion angle</u>
PID: k=342, τ_d=1.65, N=250, τ_i=39, τ_a=20, limit=±100
B-Spline: order=2, learning rate=0.1, splines=100, input range=0.3 - 0.6

<u>0° torsion angle</u>
PID: k=1000, τ_d=0.95, N=250, τ_i=39, τ_a=20, limit=±100
B-Spline: same as with 6° torsion angle

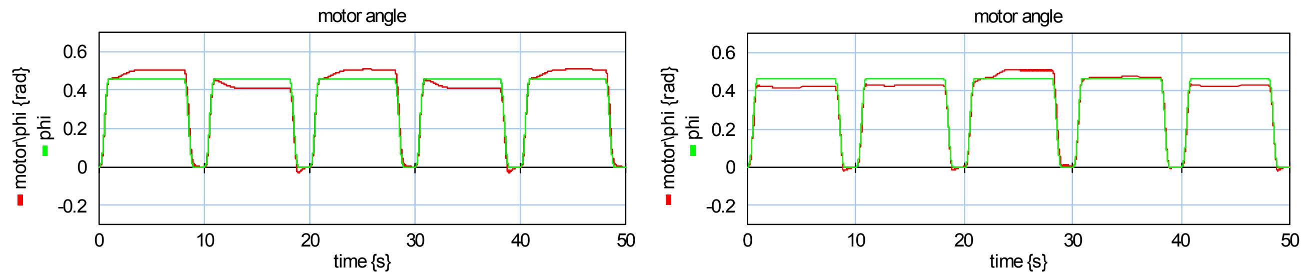

figure 82 PID only: motor angle and reference for 6° (left) and 0° (right) torsion angle

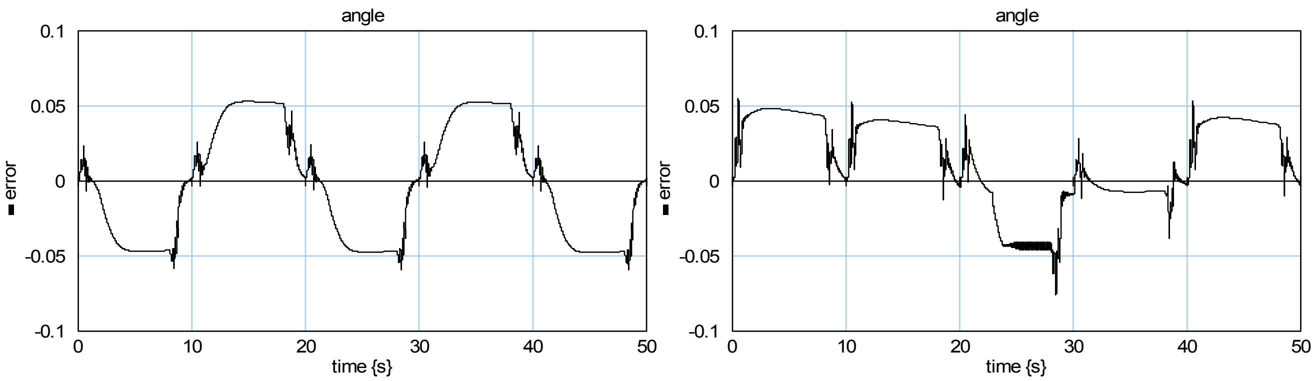

figure 83 PID only: error for 6° (left) and 0° (right) torsion angle

The motor clearly stays in its preferential positions. Outputs of the cost function after 50 seconds for 6° and 0° torsion angles are respectively 0.133 and 0.211.

Training the B-Spline network around one (electromagnetic) energetic undesired angle:

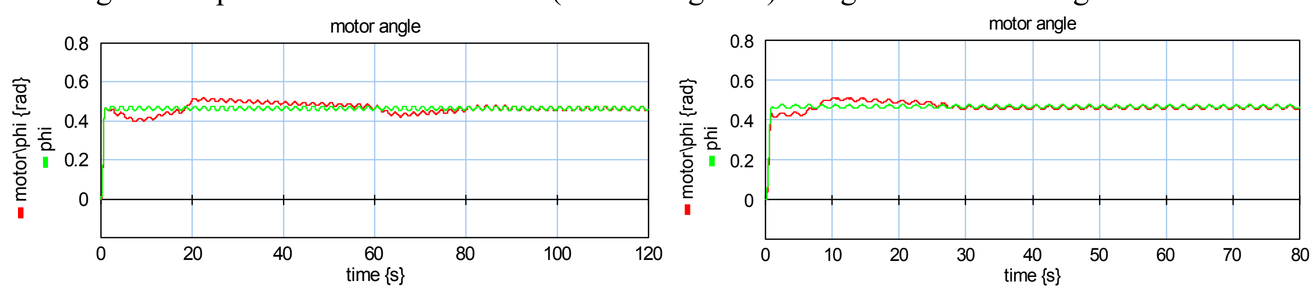

figure 84 PID+B-Spline: reference and motor angle during training process for 6° (left) and 0° (right) torsion angle

Performance after training:

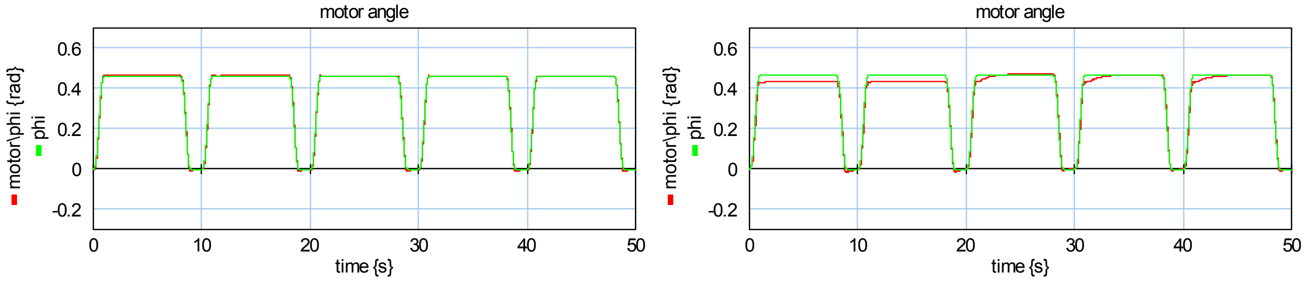

figure 85 PID+B-Spline: reference and motor angle after training for 6° (left) and 0° (right) torsion angle

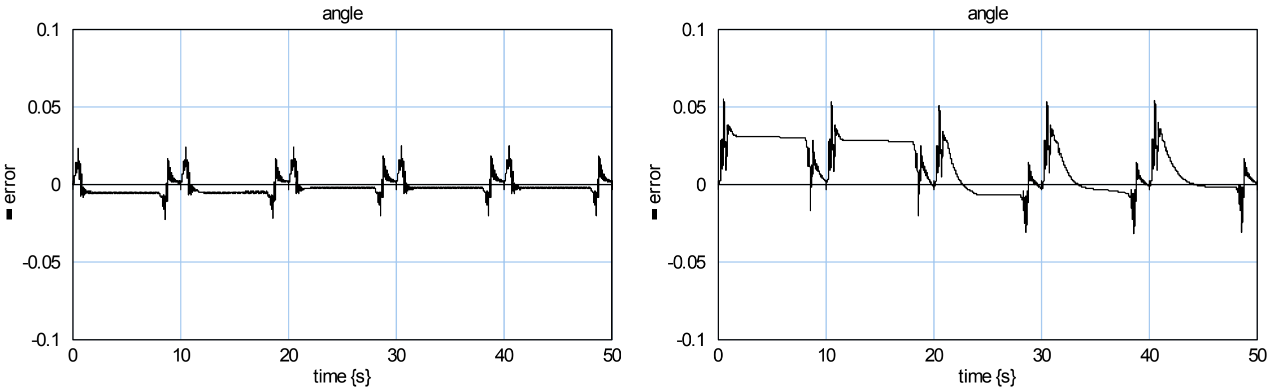

figure 86 PID+B-Spline: error after training for 6° (left) and 0° (right) torsion angle

With 6° torsion angle the preferential positions are overruled, however with 0° even the learning controller has problems keeping the motor angle at the energetic undesired reference level, due to the large reluctance torque. Outputs of the cost function after 50 seconds for 6° and 0° torsion angles are respectively 0.0518 and 0.113.

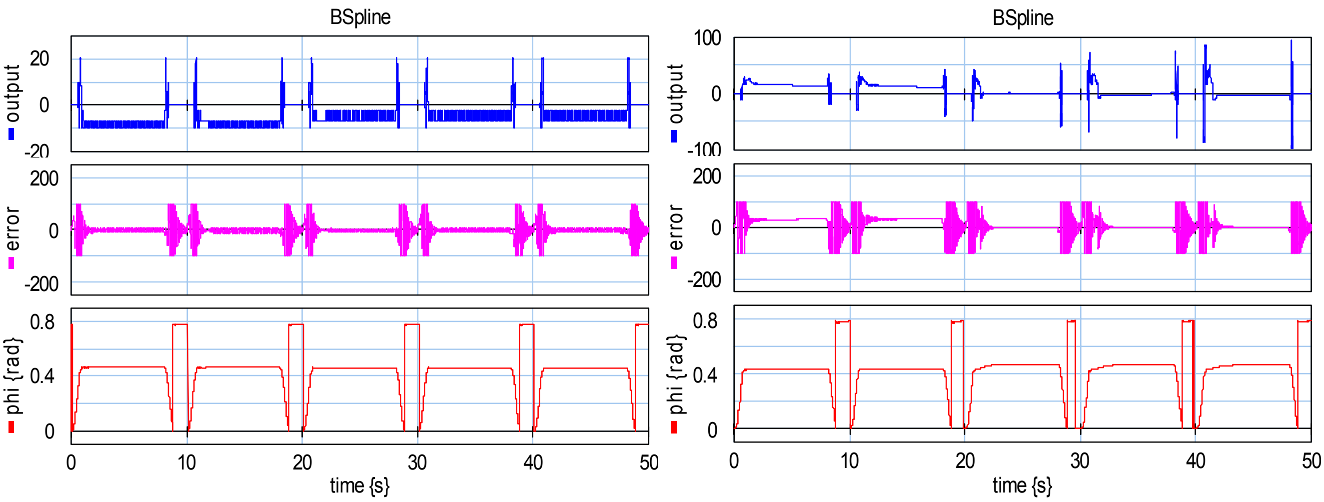

figure 87 B-Spline network I/O for torsion angle of 6° (left) and 0° (right)

360° tracking application

6° torsion angle

PID: k=342, τ_d=1.65, N=250, τ_i=39, τ_a=20, limit=±100
B-Spline: order=2, learning rate=0.1, splines=100, input range=0.0 - 0.8

0° torsion angle

PID: k=1000, τ_d=0.95, N=250, τ_i=39, τ_a=20, limit=±100
B-Spline: order=1, learning rate=0.2, splines=200, input range=0.0 - 0.8

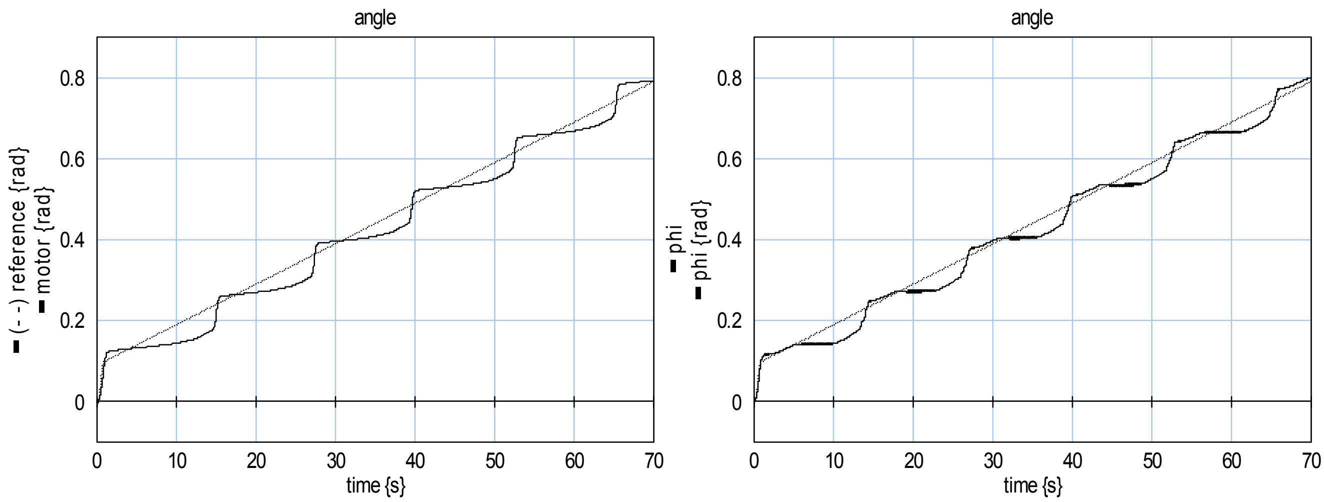

figure 88 PID only: reference and motor angle for 6° (left) and 0° (right) torsion angle

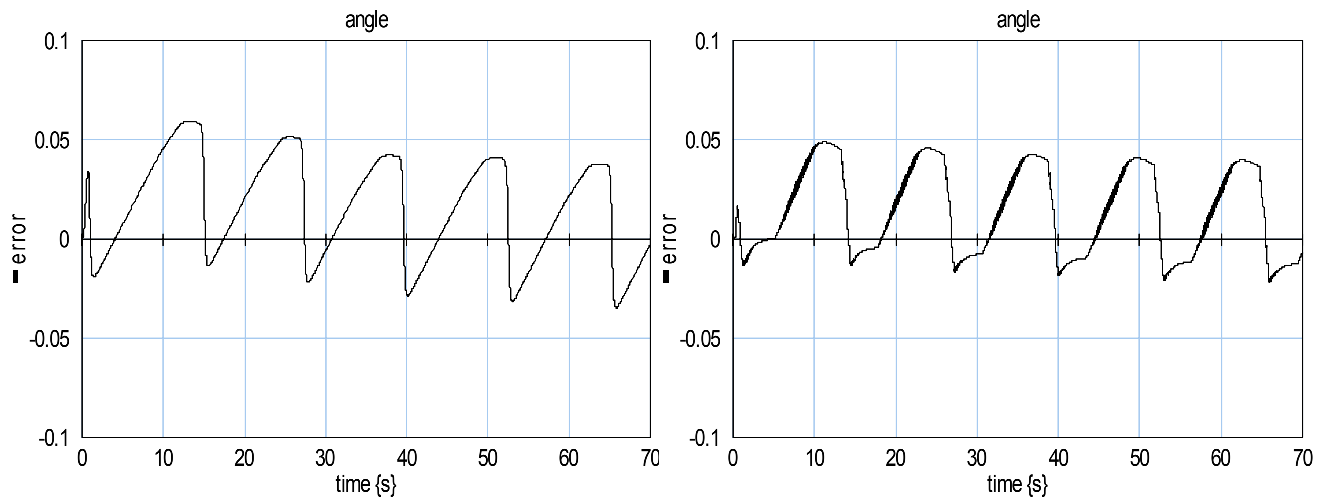

figure 89 PID only: error for 6° (left) and 0° (right) torsion angle

Outputs of the cost function after 70 seconds for 6° and 0° torsion angles are respectively 0.079 and 0.238.

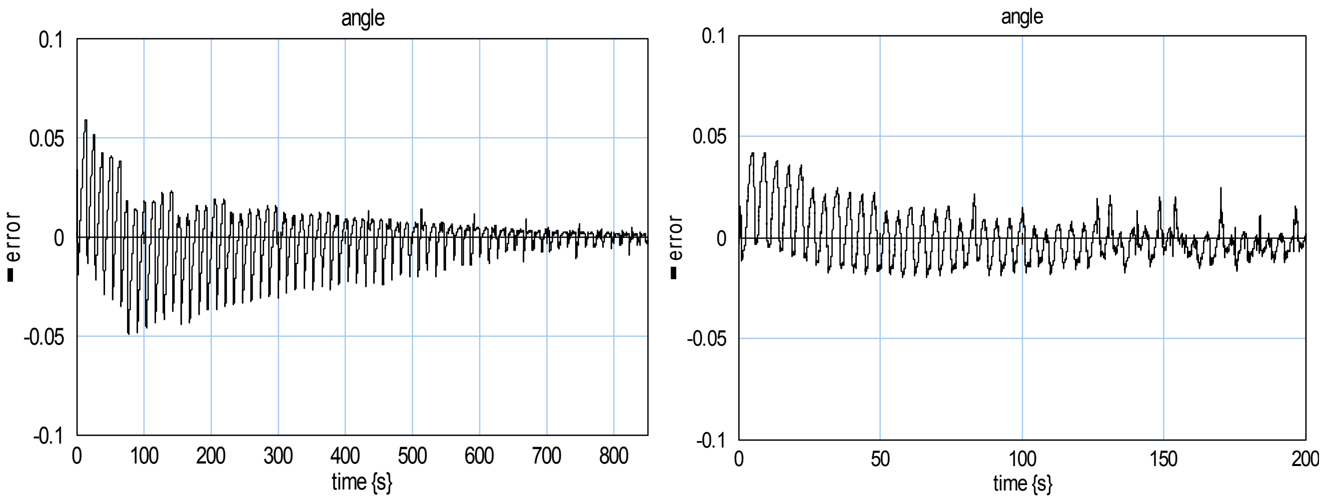

figure 90 PID+B-Spline: error during training process for 6° (left) and 0° (right) torsion angle

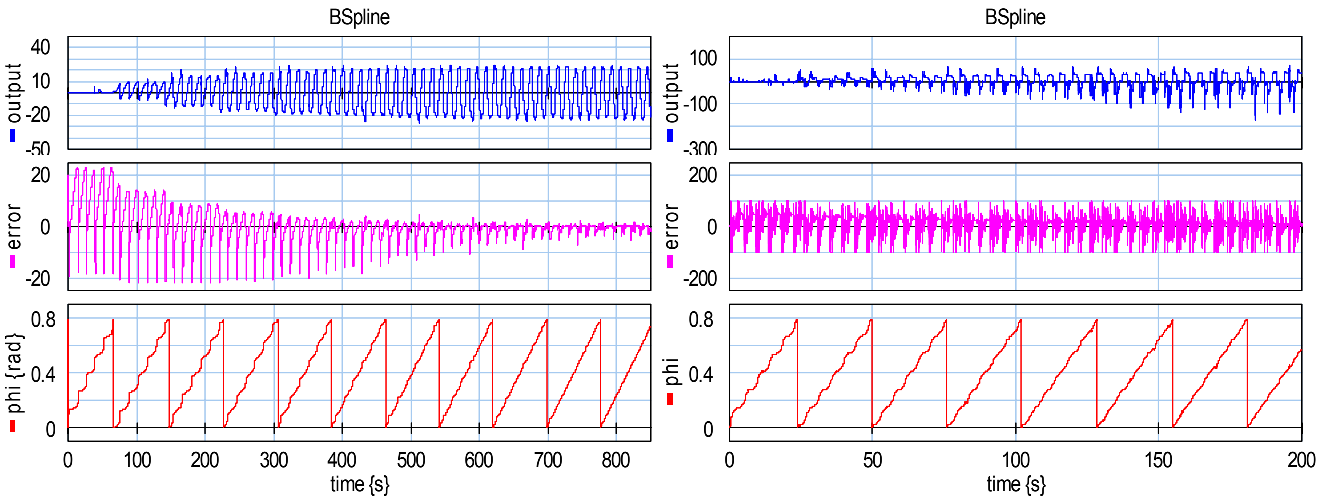

figure 91 B-Spline I/O during training process for 6° (left) and 0° (right) torsion angle

Performance after training:

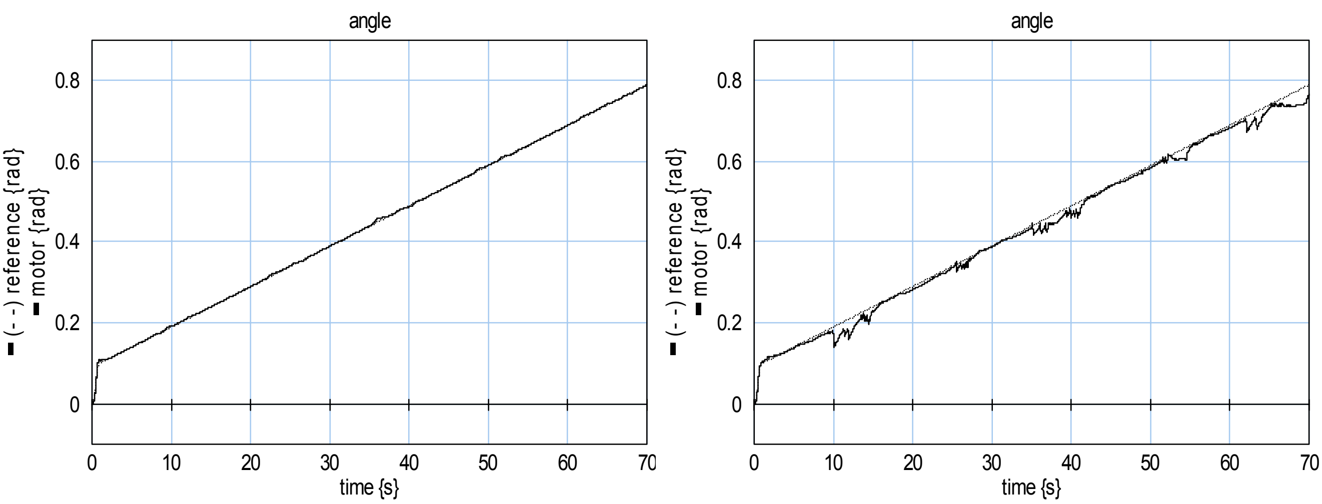

figure 92 PID+B-Spline: reference and motor angle after training for 6° (left) and 0° (right) torsion angle

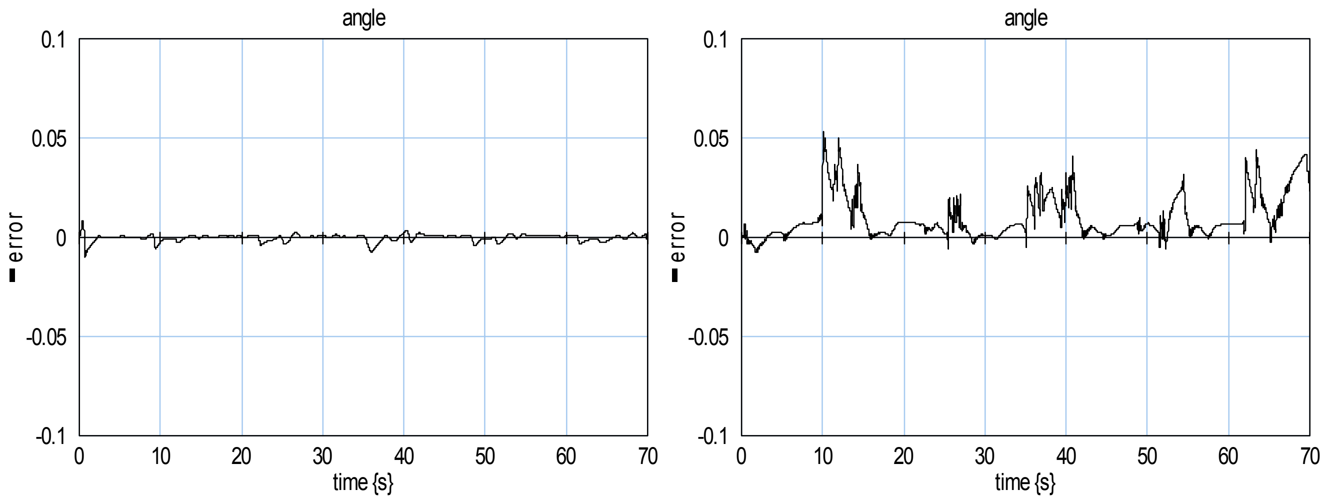

figure 93 PID+B-Spline: error after training for 6° (left) and 0° (right) torsion angle

Outputs of the cost function after 70 seconds for 6° and 0° torsion angles are respectively 0.000359 and 0.191.

Pulsed ramp

<u>6° torsion angle</u>
PID: k=1000, τ_d=0.95, N=250, τ_i=39, τ_a=20, limit=±100
B-Spline: order=2, learning rate=0.1, splines=100, input range=0.0 - 0.8

<u>0° torsion angle</u>
PID: k=1000, τ_d=0.95, N=250, τ_i=39, τ_a=20, limit=±100
B-Spline: order=1, learning rate=0.2, splines=200, input range=0.0 - 0.8

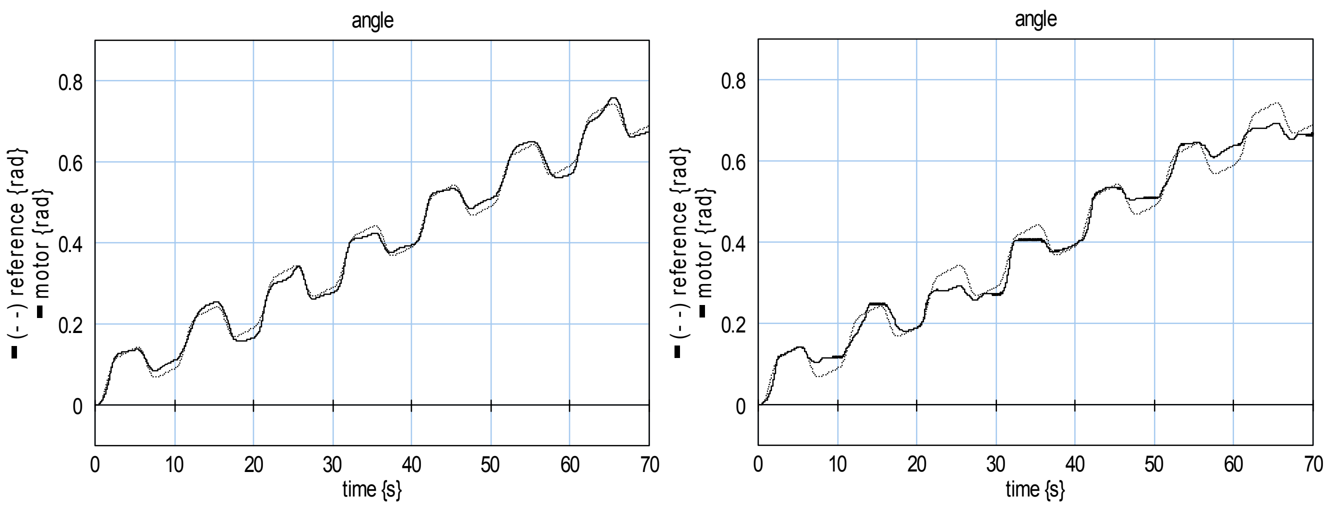

figure 94 PID only: reference and motor angle for 6° (left) and 0° (right) torsion angle

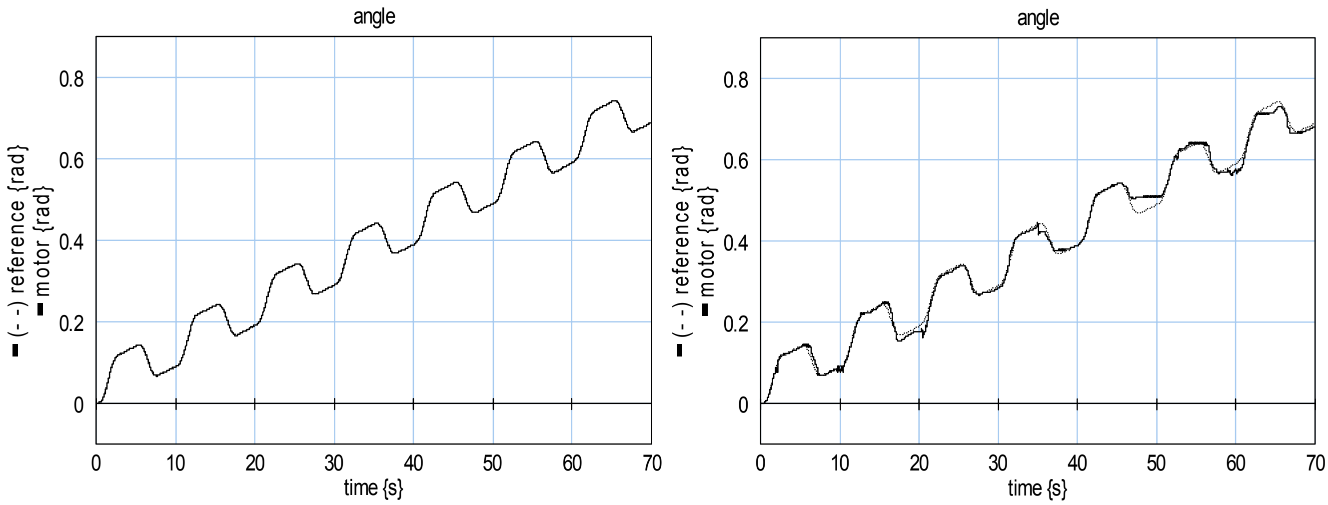

figure 95 PID+B-Spline: reference and motor angle after training for 6° (left) and 0° (right) torsion angle

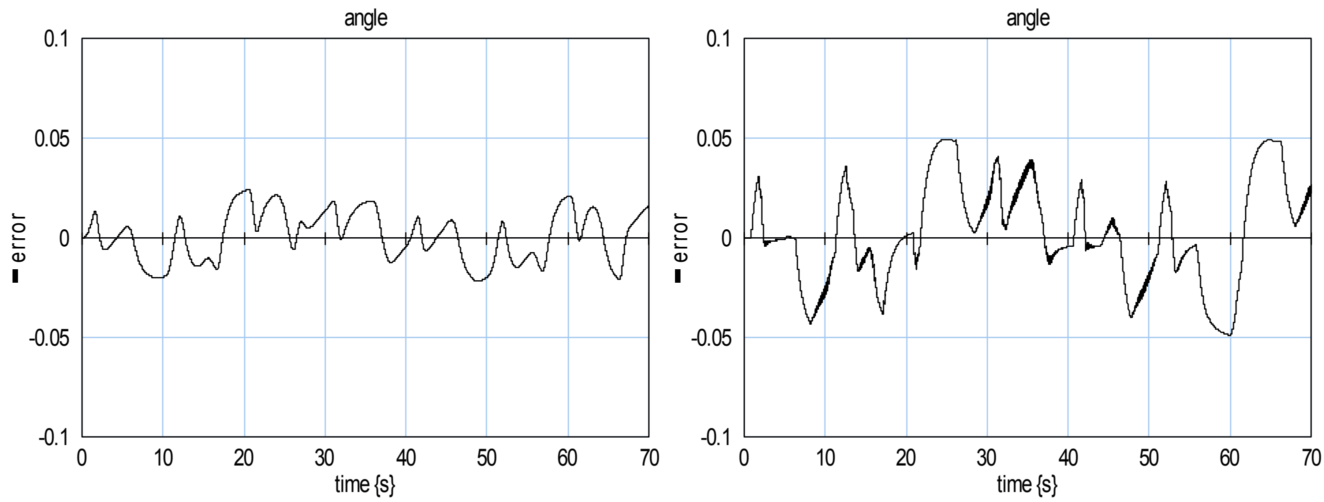

figure 96 PID only: error for 6° (left) and 0° (right) torsion angle

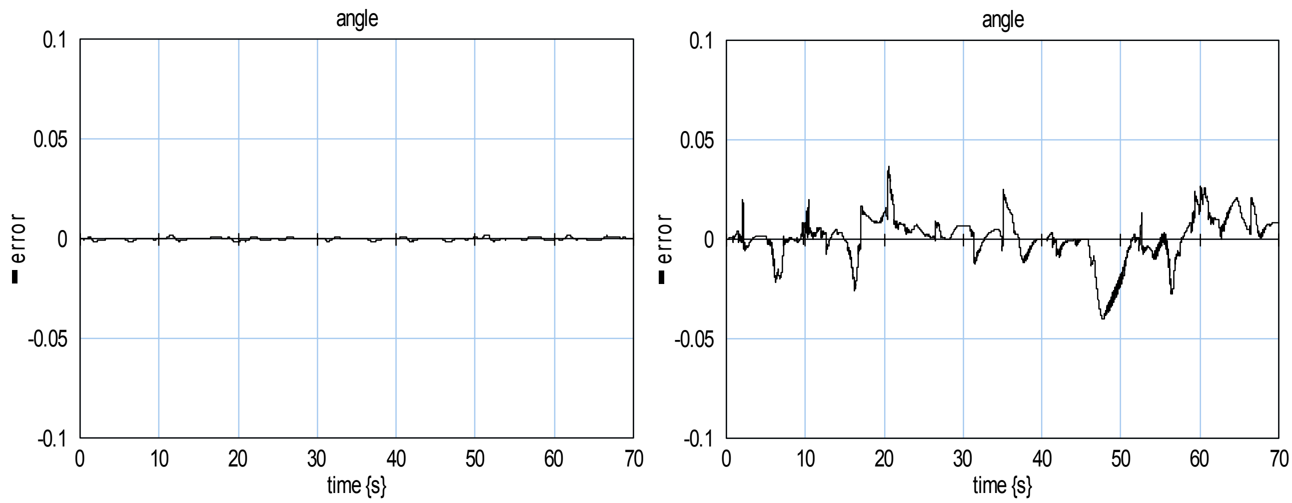

figure 97 PID+B-Spline: error after training for 6° (left) and 0° (right) torsion angle

APPENDIX C: MAXWELL'S EQUATIONS

Maxwell's equations describe the essential relations between electric and magnetic domains. Because these are the origin of the motor theory and the analysis using magnetic equivalent circuits Maxwell's equations are noted here.

First Maxwell's equation relates magnetic field H to electric current density J and electric displacement D:

$$\oint_C \vec{H} \bullet \vec{\tau} \cdot ds = \iint_S \vec{J} \bullet \vec{n} \cdot dA + \frac{d}{dt} \iint_S \vec{D} \bullet \vec{n} \cdot dA \qquad (62)$$

The magnetic field along contour C is equal to the current plus the change of electric displacement through the surface S bounded by contour C (see figure 98). Electric displacement D is related to electric field E by the dielectrical constant ε: $D = \varepsilon E$.

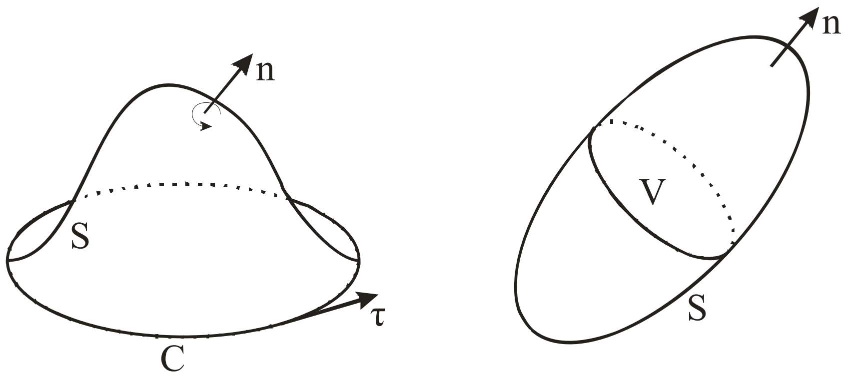

figure 98 surface S with contour C and closed surface S with volume V

Because mechanical speeds and distances of the observed system are very low compared to the speed of light, the second term in (62) can be neglected: the time-derivative of the electric field and therefore also the time-derivative of the electric displacement can be neglected as source of magnetic field. First Maxwell's equation simplifies into Ampère's law:

$$\oint_C \vec{H} \bullet \vec{\tau} \cdot ds = \iint_S \vec{J} \bullet \vec{n} \cdot dA \qquad (63)$$

Second Maxwell's equation (or Faraday's Induction Law) relates electric field E to magnetic flux density (induction) B:

$$\oint_C \vec{E} \bullet \vec{\tau} \cdot ds = -\frac{d}{dt} \iint_S \vec{B} \bullet \vec{n} \cdot dA \qquad (64)$$

The electric field along contour C is equal to the opposite of the time-derivative of the magnetic flux through surface S bounded by contour C.

Gauss' law for magnetism states that there is no flux leakage:

$$\oiint_S \vec{B} \bullet \vec{n} \cdot dA = 0 \qquad (65)$$

Magnetic field *H*, flux density *B* and the magnetization *M* are related by the permeability μ:

$$B = \mu\left(H + M\right) \xrightarrow{isotropic\,/\,linear} B = \mu_r \mu_0 \left(H + M\right) \tag{66}$$

M is the permanent magnetic field due to dipoles in the material created by polarisation. It plays an important role in the permanent magnets of a p.m. motor. Magnetization can be undone or reversed when exposed to a high magnetic field in opposite direction.

APPENDIX D: DESCRIPTION MATLAB MODELS

The electromagnetic motor model of chapter 3.2 has been implemented in Matlab using separate functions for each step in the algorithm. Below the main m-file “run.m” is described. Afterwards the functions will be shown schematically.

MAIN M-FILE: run.m

```
parameters_motorC.m
     (loads parameters of example motor C)
param.m
     (processes the parameters, prepares calculations)

FUNCTION:
[A,L,U,R,Fpm] = magn_circuit(design parameters);
     (calculates the component values of the equivalent circuit as
     described in §3.2.4: cross-sectional surface, reluctance,
     permeability and magneto motive forces as function of the
     design parameters)

FUNCTION:
Fp = stroom(current amplitude, motor configuration);
     (calculates the size and the ideal phase of the current through
     the coils as function of the motor configuration)

FUNCTION:
[Km,P,B,H] = KM(A,L,U,R,Fpm,Fp);
     (calculates the motor constant, flux, flux density and magnetic
     field strength as described in §3.2.5 - 3.2.7)

FUNCTION:
Kr = KR(A,L,H,B);
     (calculates the reluctance torque as described in §3.2.8)

motorspecs.m
     (calculates resistance, inductance and steepness using the
     definitions in eq. (18), (12) and (28))
verliezen.m
     (calculates losses as described in §3.2.9)
```

SEPARATE M-FILES

```
tijdsimulatie.m
     (time simulation of simplified motor model)
thermisch.m
     (estimation of the thermal behaviour as described in §3.3)
```

FUNCTION: magn_circuit.m

Calculates the component values of the equivalent circuit using the design parameters, by calculating following steps:

- Surface of magnets and borders as function of position on rotor
- Surface of pole shoes as function of position on stator
- Overlap between rotor and stator surfaces as function of rotor angle
- Cross-sectional surfaces of the other elements of the equivalent circuit (pole shoes, stator yoke and leakage between pole shoes)
- Magneto motive forces per phase due to the magnets as function of the rotor angle
- Reluctance of all components from the cross-sectional or overlapping surfaces, lengths and permeabilities

FUNCTION: stroom.m

Calculates the current through the coils. As described in §2.4.1 the current should be in phase with the motor constant.

- Depending on the simulation settings a block or sine wave current with correct phase is defined for all three phases
- The currents are transformed into magneto motive force sources

FUNCTION: KM.m

Solves the flux balance setup by magn_circuit.m and stroom.m using following steps:

- Setup algebraic structure corresponding to equivalent circuit (Hopkinson)
- Copy reluctances and magneto motive forces at one specific rotor angle into algebraic equations
- Solve flux from algebraic structure using eq. (52)
- Adjust permeabilities due to saturation according §3.2.9
- Repeat permeability adjustment to get equilibrium solution of nonlinear saturation
- Repeat all steps above for all other rotor angles, such that we end up with the flux as a function of the rotor angle
- Km, B and H are calculated from the flux according §3.2.5 and 3.2.7

FUNCTION: KR.m

Calculates the reluctance torque using eq. (57).

- Element wise multiplication of B, H, A and L yields E_{magn}
- Differentiation of E_{magn} to the rotor angle yields the reluctance torque

REFERENCES

1. Hendershot J.R. and Miller T.J.E., *Design of brushless permanent-magnet motors*, Magna Physics Publications - Oxford Science Publications
2. Hoeijmakers M.J., *Elektrische omzettingen*, Delft University Press, The Netherlands
3. Jansen J., *Materials Library*, third edition, Philips Report CTR505-90-RJ261, Eindhoven
4. Holm S.R. e.a., *Analytical Calculation of the Magnetic File din Electrical Machines due to the Current Density in an Airgap Winding*, Delft University of Technology, The Netherlands
5. Kokernak J.M. and Torrey D.A., *Magnetic Circuit Model for the Mutually Coupled Switched-Reluctance Machine*, IEEE Transactions on magnetics, vol. 36 no.2 march 2000
6. Thelin P. and Nee H-P, *Calculation of the airgap flux density of pm synchronous motors with buried magnets including axial leakage and teeth saturation*, KTH, Royal Institute of Technology, Sweden
7. Polinder H. and Hoeijmakers M.J., *Analytic Calculation of the Magnetic Field in PM Machines*, Delft University of Technology, The Netherlands
8. Tapia J.A. e.a., *CPPM Machine: A Synchronous Permanent Magnet Machine with Field Weakening*, University of Wisconsin-Madison and Ford Research Laboratories, USA
9. Polinder H., Hoeijmakers M.J., Compter J.C., *Modelling of a linear PM machine including magnetic saturation and end effects: maximum force to current ratio*, Delft University of Technology and Eindhoven University of Technology, The Netherlands
10. Slemon G.R., *Electric Machines and Drives,* University of Toronto, Canada
11. Schwarz K.K., *Design of Industrial Electric Motor Drives*, University of Southampton, UK
12. Beitz W. and Küttner K.H., *Taschenbuch für den Maschinenbau*, Springer-Verlag, Berlin
13. Kruif B.J. de, Vries T.J.A. de, *Improving Price/Performance ratio of a linear motor by means of learning control*, in: 2nd. IFAC Conference on Mechatronic Systems, Berkeley, California, USA, 2002, (Conference Papers)
14. Tysma Sj, Herwijnen F. van and Leijendeckers P.H.H., *Poly-Technisch Zakboekje*, Koninklijke PBNA b.v., The Netherlands

SYMBOLS

A	[m^2]	area
B	[$Wb.m^{-2}$]	magnetic flux density
E	[J]	energy
f	[Hz]	frequency
F_m	[A]	electromagnetic force
H	[$A.m^{-1}$]	magnetic field
i	[A]	current
I	[A]	current amplitude
J	[$A.m^{-2}$]	current density
K_m	[Vs/rad] or [Nm/A]	motor constant
l	[m]	length
L	[H]	inductance
N	[-]	number of windings per coil
P	[W]	power
R	[Ω]	resistance
R_m	[$A.Wb^{-1}$]	magnetic reluctance
S	[Nm.s/rad]	steepness
T	[Nm]	torque
u	[V]	voltage
U	[V]	voltage amplitude
φ	[rad]	(motor) angle
Φ	[Wb] or [Vs]	magnetic flux
λ	[Wb] or [Vs]	coupled magnetic flux
μ	[H/m]	magnetic permeability
ω	[rad/s]	angular velocity